# FORCE GENERATION BY MICROTUBULE END-BINDING PROTEINS

By

LUZ ELENA CARO

A DISSERTATION PRESENTED TO THE GRADUATE SCHOOL
OF THE UNIVERSITY OF FLORIDA IN PARTIAL FULFILLMENT
OF THE REQUIREMENTS FOR THE DEGREE OF
DOCTOR OF PHILOSOPHY

UNIVERSITY OF FLORIDA

2007

To my supportive parents, Ruby and Armando Caro,
encouraging siblings, Maritza, Mando, and Cesar,
and my eternal best friend, Antonio.

ACKNOWLEDGMENTS

I acknowledge the support of my advisor, Dr. Richard B. Dickinson, whose patience, guidance, and motivation provided the necessary tools for my successful and rewarding graduate experience. The helpful comments and constructive criticisms from my committee members were greatly appreciated. I thank Dr. Anuj Chauhan for the continued encouragement and support throughout my professional career. The insightful career advice and assistance provided by Dr. Jennifer Curtis was greatly appreciated. I recognize Dr. Anthony Ladd for introducing me to the exciting research at the University of Florida. The assistance provided by the Chemical Engineering faculty and staff was invaluable for my experience at the University of Florida.

I thank Dr. Daniel Purich for his biochemistry and professional advice which helped me to develop my research skills. I am grateful for the expertise of the members in the biochemistry group (under advisement of Dr. Daniel Purich) which helped me gain the proper biochemistry understanding needed for my graduate research; I thank Dr. William Zeile, Dr. Joseph Phillips, Dr. Fangliang Zhang.

I thank my group members who helped me learn experimental techniques and exchanged ideas pertaining to research; my graduate experience was enriched by their companionship and support: Kimberly Interliggi, Colin Sturm, Gaurav Misra, Jeff Sharp, Huilian Ma, Adam Feinburgh.

TABLE OF CONTENTS

page

LIST OF TABLES

LIST OF FIGURES

LIST OF TERMS

| | |
|---|---|
| ADP: | Adenosine diphosphate |
| APC: | Adenomatous Polyposis Coli |
| ATP: | Adenosine triphosphate |
| $a$: | Width of protofilament |
| $C_{eff}$: | Effective concentration of a free subunit of filament-bound EB1 |
| $C_T$: | Effective concentration of tracking unit at protofilament plus-end |
| $d$: | Size of tubulin protomer |
| $dbE^-$: | State of tubulin protomer attached to the subunit on the minus-side of a double- bound EB1 dimer |
| $dbE^+$: | State of tubulin protomer attached to the subunit on the plus-side of a double- bound EB1 dimer |
| $[E]_0$: | Total intracellular EB1 concentration |
| [E]: | Concentration of EB1 in solution |
| EB1: | End Binding Protein 1 |
| $E_{sp}$: | Hookean Spring energy |
| $D_f$ : | Protofilament diffusivity |
| $dt$: | Time steps taken in simulation |
| $F$: | Force applied to microtubule plus-end |
| $F_{stall}$: | Stall force – maximum achievable force |
| $f$: | Energy captured from hydrolysis that is used for affinity modulation |
| GDP: | Guanosine diphosphate nucleotide |
| GTP: | Guanosine triphosphate nucleotide |
| [GDP]: | Concentration of guanosine diphosphate nucleotide |
| [GTP]: | Concentration of guanosine triphosphate nucleotide |
| $K_1$: | Equilibrium dissociation constant for tubulin in solution binding to EB1 |

(K1 ≡ k- 1/k1)

$K_1$': Equilibrium dissociation constant for tubulin addition to track-bound protofilament (K1' ≡ k r/kf')

$K_3$: Equilibrium dissociation constant for EB1 subunit binding to track-bound filament-T-GDP (K3 ≡ k –side'/k+side')

$K$: Ratio of forward and reverse rate of EB1 subunit binding to protofilament plus-end (K ≡ k +/k-)

$K$': Equilibrium dissociation constant for EB1 subunit binding to protofilament plus-end (K' ≡ k -/k+)

$K_d$: Equilibrium dissociation constant for EB1 (or TE) binding to filament-bound T-GDP (Kd ≡ k-side/konside)

$K_d$*: Equilibrium dissociation constant for EB1 (or TE) in solution binding to T-GTP at protofilament plus-end

$K_{pi}$: Equilibrium dissociation constant for reversible phosphate binding to T protomers

$K_T$: Equilibrium dissociation constant for track binding to solution-phase EB1 (or TE or TTE)

$K_x$: Equilibrium dissociation constant for the GTP/GDP exchange reaction

$k_1$: Forward rate constant for tubulin in solution binding to EB1

$k_{-1}$: Reverse rate constant for tubulin in solution binding to EB1

$k_+$: Forward rate constant for subunit of filament-bound EB1 binding to T-GTP at protofilament plus-end

$k_+^{side}$: Forward rate constant for subunit of filament-bound EB1 binding to filament-bound T-GDP

$k_-$: Reverse rate constant for EB1 (or TE) in solution binding to T-GTP at

protofilament plus-end

$k_{-}^{side}$: Reverse rate constant for EB1 (or TE) binding to filament-bound T-GDP

$k_BT$: Thermal energy (Boltzmann constant, k, × absolute temperature, T)

$k_f$: Forward and reverse rate constants for tubulin in solution binding to protofilament plus-end

$k_{f,0}$: Initial forward rate constant for tubulin in solution binding to protofilament plus-end

$k_f^E$: Forward rate constant for EB1-bound tubulin in solution binding to T-GTP at protofilament plus-end

kMT: Kinetochore-bound microtubule

$k_{obs}$: Observed decay constant of EB1 on MT

$k_{off}$: Dissociation rate constant for EB1 dimer from protofilament

$k_{on}$: Forward rate constant for EB1 (or TE) in solution binding to T-GTP at protofilament plus-end

$k_{on}^{side}$: Forward rate constant for EB1 (or TE) binding to filament-bound T-GDP

$k_r$: Reverse rate constant for tubulin in solution binding to protofilament plus-end

$k_r^E$: Reverse rate constant for EB1-bound tubulin in solution binding to T-GTP at protofilament plus-end

$k_T$: Forward rate constant for track binding to solution-phase EB1 (or TE or TTE)

$k_T^-$: Reverse rate constant for track binding to solution-phase EB1 (or TE or TTE)

$L$: Length of protofilament in ciliary plug

LLF: Lock, Load, and Fire model

| | |
|---|---|
| MT: | Microtubule |
| $N$: | Total number of protomers in a protofilament |
| $N_p$: | Number of protofilaments tethered to motile object |
| $n$: | Position of tubulin protomer bound to track |
| $ns$: | Number of protomers between EB1 subunit at equilibrium position and final binding position |
| $P_{eq}$: | Equilibrium fraction of EB1-bound protomers on protofilament |
| $P_i$: | Phosphate |
| $p$: | Probability of protomer bound to EB1 subunit |
| $p_{end}$: | Probability of EB1 binding to the protofilament plus-end |
| $p_{eq}$: | Equilibrium probability of protomer bound to EB1 subunit |
| $p_{side}$: | Equilibrium probability of EB1 binding to filament-bound T-GDP |
| $q_+$: | Probability of protomer in state dbE+ |
| $q_-$: | Probability of protomer in state dbE- |
| $q$: | Probability of protomer attached to double-bound EB1 subunit |
| $q_{eq}$: | Equilibrium probability of protomer attached to double-bound EB1 subunit |
| S1: | State of terminal protomer in protofilament |
| S2: | State of penultimate protomer in protofilament |
| TAC: | Tip-Attachment Complex model |
| Tb: | Tubulin protomer |
| [Tb]: | Tubulin protomer concentration |
| $[Tb]_c$: | Critical tubulin concentration for free MT plus-end |
| $[Tb]^E_c$: | Critical TE concentration for free MT plus-end |
| TE: | EB1-bound tubulin protomer |
| T-GDP: | GDP-bound tubulin protomer |

| | |
|---|---|
| [T-GDP]: | T-GDP concentration |
| $[\text{T-GDP}]_{(-)c}$: | Critical tubulin concentration for T-GDP at MT plus-end |
| T-GTP: | GTP-bound tubulin protomer |
| Tk2: | Track bound to protofilament-bound EB1 |
| Tk3: | Track bound to protofilament-bound TE |
| Tk4: | Track bound to protofilament-bound dbE+ |
| Tk: | Track (tethering protein bound to motile surface) |
| Tk-E: | Track bound to EB1 in solution |
| Tk-TE: | Track bound to TE in solution |
| Tk-TTE: | Track bound to TTE in solution |
| $T_m$: | Time required for tubulin addition and filament-bound GTP hydrolysis |
| TTE: | EB1 bound to two tubulin protomers |
| $t$: | Total simulation time |
| $u$: | Probability of protomer being unbound from EB1 |
| $u_{eq}$: | Equilibrium probability of protomer being unbound from EB1 |
| $v$: | Irreversible velocity |
| $v_r$: | Reversible velocity |
| $v_{max}$: | Maximum expected velocity |
| $w$: | Probability of protomer bound to TE |
| $w_{eq}$: | Equilibrium probability of protomer bound to TE |
| $x$: | Protofilament end position |
| $z$: | Equilibrium surface position |
| $z_e$: | Equilibrium position of protofilament-bound EB1 subunit |
| $\Delta$: | Transition state distance |
| $\Delta G$: | Net free energy change of the tubulin cycle |

| | |
|---|---|
| $\Delta G_0$: | Initial free energy change of the tubulin cycle |
| $\Delta G_{(-)loss}$: | Free energy of T-GDP dissociation from MT minus-end |
| $\Delta G_{(+)add}$: | Free energy of T-GTP addition to MT plus-end |
| $\Delta G_{exchange}$: | Free energy of GDP/GTP exchange in solution |
| $\Delta G_{hydrolysis}$: | Free energy of MT-bound GTP hydrolysis |
| $\Delta G_{Pi\text{-}release}$: | Free energy of MT-bound phosphate (Pi) release |
| $\delta$: | Viscous drag coefficient |
| $\gamma$: | Hookean spring constant |
| $\eta$: | Viscosity |
| $\kappa$: | Stiffness of MT protofilament under compression |
| $\rho^2$: | Surface density of EB1 on motile object |
| $\tau$: | Time required for ciliary plug to shift and rebind |

Abstract of Dissertation Presented to the Graduate School
of the University of Florida in Partial Fulfillment of the
Requirements for the Degree of Doctor of Philosophy

FORCE GENERATION BY MICROTUBULE END-BINDING PROTEINS

By

Luz Elena Caro

December 2007

Chair: Richard B. Dickinson
Major: Chemical Engineering

Microtubules are cytoskeletal filaments essential for multiple cell functions, including motility of microorganisms and cell division. Of particular interest is how these biological polymers generate the forces required for movement of chromosomes during mitosis and for formation of cilia and flagella. Defective microtubule-based force generation can lead to various pathological complications; therefore, an understanding of microtubule force generation is important for cancer research and biotechnology.

The mechanism by which elongating microtubules generate force is unknown. Several proteins, including End-Binding Protein 1 (EB1) and adenomatous polyposis coli (APC), specifically localize to microtubule elongating ends where the microtubule is tightly bound to a motile object and generating force. The role of these end-tracking proteins is not fully understood, but they likely modulate microtubule-motile surface interactions, and may aid in force production.

The objective of my research is to elucidate the role of polymerizing microtubules and end-binding proteins, specifically EB1, in force-dependent processes by formulating a model that explains their interaction and role in force generation. The commonly assumed Brownian Ratchet model describing the forces caused by elongating microtubules cannot easily explain

force generation during rapid elongation and strong attachment of the microtubule to the motile object. I propose a novel mechanism in which EB1 proteins behave as end-tracking motors that have a higher affinity for guanosine triphosphate-bound tubulin than guanosine diphosphate-bound tubulin, thereby allowing them to convert the chemical energy of microtubule-filament hydrolysis to mechanical work. These microtubule end-tracking motors are predicted to provide the required forces for cell motility and persistent attachment between the motile surface and polymerizing microtubules.

I have developed mechanochemical models that characterize the kinetics of these molecular motors based on experimentally determined binding parameters and thermodynamic constraints. These models account for the association of EB1 to tethered and untethered elongating microtubule ends, in the absence or presence of force, and with or without EB1 binding to solution-phase tubulin. These models explain the observed exponential profile of EB1 on untethered filaments and predict that affinity-modulated end-tracking motors should achieve higher stall forces than with the Brownian Ratchet system, while maintaining a strong, persistent attachment to the motile object.

# CHAPTER 1
# INTRODUCTION

Forces produced by microtubule polymerization are required for chromosomal movement during mitosis and ciliary/flagellar formation (Dentler and Rosenbaum, 1977; Inoue and Salmon, 1995; Dogterom and Yurke, 1997). End-tracking proteins (a.k.a. tip-tracking proteins), such as end-binding protein 1 (EB1) and adenomatous polyposis coli (APC), have previously been shown to bind specifically to the polymerizing microtubule plus-end where the microtubule is tightly bound, at the kinetochore and at the tips of growing cilia/flagella (Allen and Borisy, 1974; Dentler, 1981; Severin et al., 1997), suggesting a possible role for end-tracking proteins in force generation at these sites. A few models demonstrate how end-binding proteins may be involved in microtubule force-generation, suggesting that end-tracking proteins bind weakly to the microtubule plus-end and serve as a linker between the MT and a motile surface (e.g., kinetochore) (Hill, 1985; Inoue and Salmon, 1995; Rieder and Salmon, 1998; Maddox et al., 2003; Maiato et al., 2004). However, these models cannot explain the strong attachment of the microtubule to a motile object during elongation, nor the energetics and mechanism of the interaction between the end-binding proteins and a motile surface. The objective of my thesis research was to help elucidate the role of microtubule elongation mediated by end-binding proteins in force generation. Our models explain and characterize the interaction of end-binding proteins with growing microtubule ends and their role in force generation

Understanding the functions of microtubules and end-tracking proteins in cellular motility and cell proliferation is of great importance to the medical field, particularly in the area of cancer research. For example, the end-tracking protein APC not only plays a potentially key role in microtubule-chromosome attachment during cell division, but it also suppresses excessive cell production that could lead to colon cancer. Cells with a specific mutation in APC, which prevent

its binding to microtubules and EB1, lead to aneuploid progency and an absence of APC's tumor suppression function (Fodde et al., 2001b; Kaplan et al., 2001). By providing insight into the potential function of these proteins and the interaction among them is just one example of how our research can provide a significant impact in cell biology.

## 1.1 Microtubules

Microtubules (MTs) are versatile polymers that occur in nearly every eukaryotic cell. They provide form and support in cells, aid in mitosis, guide transport of organelles, and enable cell motility (Olmsted and Borisy, 1973; Yahara and Edelman, 1975; Dentler and Rosenbaum, 1977). Microtubules are hollow, tubular structures composed of 8-nm α/β-tubulin heterodimers; where the β–subunit can bind to either a guanosine triphosphate (GTP) or guanosine diphosphate (GDP) nucleotide (Farr et al., 1990). Tubulin bound to GTP assembles head-to-tail to form the 13 asymmetric, linear protofilaments of a microtubule (Figure 1-1) (Chretien et al., 1995; Chretien and Fuller, 2000). Each protofilament has the same polarity, with a β-tubulin at one end (minus or slow-growing end), and an α-tubulin at the other (plus or fast-growing end) (Chretien et al., 1995; Chretien and Fuller, 2000). The structural polarity of the microtubules is important in their growth and ability to participate in many cellular functions. During microtubule polymerization (MT growth), GTP-tubulin protomers add to the plus-end of a MT, the subunits then hydrolyze their bound GTP and subsequently release the hydrolyzed phosphate. During depolymerization (MT shortening), GDP-tubulin subunits are released from the MT minus-ends at a very rapid rate (Desai and Mitchison, 1997).

The elongation velocity of a microtubule during polymerization, $v$, is reported as 167 nm/s for the free, microtubule plus-end during mitosis (Piehl and Cassimeris, 2003). Assuming

irreversible elongation at the MT plus-end *in vivo*, this value can be used to estimate the plus-end protofilament effective on-rate constant of tubulin ($k_f$) association,

$$k_f = \frac{v}{d \cdot [Tb]} \tag{1-1}$$

where $d$ is the length of a protomer and [Tb] the intracellular GTP-tubulin concentration (~10 μM; (Mitchison and Kirschner, 1987); yielding $k_f = 2\ \mu M^{-1}\text{-}s^{-1}$. The critical concentration for tubulin polymerization *in vitro* is $[Tb]_c = 5\ \mu M$, which can be used to calculate an effective tubulin off-rate ($k_r$) of 10.6 $s^{-1}$, assuming

$$[Tb]_c = k_r / k_f \cdot \tag{1-2}$$

This calculated off-rate is used to determine the reversible, elongation rate of the microtubule plus-end (85 nm/s) by

$$v_r = \left(k_f \cdot [Tb] - k_r\right) \cdot d\,. \tag{1-3}$$

For the purposes of model comparisons in subsequent chapters, these rate constants for binding and dissociation of tubulin are assumed, and $v$ and $v_r$ are taken as nominal velocities of irreversible and reversible elongation, respectively, of MT plus-ends without the involvement of end-tracking proteins.

Microtubule polymerization/depolymerization provides the forces required for cilia and flagella assembly as well as chromosomal alignment during mitosis. During microtubule elongation in both processes, the plus-end of the MT remains attached to the motile object (i.e., the ciliary/flagellar assembly plug or kinetochore, respectively) (Allen and Borisy, 1974; Dentler, 1981; Severin et al., 1997). Microtubule assembly is known to play a key role throughout mitosis, the process of division and separation of the two identical daughter chromosomes (Inoue, 1981; Salmon, 1989; Rieder and Alexander, 1990) . In an early stage of

mitosis, replicated chromosomes (sister chromatids) are attached to each other at the centromere, which also serves as the binding site for the proteinaceous kinetochore structure (Figure 1-2) (Lodish et al., 1995). The outer plate of kinetochores contains proteins that bind to kinetochore microtubules (kMTs). Other types of microtubules are also involved in mitosis, including astral and polar MTs. However, kMTs are of particular interest because of their role in properly arranging cellular chromosomes by generating force at the kinetochore (Lodish et al., 1995).

The six phases of mitosis include prophase, prometaphase, metaphase, anaphase, and telophase. During prometaphase, kMTs of different length emanate away from opposite poles of the cell, and bind their plus-end to the kinetochores of chromosomes. By rapid addition and loss of tubulin protomers at the kinetochore, the kMTs oscillate back and forth (directional instability), generating the force required to balance the length of kMTs on opposite ends of each chromosome (Skibbens et al., 1993). These oscillations eventually results in the alignment of the chromosomes at the spindle equator (congression). In metaphase, kMTs from opposite poles experience a net polymerization at the kinetochore and net depolymerization at the poles (MT flux) (Maddox et al., 2003), exerting tension on each of the chromosomes (Inoue, 1982). As a result, the chromosomes maintain their alignment along the equatorial plane. The spindle checkpoint then ensures chromosomes are properly attached to the spindle before anaphase onset by releasing an inhibitory signal that delays anaphase if kinetochores are unattached (Rieder et al., 1994; 1995). The kMTs proceed to depolymerize while still attached to the kinetochores during anaphase (Coue et al., 1991), pulling the sister chromatids apart and moving them toward opposite poles for cellular division (cytokinesis).

Kinetochores stabilize microtubules against disassembly by attaching specifically to elongating GTP-rich MT plus-ends (Severin et al., 1997). A complex of proteins is required for

kinetochore capture by kMTs, but their interaction have not been elucidated (Mimori-Kiyosue and Tsukita, 2003). If one of the kinetochore-associated proteins could recognize and track the GTP-rich end, this protein could potentially provide a mechanism that would couple kinetochore movement to force generated by MT polymerization during mitosis. Several proteins that localize at the kinetochore-kMT attachment during mitosis have also been shown to bind to the plus-ends of MTs (end-tracking proteins), suggesting their likely role in such a mechanism. Of particular interest here are the plus-end tracking proteins EB1 and adenomatous polyposis coli. Although the interaction among these two proteins and the protein/microtubule relationship is still unclear, a significant amount of recent research demonstrates their potential role in kinetochore motility and kMT attachment, as discussed presently.

## 1.2 End-Tracking Proteins

Several MT end-tracking proteins are thought to facilitate force generation by microtubule polymerization (Schuyler and Pellman, 2001). End-tracking proteins localize to the MT plus-end, and when fluorescently labeled, they mark the translating polymerizing ends of MTs. Recent studies demonstrate the ability of a variety of proteins to track the ends of growing MTs, including CLIPs, CLASPs, $p150^{glued}$, APC, EB1, etc. It is suggested these end-tracking proteins aid in control of MT dynamics and in attachment of MTs to a motile surface (i.e., the cell membrane or kinetochore) in several organisms, such as fungi and humans.

### 1.2.1 EB1

Of particular interest here is the EB1 protein, because it was found to localize at points where polymerizing MTs generate force (mitosis, cell growth, flagellar movement, etc). EB1's specific localization suggests that EB1 has a role in modulating the attachment of the MTs to motile surfaces and regulating MT dynamics at the attachment site to generate the forces during these cellular processes.

EB1 is a dimeric, 30-kDa leucine zipper protein (Mimori-Kiyosue et al., 2000) with two MT binding domains. EB1 binds to microtubules throughout the cell cycle. During mitosis and cell growth, EB1 specifically localizes to the GTP-rich tubulin protomers (polymerizing unit) at the polymerizing plus-ends of microtubules. EB1 quickly disappears from the plus ends of depolymerizing GDP-rich MT's, indicating that the higher EB1 density at plus ends requires polymerization and/or a GTP-rich MT end. This association/dissociation behavior suggests that EB1 has a role in targeting the MTs to a motile surface and/or regulating MT dynamics at the attachment site (cell membrane or kinetochore) (Mimori-Kiyosue and Tsukita, 2003). This hypothesis is supported by demonstrating that EB1-null *Drosophila* cells cause mitotic defects including mis-positioning of kinetochores during congression (Rogers et al., 2002). Specific localization of EB1 to GTP-rich MT plus-ends is not understood, but may be the result of direct binding of EB1 to the GTP-stabilized conformation of the MT plus end, co-polymerization with tubulin in solution, or recruitment by other proteins, and dissociation from GTP-bound MT subunits (Figure 1-3).

A study performed by Tirnauer et al. (2002b) provided important quantitative data that can be used to evaluate and provide parameters for models of EB1 interactions with MTs. As shown in Figure 1-4. They observed an exponentially decreasing density of EB1 from the MT tips to a uniform density on the MT sides, with 4.2x greater EB1 density relative to the sides. They measured the equilibrium dissociation constant of EB1 to MT sides in vitro to be $K_d = 0.5$ μM. Equilibrium binding EB1 from the cytoplasm to MT sides also explains the faint uniform fluorescence of EB1 along the side of polymerizing MTs *in vivo* (Mimori-Kiyosue et al., 2000).

The above results suggested that EB1 may either bind near plus ends with higher affinity than MT sides, or it could copolymerize with tubulin at plus ends before release at filament sides,

which would require association between EB1 and tubulin in solution. However, direct binding between EB1 and tubulin protomers in solution is uncertain. Vincent Gache's (2005) group used sucrose gradient centrifugation to find that bovine brain T-GTP did not bind to an EB1 construct. Contrary to his finding, Juwana et al. (1999) demonstrated that recombinant EB1 co-precipitates with purified bovine tubulin an immunoaffinity assay, despite the 100-time lower concentration of EB1 than T-GTP (Tirnauer et al., 2002a; Tirnauer et al., 2002b). However, other studies report no interaction between purified EB1 and tubulin. For example, Ligon et al. (2006) showed that full length human EB1 did not bind to a tubulin-affinity matrix. Nevertheless, lack of binding *in vitro* does not rule out EB1's interaction with tubulin protomers *in vivo*, which may require cytoplasmic components or conditions not present in these *in vitro* experiments. Consistent with this possibility, EB1 and tubulin alone *in vitro* do not promote microtubule polymerization (Nakamura et al., 2001; Tirnauer et al., 2002b; Ligon et al., 2003).

### 1.2.2 Adenomatous Polyposis Coli (APC)

EB1 may be recruited to the MT plus-ends by other proteins such as APC. APC is a dimeric tumor suppressor protein that plays an important protein role in preventing colon cancer. APC is known to co-localize and interact with both EB1 and polymerizing microtubule plus-ends at the kinetochore and at the cell cortex (Juwana et al., 1999). Like EB1, APC falls off the microtubule upon plus-end depolymerization. The C-terminal domain of APC (C-APC) is responsible for its association with EB1 and microtubules (Bu and Su, 2003), which is diminished upon phosphorylation of APC. In the absence of C-APC, there is an ineffective connection between kMTs and the kinetochore (Fodde et al., 2001a; Kaplan et al., 2001; Green and Kaplan, 2003), about 75% of cells exhibit failed chromosome congression (Green and Kaplan, 2003), and chromosome segregation is defective (which may be responsible for colon cancer) (Fodde et al., 2001a; Kaplan et al., 2001; Green and Kaplan, 2003). Studies also indicate

that neither the microtubule-binding domain nor the EB1 binding domain of APC can be compromised to obtain proper chromosomal segregation. In the absence of the EB1-binding domain, APC localizes non-specifically to MTs (Askham et al., 2000), and in the presence of only the EB1 binding domain, APC distributes throughout the entire cell without binding to microtubules or kinetochores (Green and Kaplan, 2003). These observations suggest that APC may modulate plus end attachment of EB1 to kMTs, help kMTs target the kinetochore, and (in association with EB1) aid in regulating kMT polymerization during mitosis.

Other kinetochore-associated proteins ($p150^{Glued}$, CLIP-170, and CLASPs) also have direct interactions with EB1, have the ability to bind to the MT plus-end, and are located at the kinetochore-MT interface (Folker et al., 2005; Hayashi et al., 2005; Mimori-Kiyosue et al., 2005). Therefore, these components may also be involved in activation of EB1 at the MT tip and/or linking the EB1-bound MT plus-end to the kinetochore.

### 1.2.3 Ciliary and Flagellar Movement

Another example of force generation mediated by polymerizing microtubules that remain attached to the motile object is ciliary/flagellar formation and regeneration. During formation of these organelles, membrane-bound capping structures (or MT "plugs") are persistently associated with the plus-ends of polymerizing MTs during MT assembly and disassembly (Suprenant and Dentler, 1988). These capping structures consist of (a) a plug-like unit that inserts into the lumen of the microtubule, and (b) plate-like structure that joins the plug to the membrane. Interestingly, components of the capping structure have been found to resemble proteins within the kinetochore, as indicated by their antigenic cross-reactivity (Miller et al., 1990), and these findings suggest that the kinetochore and ciliary/flagellar capping structures may interact with polymerizing microtubules in a similar manner. In this regard, EB1 co-localizes with the plus-ends of microtubules within cilia/flagella as well as those attached to

kinetochores (Pedersen et al., 2003; Schroder et al., 2007; Sloboda and Howard, 2007). Depleted or mutated EB1 microtubule ends significantly reduces the efficiency of primary cilia assembly in fibroblasts (Schroder et al., 2007). Because the sites of EB1 localization are involved in force generation in the above organelles, the MT end-tracking properties of EB1 are likely to play a role in MT elongation-dependent force generation.

## 1.3 Force Generation Models

Although much progress was made identifying microtubule-associated proteins and their locations, how MT elongation is coupled to force generation has not been determined. Various force-generating models have been considered, including force from microtubule polymerization, force from motor-protein activity, and force from affinity modulation (Mitchison and Salmon, 2001).

### 1.3.1 Brownian Ratchet Models

It is commonly assumed that the Brownian Ratchet model describes the protrusive forces caused by elongating microtubules (Peskin et al., 1993; Mogilner and Oster, 1996). The thermodynamic driving force in this model is the free energy change of protomer addition to free protofilament ends (Hill, 1981; Theriot, 2000). An essential feature of this model is that thermal fluctuations open a gap between the free protofilament plus end and the motile surface to allow addition of each new protomer. Because the protofilaments must freely fluctuate from the surface, the Brownian ratchet mechanism therefore cannot easily explain force generation during rapid elongation and strong attachment of the elongating microtubule end to the motile object.

The thermodynamic stall force associated with the Brownian Ratchet model is limited by the free energy of protomer addition, and is given by

$$F_{stall} = \left(N_p \cdot k_B T / d\right) \ln\left([\mathrm{Tb}]/[\mathrm{Tb}]_c\right), \tag{1-4}$$

where $N_p = 13$ is the number of protofilaments, $k_B T = 4.14$ pN-nm is the thermal energy (Boltzmann constant × absolute temperature), and $d = 8$ nm is longitudinal dimer-repeat distance. Under typical intracellular tubulin (Tb) concentrations of 10-15 μM and a plus-end critical concentration $[Tb]_c = 5$ μM (Walker et al., 1988), then $F_{stall}$ = ~5-7 pN, or ~ 0.5 pN per protofilament.

### 1.3.2 Sleeve Model

The Hill "sleeve" model couples polymerization of MTs with the force generated at the anti-pole ward moving kinetochore in cells. The model assumes MTs are inserted into a sleeve and tubulin dimers are added to the growing MT through the center of the sleeve. Movement of a MT through the sleeve as it grows is accounted for by a random-walk approach, where the free-energy source is the binding of GTP-tubulin protomers to MT ends (Hill, 1985).

The Tip Attachment Complex model (TAC) incorporates the idea of a "sleeve" in order to model force-generation by MT polymerization in the presence of linker proteins. In TAC models, the tip of the microtubule inserts into a "sleeve" containing linker proteins that bind weakly to the subunits at/near the ends of MTs, and are assumed to grow freely by means of a Brownian ratchet mechanism (Inoue and Salmon, 1995). The weak-binding properties of the TAC linker proteins are assumed to allow the TAC to advance with the growing MT tip without hindering elongation. Therefore, the assumed bonds between the TAC linker proteins and MT have the seemingly contradictory properties of being strong enough to sustain attachment of the motile object, while at the same time being weak enough for their rapid unbinding/rebinding to permit unhindered elongation. In contrast, the models we are proposing suggest that linker proteins behave as end-tracking motors that have unique binding proteins allowing them to

maintain a strong, persistent attachment between the protofilament and a motile surface during MT elongation.

### 1.3.3 Kinetochore Motors

Several researchers have proposed a motor-induced force-generation model. One such model is known as the "reverse Pac-Man" mechanism (Maddox et al., 2003), where plus-end directed motors move kinetochores anti-pole ward during plus-end kMT polymerization (Inoue and Salmon, 1995). The plus-end directed motor protein, CENP-E, was assumed to play this role because of its localization to the kinetochore and its role in sensing kMT attachment at the kinetochore (Abrieu et al., 2000). However, recent experimental evidence shows that the CENP-E protein is not required for chromosome congression (McEwen et al., 2001). This result does not dismiss the possibility that MT motors contribute to anti-poleward kinetochore motility in the cell; there are other kinetochore-associated motor proteins (i.e., MCAK) of unknown function. One recent force-generation model, the "slip-clutch" model, integrates both the reverse Pac-Man and lateral- TAC mechanisms. This model represents the polymerization state of the kinetochore by a "slip-clutch" mechanism involving molecular motors and "linker" proteins that are attached to the kinetochore and bind along the wall of MTs. The energetics of such a mechanism have not yet been analyzed, but it suggests that the proteins involved provide force at the kinetochore, and prevent strong forces from pulling MT plus ends out of their kinetochore attachment sites (Maddox et al., 2003).

### 1.3.4 Filament End-Tracking Motors

Dickinson & Purich (2002) first proposed a model for actin-based motility whereby end-tracking proteins tethered elongating filaments to motile objects and facilitated force generation. In this mechanochemical model for actin subunit addition, surface-bound end-tracking proteins bind preferentially to newly added ATP-bound terminal subunits on each subfilament and release

from ADP-bound penultimate subunits. This cycle facilitates force generation of persistently tethered filaments by capturing the free energy of ATP hydrolysis in the monomer addition cycle. The ATP hydrolysis-driven processive tracking on the filament end gives the end-binding protein the characteristics of a molecular motor. We later proposed that the interaction of microtubule end-tracking proteins with terminal GTP subunits could similarly explain force generation and persistent attachment of MT's at motile objects (Dickinson et al., 2004). The models presented in this thesis are quantitative extensions of that initial model.

## 1.4 Thermodynamic Driving Force

The thermodynamic advantage of GTP-driven affinity modulated interactions can be seen by accounting for the free energy requirements of the tubulin polymerization cycle. The net free energy of the tubulin cycle ($\Delta G$) is partitioned among the five key steps of the tubulin cycle: tubulin addition (polymerization), filament GTP hydrolysis, phosphate ($P_i$) release, depolymerization, and GDP/GTP exchange in solution (Figure 1-5). The net free energy of this cycle is the sum of these individual free energies

$$\Delta G = \Delta G_{(+)add} + \Delta G^{F}{}_{hydrolysis} + \Delta G_{P_i-release} + \Delta G_{(-)loss} + \Delta G_{exchange}, \tag{1-5}$$

this is equal to the net free energy of GTP hydrolysis:

$$\Delta G = \Delta G_0 - k_B T \ln([GTP]/[GDP][P_i]), \tag{1-6}$$

where $\Delta G_0 \cong 11 k_B T$ is the standard-state free energy change for tubulin *in vivo* (Howard, 2001). The free energy changes for the individual assembly steps are listed in Table 1-1, where $K_{Pi}$ is the equilibrium dissociation constant of reversible phosphate binding to GDP-tubulin protomers and $K_X$ is the equilibrium constant for the GTP/GDP exchange reaction. Based on literature values (Table 1-2), the free energy from the combined filament-bound hydrolysis and phosphate-release steps account for $\sim 11\ k_B T$ of energy, which is nearly half of the total energy of the tubulin cycle

($\Delta G \approx$ - 22 $k_BT$; (Howard, 2001), and is significantly greater than the free energy of monomer addition at the MT plus-ends (~5.8 $k_BT$). Hence, considerably greater forces can be expected by exploiting the ability of end-trackers like EB1 that bind preferentially to T-GTP protomers, thereby providing a pathway for harnessing the energy released by MT-bound GTP hydrolysis to facilitate protomer addition and resultant force generation.

## 1.5 Summary

Microtubule polymers play an essential role in force generated during cell division, ciliary movement, and many other cell processes. The polarity of MTs is key features that allow them to provide guided transport and to target specific proteins, such as end-tracking proteins, EB1 and APC. EB1 is known to specifically localize to the GTP-rich end of MTs when MTs are polymerizing at the leading edge of growing cells and when MTs are polymerizing at the kinetochore during mitosis. These properties suggest a critical role of EB1 force generation by MTs. Prior force-generation mechanisms involving end-binding proteins and MTs have been proposed including TAC and models involving ATP-driven MT motors kinesis and dynein, which move on MT sides. This thesis explores the hypothesis that end-tracking motor facilitate plus-end attachment and force generation, by harnessing the energy nucleotide triphosphate (NTP) hydrolysis and converting it to mechanical work. The key feature of this model is that the end-tracking proteins binding specifically to the NTP-bound monomers on the filaments, a feature correlates well with the properties of the MTs and their corresponding end-tracking proteins.

## 1.6 Outline of Dissertation

The layout of this dissertation is as follows. Chapter 2 describes a preliminary mechanochemical MT end-tracking model which was first developed to demonstrate how end-tracking proteins on a motile object (e.g., kinetochore) can facilitate MT attachment, elongation

and force generation. This model demonstrates the principles of filament end-tracking and force generation and assumes EB1 is immobilized at the motile object, but it does not account for the interaction of EB1 from solution with MTs. End-tracking models based on interactions of monovalent or divalent solution-phase EB1 with MT protofilaments are modeled in Chapters 3 and 4, respectively. Chapter 3 first treats the simpler case of monovalent EB1 to illustrate how the exponential EB1 density on MT tips results from affinity modulated interactions and how simply allowing EB1 to bind reversible to flexible proteins (e.g., APC) in the kinetochore comprises an end-tracking motors. Chapter 4 then addresses the more realistic (and complex) case of divalent EB1, which makes similar predictions at the monovalent case, but predicts enhanced processivity due to EB1's divalent interactions with the MT lattice. Both Chapters 3 and 4 discuss the growth of a single protofilament allowing EB1 binding, the probabilistic model used to determine optimal kinetic parameters, and stochastic simulations of protofilament growth against a load. Chapter 5 explores an MT model with EB1 end-tracking from a rigid "plug," reflecting ciliary /flagellar growth. Finally, Chapter 6 summarizes the work completed and suggests future directions.

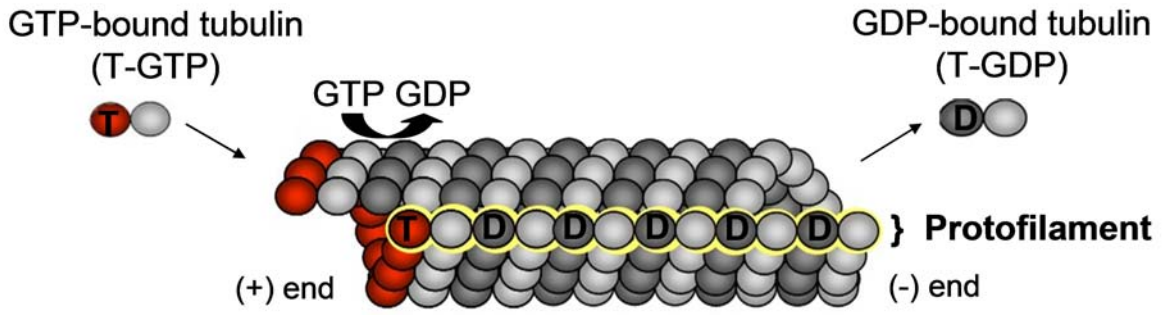


Figure 1-1. Microtubule structure. Tubulin bound to GTP polymerize into 13-protofilament polymers: microtubules. Because tubulin is a heterodimer, the microtubule has a structural polarity with a plus and minus end. During MT polymerization, T-GTP binds to the MT plus-end, which induces hydrolysis of the penultimate tubulin subunit causing filament-bound GTP to be converted to GDP. T-GDP dissociates from the minus end.

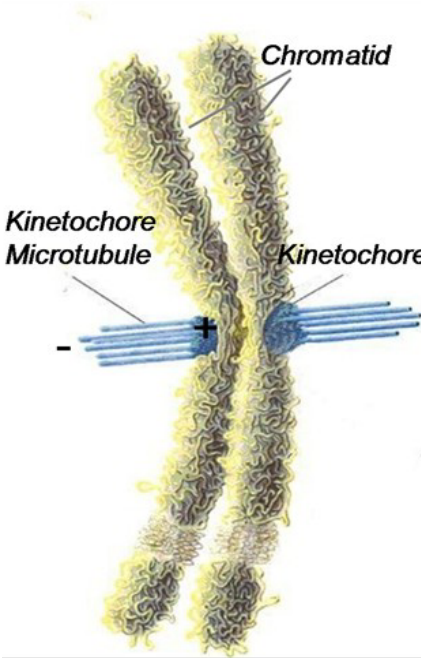


Figure 1-2. Chromosomal binding site of microtubules. Two sister chromatids bind at the centromere to form a chromosome. Kinetochore microtubules bind to the chromosome in the kinetochore at the centromere [Reprinted with permission from Lodish, H. 1995. Molecular Cell Biology (Figure 23-28, p. 1094). New York, New York.]

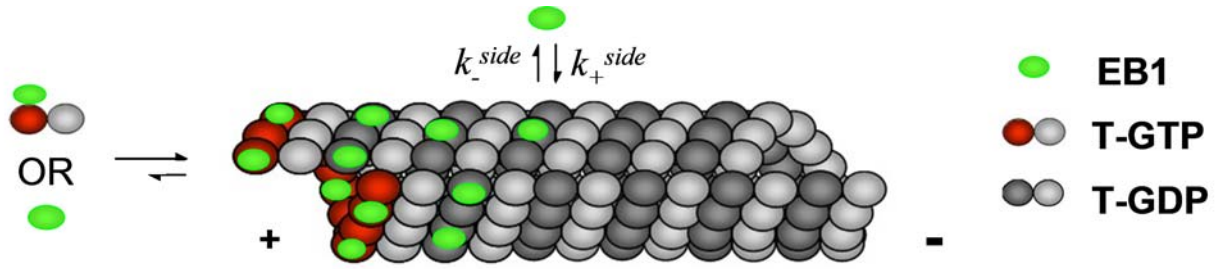


Figure 1-3. EB1 binding to microtubule lattice. EB1 has equal association and dissociation rates on GDP-bound microtubule lattice. EB1 may bind directly to the microtubule plus-end or copolymerize with tubulin in solution first.

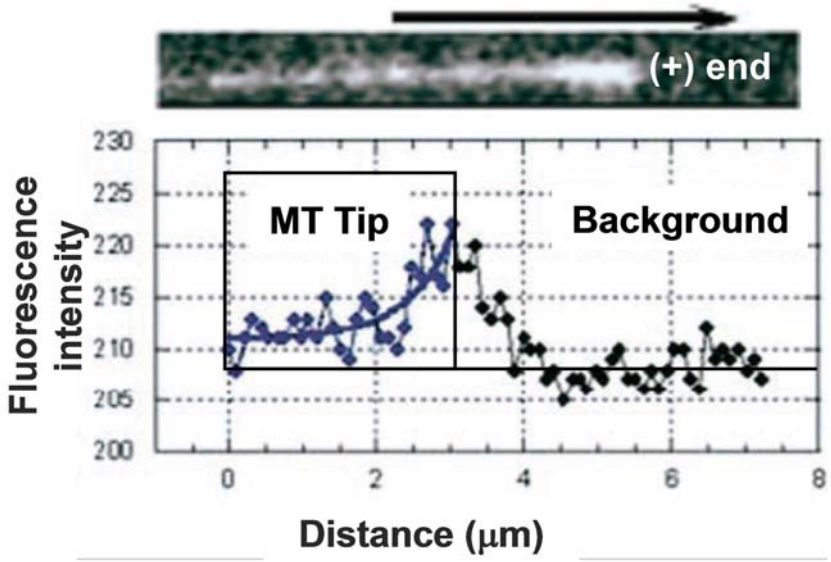


Figure 1-4. Concentration of EB1 along length of microtubule. By measuring the fluorescence intensity of EB1 on the microtubule, there is an experimentally determined decay of EB1 concentration along the protofilament. [Reprinted with permission from Tirnauer, J. 2002. EB1-microtubule interactions in *Xenopus* egg extracts: role of EB1 in microtubule stabilization and mechanisms of targeting to microtubules. Molecular Biology of the Cell. (Pg. 3622, Figure 4).]

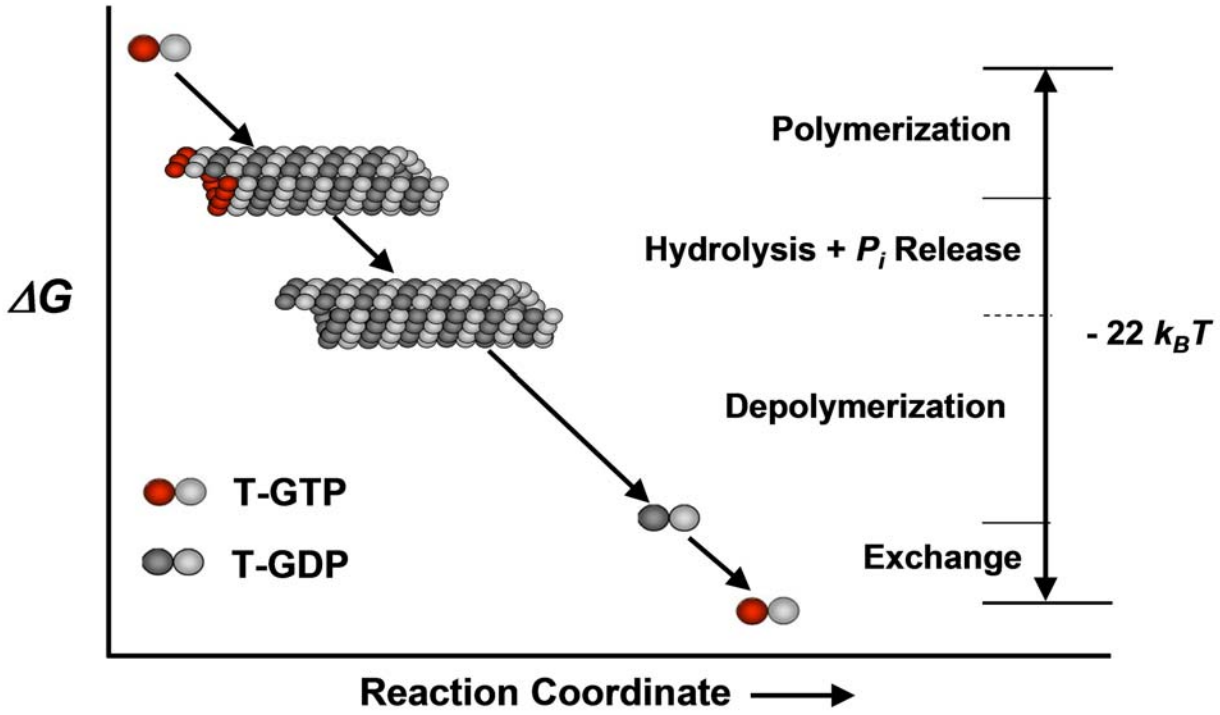


Figure 1-5. Thermodynamics of GDP to GTP tubulin exchange cycle. The free energy change of the tubulin cycle, $\Delta G$, is -22 $k_BT$, which is partitioned among the various steps: polymerization, hydrolysis and phosphate release, depolymerization, and GTP-GDP exchange in solution.

Table 1-1. Thermodynamic equations characterizing the multiple steps for GDP to GTP conversion

| Definition | Equation |
|---|---|
| Addition of T-GTP to MT plus-end | $\Delta G_{(+)add} = -k_B T \ln\left([Tb]/[Tb]_c\right)$ |
| Phosphate (*Pi*) release | $\Delta G_{P_i-release} = k_B T \ln\left([P_i]/K_p\right)$ |
| Loss of T-GDP from MT minus-end | $\Delta G_{(-)loss} = k_B T \ln\left([T-GDP]/[T-GDP]_{(-)c}\right)$ |
| GDP/GTP Exchange | $\Delta G_{exchange} = k_B T \ln([Tb]\cdot[GDP]/[T-GDP]\cdot[GTP]) - k_B T \ln(K_X)$ |
| Hydrolysis of MT-bound GTP in terms of free energy of other steps | $\Delta G^{F}{}_{hydrolysis} = \Delta G_0 + k_B T \ln\left(K_{P_i} K_X \frac{[T-GDP]_{(-)c}}{[Tb]_c}\right)$ |

Table 1-2. Equilibrium constants used in energy equations

| Symbol | Reaction | Value | Reference |
|---|---|---|---|
| $K_x$ | GTP/GDP exchange | 3.00 * | (Zeeberg and Caplow, 1979) |
| $K_p$ | $P_i$ binding to filaments | 25.00 mM | (Carlier et al., 1988) |
| $[Tb]_c$ | T-GTP addition to MT plus-end | 0.03 μM | (Howard, 2001) |
| $[T\text{-}GDP]_{(-)c}$ | T-GDP addition to MT minus-end | 90.00 μM | (Howard, 2001) |

*Calculated from the ratio of measured equilibrium dissociation constants of nucleotide binding to the protomer, i.e., $K_x = K_{GDP}/K_{GTP}$

# CHAPTER 2
# MICROTUBULE END-TRACKING MODEL

This chapter describes a preliminary model that simulates the growth of a 13-protofilament microtubule (MT) in the presence of surface-tethered EB1 end-tracking motors. While this model does not account for EB1 binding from solution, it does illustrate the principle of MT end–tracking and force generation on a motile object. As described in the previous chapter, the key feature of the EB1 end-tracking motor is that it captures filament-bound GTP hydrolysis energy and converts it to mechanical work. In the model presented here, EB1's dimeric structure allows it to maintain persistent attachment of the MT plus-end and the motile surface (i.e., a processive motor) and it is expected to allow for larger stall forces than the Brownian Ratchet Model. EB1 is modeled as a Hookean spring whose binding to the MT depends on its Gaussian-based probability density, which is a function of EB1's equilibrium and binding positions. An external load applied to the motile surface affects the probability of EB1 binding and the velocity and maximum achievable force of the microtubule. The velocity as a function of applied force and the resulting stall forces are simulated and analyzed.

## 2.1 EB1 End-Tracking Motors

The preferred binding of EB1 to MT plus-ends is reminiscent of the interaction between end-tracking proteins and actin in the actoclampin end-tracking motor model and suggests that end-binding proteins may behave as end-tracking motors. To explore this possibility, we model EB1 as a protein tethered to a motile surface on one end and interacting with the MT plus-end through its MT-binding domain on the other end. There are two key features of a MT end-tracking motor: affinity-modulated interaction driven by hydrolysis of GTP on the filament end, and multiple or multivalent interactions with the filament end to maintain its possession to the motile surface. EB1 is assumed to bind preferentially to filament GTP subunits and release

from GDP subunits, thereby capturing some of the available hydrolysis energy, stabilizing GTP-bound terminal subunits, and increasing the net free energy of protomer addition. Because EB1 dimers are multivalent and multiple EB1 molecules can interact with each MT end, the end-tracking motors to maintain a strong interaction with the protofilament even when other end-tracking units release, thereby allowing the motor can advance processively along the polymerizing MT end. This processive action is driven by GTP hydrolysis and is the primary characteristic of other molecular motors, such as kinesin, except in this case hydrolysis occurs on the MT rather than on the MT-binding protein.

## 2.2 Microtubule Growth Model

Our preliminary MT end-tracking model illustrated in Figure 2-1 simulates the growth of a 13-protofilament microtubule bound to surface-tethered EB1 motors and analyzes the force effects on the growth of the microtubule. By capturing part of the filament-bound GTP hydrolysis energy and converting it to mechanical work, the resulting stall force is expected to exceed that of the Brownian Ratchet Mechanism, which is driven solely by free energy of monomer addition. The model assumes that EB1 is tethered to the motile object and does not bind to tubulin protomers from solution, although solution phase EB1 exists in the cytoplasm and likely interacts with tubulin in solution (see Chapter 1). These complications are addressed in the subsequent chapters. The key reactions for the present model are shown in Figure 2-2 and include several possible end-tracking "stepping motor" pathways for two EB1 dimeric subunits (referred to hereafter as EB1 "heads") operating at the plus-end of each MT protofilaments. Considering Stage A, where only one EB1 head is bound to terminal GTP-bound subunit, as the beginning of the cycle, monomers can add directly from solution (Reaction 1), which triggers hydrolysis on the now penultimate subunit, resulting in Stage B. The second EB1 head then binds the new terminal subunit (Reaction 2, resulting in Stage C). The first EB1 head then

releases from the penultimate subunit (Reaction 3) to restore Stage A, with the net effect of the cycle of having added one protomer. We also allow for binding of the second EB1 head in the wrong direction (Reaction 5) or T-GTP addition when both heads are bound (Reaction 4), either of which results resulting in Stage D. Note that of the two EB1 heads remains associated with terminal T-GTP until hydrolysis of its GTP is induced when a new tubulin protomer adds to the protofilament end and/or when the second EB1 head binds the newly added Tb protomer. Hydrolysis weakens the "older" EB1-MT bond, thereby releasing that EB1 head to bind to the next added Tb protomer in the cycle. Because at least one EB1 head should be bound at any time during the end-tracking cycle, the protofilament remains associated with the motile object (i.e., the motor is processive). (Long-term processivity may not be essential when there is a high density of EB1 molecules on the surface near the protofilament; even if both heads are released, other EB1 molecules would quickly capture the protofilament end.)

In the absence of hydrolysis-induced affinity modulation, the principle of detailed balance would fix the relation among the various equilibrium dissociation constants in Reactions 1-3 shown in Figure 2-2, such that $K_1 K_2 = [\mathrm{Tb}]_c K_3$, where $K_1 = k_r / k_f$, $K_2 = k_- / k_+$, and $K_3 = k_-^{side} / k_+$ are the equilibrium dissociation constants for Reactions 1, 2, and 3, respectively. However, affinity modulation is assumed to increase $k_-^{side}$ thereby increasing $K_3$ by a factor $f$, such that $K_1 K_2 = [\mathrm{Tb}]_c K_3 / f$. The value of $f$ reflects the portion of the GTP hydrolysis energy that can be transduced into work in each end-tracking cycle. Because hydrolysis and protomer addition are the two sources of energy used for force generation in this mechanism, the thermodynamic stall force is characterized by

$$F_{stall} = (N \cdot k_B T / d) \ln([Tb] \cdot K_3 K / K_1) = (N \cdot k_B T / d)(\ln([Tb]/[Tb]_c) + \ln(f)). \quad (2\text{-}1)$$

The first term on the right hand represents the contribution of tubulin addition without GTP hydrolysis (same as that of a free MT in the Brownian Ratchet model). The second term corresponds to the benefit of having GTP-hydrolysis-driven affinity modulation. For example, $f = 1000$ corresponds to ~7 $k_BT$ additional energy captured per cycle, putting $F_{stall}$ at ~54 pN, a value that is much higher than the ~7-pN stall force predicted for a Brownian Ratchet driven solely by the free energy of protomer addition (c.f., Eq. 1-4).

While Eq. 2-1 provides a thermodynamic limit, MT growth by the end-tracking cycle may kinetically stall at a lower force, whose value can be determined by stochastic simulation. To simulate the elongation of the 13 protofilaments of an EB1-bound microtubule, we made several simplifying assumptions about the binding properties of EB1 to the protofilament lattice. We assume that only one EB1 dimer operates processively on each of the 13 protofilaments at any one time. Any lateral effects among adjacent protofilaments on their elongation are neglected. Because the EB1 dimer has flexible segments between its coiled-coil region and its two MT-binding heads (Honnappa et al., 2005), we modeled each EB1 head as a Hookean springs with spring constant $\gamma$. The contribution of the spring energy, $E_s$ given by

$$E_s = \frac{\gamma \cdot (z - z_e)^2}{2} \tag{2-2}$$

where $z$ and $z_e$ are the instantaneous and equilibrium positions, respectively, of EB1's MT binding domain. All EB1 molecules bound to the motile object are assumed to have the same equilibrium position, hence $z_e$ determines the position of the translating motile object relative to the MT (assumed fixed in space). Assuming EB1 is present at the motile object with a mean lateral spacing, $\rho$, the effective local concentration of EB1 at the motile object is

thus $C_{eff}(z) = \rho^{-2} p(z)$, where *p(z)* is the Boltzmann's distribution of the EB1 binding position, i.e.,

$$p(z) = \frac{e^{-\gamma(z-z_e)^2/2k_BT}}{\sqrt{2\pi k_B T/\gamma}} \tag{2-3}$$

where $k_B$ is Boltzmann's constant, and $T$ is the absolute temperature. The position-dependent binding rate constant $k_+(z)$ ($s^{-1}$) of the EB1 head to the MT lattice at distance $z$ is taken as $k_+(z) = k_{on} C_{eff}(z)$ or:

$$k_+(z) = k_{on} \rho^{-2} \frac{e^{-\gamma(z-z_e)^2/2k_BT}}{\sqrt{2\pi k_B T/\gamma}} \tag{2-4}$$

where $\rho$ is the EB1 spacing distance, $k_1$ is the forward association rate constant ($\mu M^{-1}s^{-1}$ or $nm^3/s$) for EB1 binding to a T-GDP subunit from solution. Because binding sites are at discrete positions spaced by distance $d = 8$ nm, then $z = nd$ in Eq. 2-4.

While it is possible that a stressed bond may have an increased or decreased dissociation rate (i.e., "slip" bond or "catch" bond, respectively) under several piconewtons of force (Bell, 1978; Dembo, 1994); (Dembo et al., 1988), we assume the simplest case where the EB1 bonds are neither catch nor slip under the forces involved here, and force is not assumed to not affect the dissociation rate constants of EB1 releasing from MT sides.

The characteristic time for forces to relax between transitions is ~ $\delta/13\gamma$, where $\delta$ is the viscous drag coefficient $\delta$ (drag force/velocity) of the motile object propelled by the MT. For a ~100-nm motile object, this time would be ~10-100 μs, much faster than the cycle time for protomer addition. Therefore, we assume the instantaneous position of the motile object remains in mechanical quasi-equilibrium with the external load, $F$, such that its position $z_e$ is determined by the balance of spring forces due to the bound EB1 heads. The equation for the external load is

given by Equation 2-5; the position of bound EB1 heads in each stage can be determined from Figure 2-3.

$$F = \sum_{\text{state A}} \gamma(n_i d - z_e) + \sum_{\text{state B}} \gamma((n_i - 1)d - z_e) + \sum_{\text{state C}} \gamma((2n_i - 1)d - z_e) + \sum_{\text{state D}} \gamma((2n_i - 3)d - z_e) \quad (2\text{-}5)$$

Solving Equation 2-5 for $z_e$ thus allows *p(z)* and the resulting transition probabilities for transition between states ($k \cdot \Delta t$) and a time step of $\Delta t$ to be calculated for each EB1 head at each time point in the simulation. In the simulation results shown in Figures 2-4, 2-5, 2-6, and 2-7, $\Delta t$ was taken to 2 μs. This time increment was chosen to be ten percent of the inverse of the largest kinetic constant to ensure that the kinetics of all reactions was accounted for.

### 2.2.1 Parameter Estimations

The key parameters in this model include [Tb], $[Tb]_c$, $\gamma$, $\rho$, and the kinetic rate constants shown in Figure 2-2. The intracellular tubulin concentration [Tb] was assumed to be 10 μM (Mitchison and Kirschner, 1987). We use the value of the plus-end critical concentration $[Tb]_c$ = 5 μM estimated by Walker et al. (1988) from the ratio of on- and off-rate constants for elongation (8.9 $\mu M^{-1}s^{-1}$ and 44 $s^{-1}$, respectively). The macroscopic on-rate constant (8.9 $\mu M^{-1}s^{-1}$) from MT elongation rate measurements reflects the collective assembly of the 13 protofilaments on the MT tip; however, the growth rule for individual protofilaments is uncertain. We therefore made the simplest assumption that each protofilaments operates independently and elongates reversibly with on-rate constant $k_f$= 8.9/13 $\mu M^{-1}s^{-1}$ or 0.68 $\mu M^{-1}s^{-1}$ and $k_r$ = 44/13 $s^{-1}$ or 3.4 $s^{-1}$. The MT reversible elongation speed used in the model was assumed to that determined by Piehl and Cassemeris (167 nm/s) and not the velocity calculated by the on and off-rates from Walker et al. The spring constant $\gamma$ of an EB1 head was estimated as $\gamma = k_B T/\sigma^2$ where $\sigma \sim$ 10 nm is the estimated standard deviation in the z-position of an EB1 head based on EM micrographs

(Honnappa et al., 2005). The spacing $\rho = 7.5$ nm was chosen assuming EB1 dimers are closely packed on the motile object. The association rate constant for an EB1 dimer on a MT-bound T-GDP subunit, $k_{on} = 25\ \mu M^{-1}s^{-1} = 5\times10^{7}\ nm^3/s$, was assumed by taking a typical association rate constant for protein binding in solution (Eigen and Hammes, 1963). The off-rate constant $k_{off} = 0.24\ s^{-1}$ for an EB1 dimer from MT GDP-subunits was calculated from the measured velocity and the exponential decay-length of EB1 dissociating from the wall of a polymerizing MT (Tirnauer et al., 2002a). However, this value reflects the probability of both EB1 heads being released simultaneously, which is assumed to be proportional to the off-rate of one EB1 head, $k_{-}^{side}$, multiplied by the probability of the other head being dissociated, which is $K_3/(1+K_3)$, such that $k_{off} = k_{-}^{side}\,[K_3/(1+K_3)]$, where $K_3 \equiv k_{-}^{side}/k_{+}$ and $k_+$ is calculated at $z - z_e = d/2$ from Equation 2-4. The primary simulation parameter was the total simulation time, $t$, which was set at 4 seconds. For $f$=1 to $f$=10,000, data points for $F \geq 20\,pN$ were obtained using a simulation time of 24 seconds to allow sufficient time for the microtubule to equilibrate.

### 2.2.2 Elongation Rate in the Absence of External Force

A typical simulated trajectory for a surface-tethered, polymerizing microtubule in the absence of external load is given in Figure 2-4. Assuming an affinity modulation of 1000, and choosing optimal values for $k_{on}$ and $\rho$ (Appendix B.1 contains the MATLAB© code), the resulting MT position increases linearly with time. The tubulin on-rate was chosen to yield the experimentally determined velocity of 167 nm/s for microtubules during mitosis (Piehl and Cassimeris, 2003). Figure 2-5 is a representation of the protofilament lengths and average equilibrium surface position corresponding to ($t = 4s$, $v$=165 nm/s). As seen in Figure 2-5, the maximum difference between the shortest and longest filaments is four subunits. This small difference reflects how the end-tracking model can also ensure high fidelity: the protofilaments

do not advance too far past one another during polymerization. This diagram shows that the end-tracking motors also maintain the average equilibrium position near the filament ends. The equilibrium surface position, $z$, is not located at the average filament end position since it is dependent on the individual springs' binding location.

### 2.2.3 Force effects on elongation rate

To analyze the effect of applied force on the polymerization rate of EB1 tethered microtubules, $F$, was varied over a range of -4 pN to 34 pN. Figure 2-6 shows that the speed of MT polymerization decreased with increasing external load for all values of f calculated. When the end-tracking protein was not affinity-modulated ($f = 1$), the velocity decreased linearly with increasing external force. As $f$ was increased, the end-tracking motor was able to capture some of the filament hydrolysis energy to elongate more rapidly under significant forces, with the velocity depending approximately exponentially on the compressive force. Negative (tensile) forces applied to the surface increased the polymerization rate of growing MTs slightly until the maximum rate was reached. Moreover, tensile forces increased the probability of EB1 binding to the GTP-bound filament, and promoted the forward MT assembly process. Although large tensile forces should dissociate the filament end-tracking motors from the MT and thereby detach the MT from motile object, the possible of complete dissociation of the EB1 molecule was allowed in our simulations.

As the modulation factor $f$ increased from 1 to 10, the dependence of velocity on the force resulted in a faster elongation (Fig. 2-5) and a greater maximum achievable force. Once the modulation factor became greater than 10, there was no significant effect of $f$ on the polymerization rate, and the microtubule achieved similar stall forces. These observations can be explained by the force-limitations on the reaction kinetics. By increasing $f$, the forward

reaction in step 2 is favored, increasing the rate of polymerization. Once $f$ becomes greater than 10, the forward reaction in both steps 2 and 5 become essentially irreversible (Equation 1-1). Further increasing the modulation factor has minimal effect on the rate of reaction, MT polymerization, and stall force.

The kinetic stall force for each simulation was taken as the force at which the speed of the MT is less than 0.1% of the velocity when there is no force ($F$=0). The thermodynamic stall forces predicted for the microtubules at various values of $f$ were calculated from Equation 2-5, and are compared to these simulated stall forces in Figure 2-7. The simulated and calculated results are comparable when the EB1 motor has little affinity modulation (from $f$=1 to $f$=10); for $f$=1, the thermodynamic and simulated stall force is approximately 7 pN. However, as $f$ increases, the simulated stall force deviates from the expected thermodynamic limit. This phenomenon can be explained by the kinetic and thermodynamic properties. When the end-tracking motors are not affinity modulated (at $f$=1) the critical tubulin concentration for MT assembly remains relatively large, and the velocity is thermodynamically limited; once the thermodynamic stall force is achieved, the MT will experience negative velocities, or net depolymerization. At larger modulation factors ($f$ > 1), the effective critical concentration is reduced and the MT dynamics are kinetically, rather than thermodynamically, limited, and the velocity can be approximated by a force-dependent exponential equation (Figure 2-5). That is, for large values of $f$, MTs are predicted to kinetically stall at much lower forces than the thermodynamic stall force.

## 2.3 Summary

This preliminary model simulates the growth of a 13-protofilament MT bound to surface-tethered EB1 motors and serves to demonstrate the principles of force generation by processive MT end-tracking motors. The key features of these end-tracking motors are (1) their

ability to capture filament-bound GTP hydrolysis and convert them to mechanical work (2) their dimeric structure which allow them to maintain persistent attachment of the MT plus-end to the motile surface. EB1 was modeled as a Hookean spring whose association rate with the MT is governed by the probability density function of the spring and varies depending on an external applied force. The dissociation rate of EB1 from the MT was determined by its affinity to T-GTP versus T-GDP subunits, or affinity modulation factor, *f*. The resulting velocity as a function of applied force was determined at varying values of *f*. The model demonstrates EB1's ability to maintain fidelity of the MT, with a maximum difference in protofilament length of four subunits. In addition, an increasing affinity modulation of EB1 results in an increase in stall force, with a maximum stall force that is significantly greater than that predicted by the Brownian Ratchet mechanism.

The primary limitation of this model is that EB1 does not bind to tubulin in solution, nor does it account for solution-phase EB1. The proposed co-factor assisted end-tracking model not only addresses the importance of a co-factor such as APC, which could be critical in the monomer addition step, but also the issue of solution phase EB1 and tubulin binding. This solution binding may be essential, and is addressed further in Chapters 3 and 4.

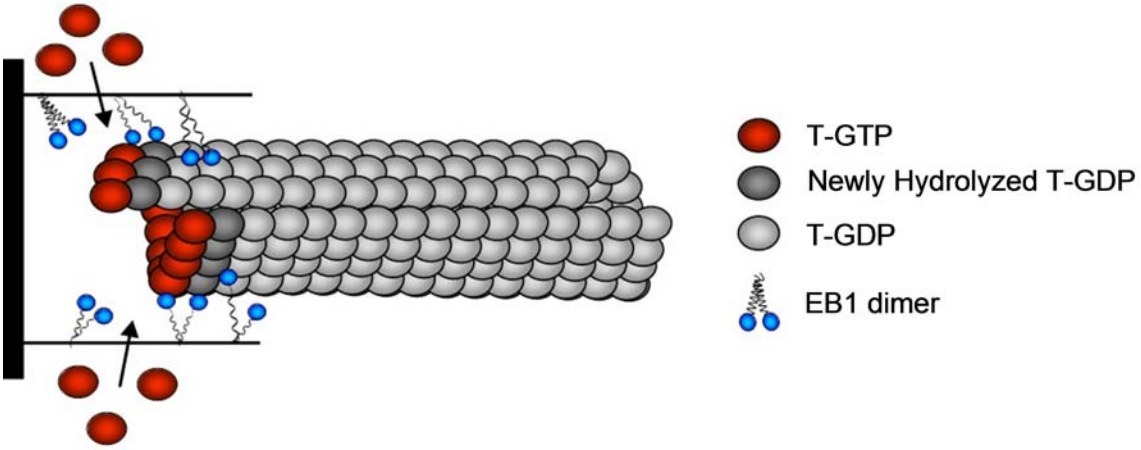


Figure 2-1. Model for microtubule force generation by EB1 end-tracking motor. Model that represents the distal attachment of tubulin protomers at the MT plus-end. A uniform density of EB1 dimers on the motile object links the MT protofilaments to the surface.

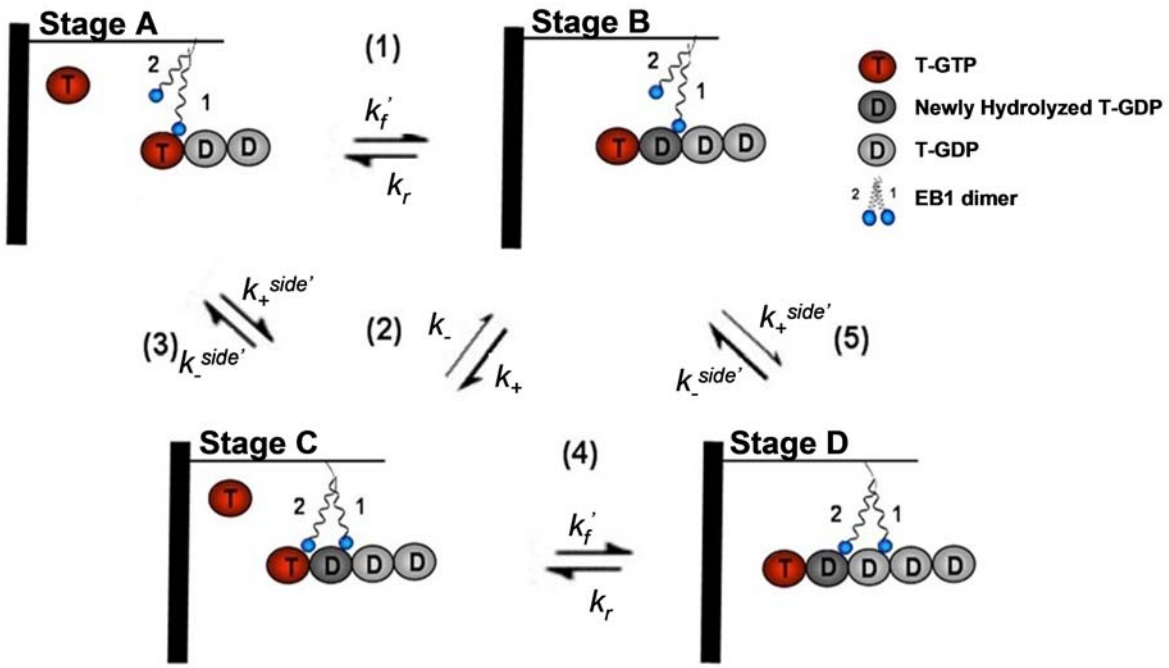


Figure 2-2. Reaction mechanisms of EB1 end-tracking motor. Mechanism of the EB1 end-tracking motor on the plus-end of one of the MT protofilaments (from upper left): One EB1 head is initially bound to the terminal GTP-tubulin subunit. Step 1: A tubulin protomer binds to the filament end from solution. Step 2: The second EB1 head binds to the newly added terminal subunit. The complex can now follow two different pathways, 3 or 4. Step 3: Binding of second EB1 head to MT end induced hydrolysis of penultimate subunit and attenuates affinity of EB1 bound to the penultimate subunit; this EB1 head is released from the MT and the protofilament is returned to its original state. Step 4: A tubulin protomer adds to the filament end from solution, inducing hydrolysis of the penultimate subunit. Step 5: Affinity of distal EB1 to hydrolyzed subunit is attenuated and is released from the MT.

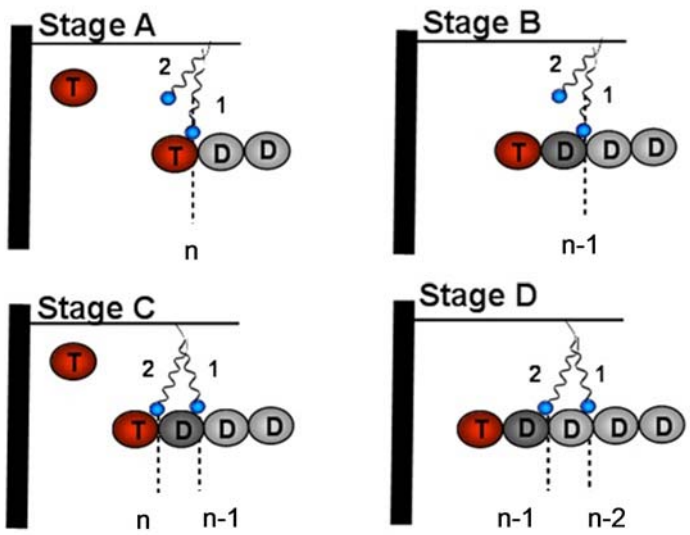


Figure 2-3. Force dependence on EB1 binding and equilibrium surface position. Binding position of EB1 dimers in each stage, where n represents the position of the bound tubulin subunit along the protofilament.

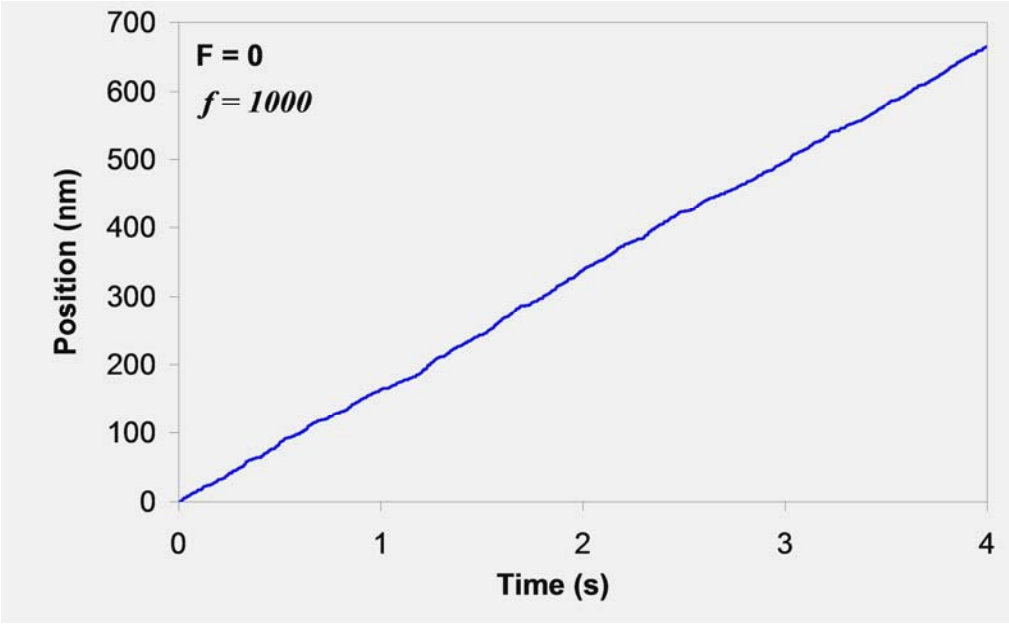


Figure 2-4. Microtubule elongation in the absence of external force. (A) The position of a 13-protofilament MT tethered to a surface by EB1 end-tracking motors is plotted as a function of time. No external forces are applied to the surface, the modulation factor is set to 1000, and optimal values of $k_{on}$, $\sigma$, and $L$ are used (See Appendix B.1). The average velocity of 172 nm/s is near the set value of 167 nm/s.

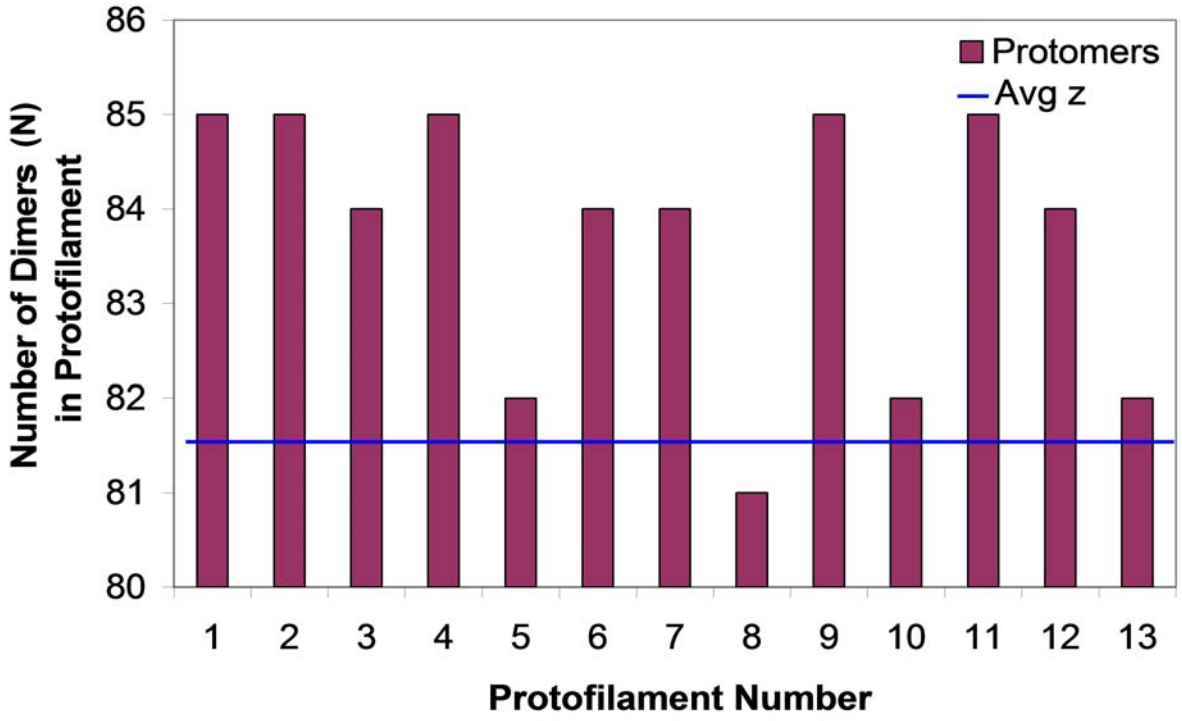


Figure 2-5. Distribution of protofilament lengths for microtubule end-tracking model. Filament lengths for microtubule described in Figure 1 ($t = 4s$ , $v = 660nm/s$). The maximum difference between the shortest and longest filaments is four subunits. The solid blue line represents the average equilibrium position of the microtubule.

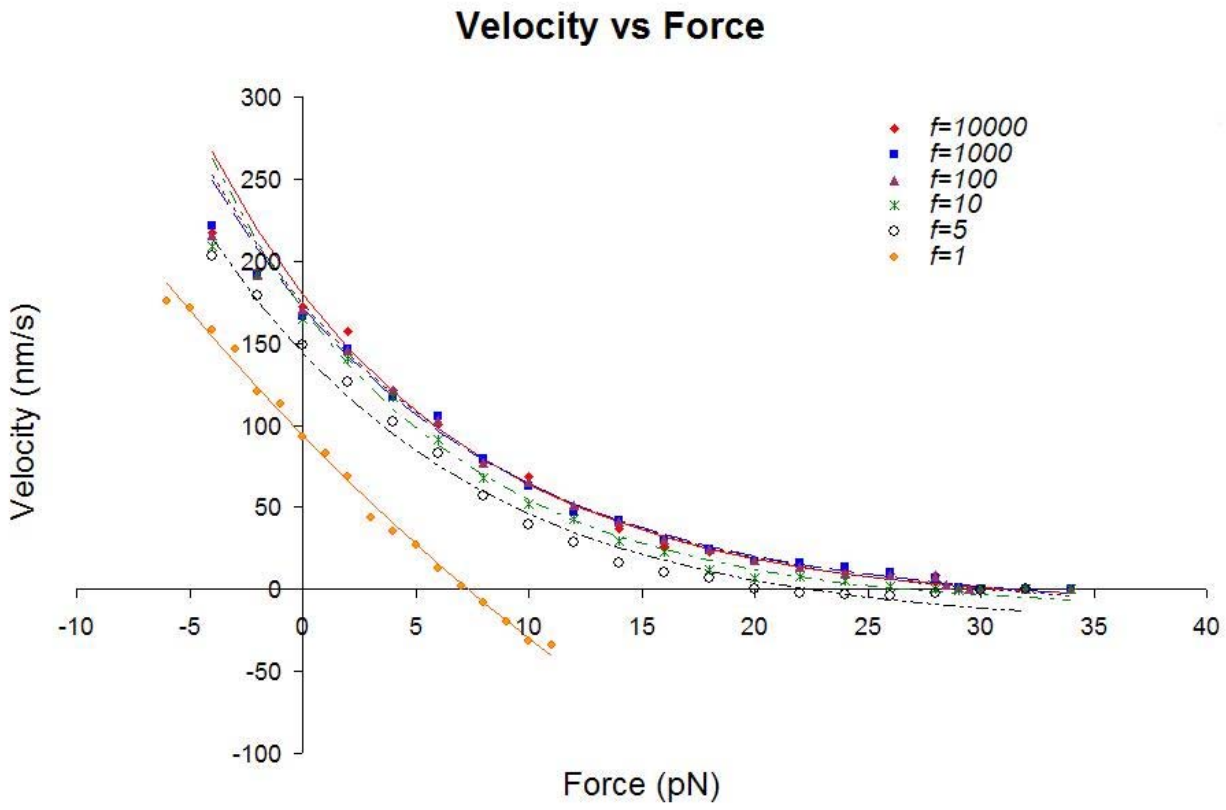


Figure 2-6. Effect of applied force on MT elongation rate. The dependence of velocity on force is presented for models with various modulation factors: 1, 5, 10, 100, 1,000, and 10,000. For $f$=1, the velocity decreases linearly with force, shown by the fitted line. For $f$=5 to $f$=10,000, the velocity decreases exponentially with increasing force. The data is fitted to a three-parameter exponential equation represented by the solid line. The stall force for each simulation is estimated as the force at which the velocity is less than 0.1% of the velocity when $F$=0. The simulation time was set at 4s. For $f$=5 to $f$=10,000, data points for $F \geq 20\,pN$ were obtained using a simulation time of 24 seconds to allow sufficient time for the microtubule to equilibrate.

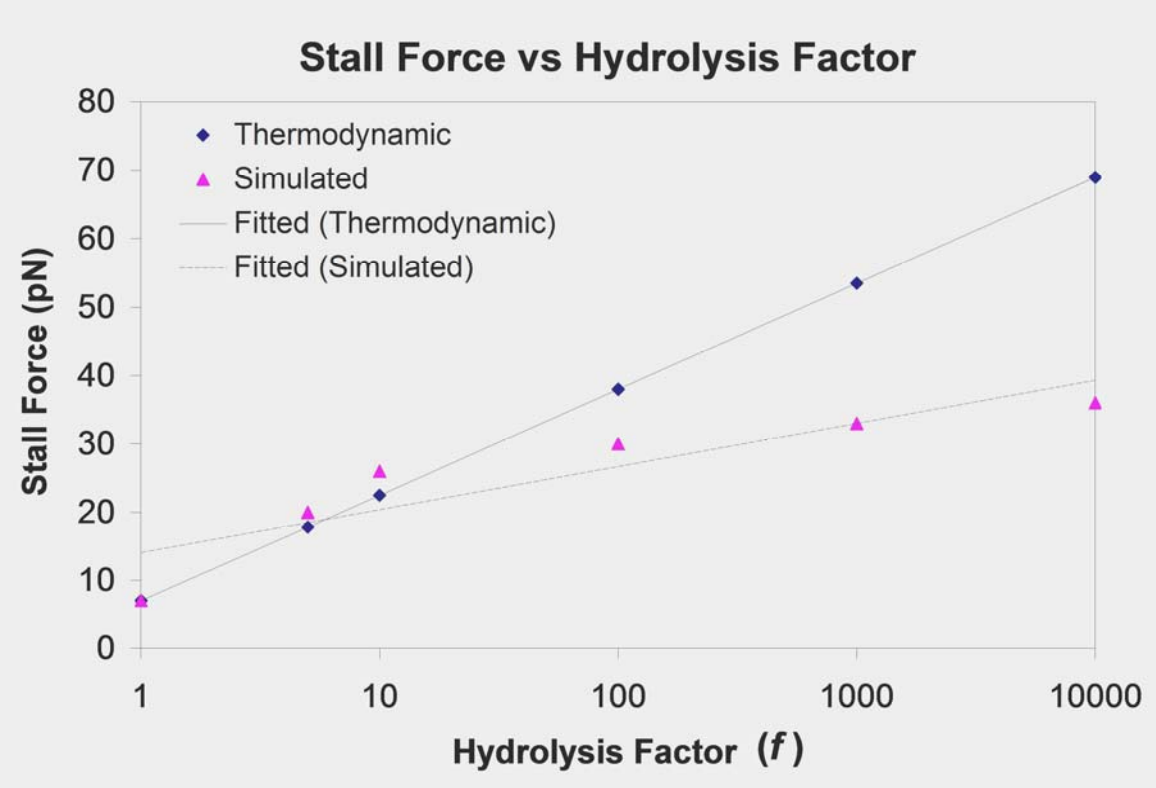


Figure 2-7. Thermodynamic versus simulated stall forces. The thermodynamic stall force was calculated for the various MT end-tracking motor represented in Figure 4 by using equation 2-5. Comparison of the calculated and simulated stall forces is shown. When the hydrolysis affects the microtubule dynamics very little ($f$=1 to $f$=5) the model provides a good prediction for the EB1 end-tracking model. At higher $f$ values, the data deviates from thermodynamic predictions. The simulated stall force only slightly increases once $f$ becomes greater than 100. The solid lines represent logarithmic fit to each of the data presented.

# CHAPTER 3
# PROTOFILAMENT END-TRACKING MODEL WITH MONOVALENT EB1

The microtubule end-tracking model developed in Chapter 2 neglected solution-phase End Binding protein 1 (EB1) and binding to microtubules and tubulin protomers. While not essential for end-tracking, binding of EB1 from solution is evident in the exponential profiles of bound EB1 at elongating free plus-ends and the apparent equilibrium density of EB1 along the length of the microtubule (MT) (Chapter 1 and Figure 1-3). To account for binding solution-phase EB1, we first developed a simplified model that simulates the growth of a single protofilament in the presence of a monovalent EB1 protein... A model for more complex and realistic case of dimeric EB1 binding is presented in the next chapter.

In the previous chapter, it was assumed that the EB1 protein behaves as an end-tracking motor, with preferential binding to T-GTP over T-GDP, and an affinity modulation factor greater than 1. In this chapter, the assertion that EB1 has a higher affinity for GTP subunits is supported by showing that the observed 4.2 tip-to-side ratio of EB1 density requires GTP-hydrolysis-driven affinity modulated binding. We do so by first modeling free filament growth with EB1 binding, but without attachment of EB1 a motile object, and comparing the predicted EB1 density along the length of the MT to the experimental results. We then allow EB1 to interact with a linker protein at the motile object (e.g., Adenomatous Polyposis Coli, APC) and predict the resulting MT dynamics and force generation. The force-velocity relationship of this the end-tracking model is then compared to those of the simple Brownian Ratchet mechanism.

## 3.1 Non-Tethered Protofilament Growth

We first consider growth of a single microtubule protofilament in the presence of a solution-phase monovalent EB1 and then show in Section 3.2 how linking the growing tip to a

surface containing a flexible binding protein for EB1 forms an end-tracking motor similar to that described in Chapter 2.

The various reactions considered in the free MT model are shown in Figure 3-1. Tubulin protomers (Tb) can add directly to filament ends (equilibrium dissociation constant $[\mathrm{Tb}]_c$), or they can first bind to EB1 (E) in solution ($K_1$) then add as an EB1-tubulin complex ($[\mathrm{Tb}]_c^E$) . In either pathway, tubulin addition is assumed to be followed by prompt GTP hydrolysis on the penultimate subunit. Because EB1 is assumed to have a lower affinity for GDP subunits (equilibrium dissociation constant $K_d > K_d^*$), the energy provided by GTP hydrolysis later releases the EB1 from non-terminal subunits.

### 3.1.1 Thermodynamics of EB1-tubulin interactions

As described in Chapter 1, free energy of the direct binding pathway is given simply by

$$\Delta G_{(+)add} = -k_B T \ln \frac{[\mathrm{Tb}]}{[\mathrm{Tb}]_c} \tag{3-1}$$

but the free energy of the net reaction involving binding and release of EB1 is

$$\Delta G_{(+)add} = -k_B T \ln \frac{[\mathrm{Tb}]}{[\mathrm{Tb}]_c} - k_B T \ln \frac{[E]}{K_d^*} + k_B T \ln \frac{[E]}{K_d} \tag{3-2}$$

hence more negative than that of monomer addition. In this way, EB1 binding temporarily stabilizes the protofilament plus-end and facilitates the net reaction of monomer addition. The principle of detailed balance requires that Eq. 3-2 holds whether E binds first to Tb in solution or E binds to the terminal subunit following monomer addition. Eq. (3-2) can be re-written

$$\Delta G_{(+)add} = -k_B T \ln \frac{[\mathrm{Tb}]}{[\mathrm{Tb}]_c} - k_B T \ln f \tag{3-3}$$

where $f = K_d/K_d^*$ is the affinity modulation factor. Like in the previous chapter, at $f = 1$ would represent the case in which EB1 binds to both GTP- as well as GDP-tubulin with equal affinity.

A value greater than one means signifies that the affinity of EB1 to GTP is greater than its affinity to GDP.

To determine the solution phase concentration of E and TE, we assume [E] is determined by equilibrium binding with Tb and to sides of the MTs within the cell (at subunit concentration [MT]). As derived in the Appendix (A.1), this assumption yields

$$[E] = \frac{[E]_0}{1 + \frac{[Tb]}{K_1} + \frac{[MT]}{K_d}} \tag{3-4}$$

and

$$[TE] = \frac{[E]_0 [Tb] / K_1}{1 + \frac{[Tb]}{K_1} + \frac{[MT]}{K_d}} \tag{3-5}$$

### 3.1.2 Kinetics of EB1-tubulin interactions

We have assumed that the affinity modulation factor must be greater than 1 for EB1 to track on the plus-ends of protofilaments (i.e., EB1 must have a higher affinity for GTP rather than GDP). To test this assertion, we developed a probabilistic model accounting various EB1 binding pathways shown in Figure 3-2: EB1 binds directly to the GTP-rich protofilament plus-end, EB1 associates with T-GDP on the side of the protofilament, or EB1 copolymerize with tubulin in solution. This model was used to predict the probability of EB1 binding to the protofilament plus-end, $p_{end}$, and the equilibrium probability of EB1 binding protofilament sides, $p_{eq}$. The value of $p_{eq}$ was obtained by the steady-state of a differential equation describing the probability of EB1 binding to an MT side (far from the plus end) as a function of concentrations and reactions rates, which is given by

$$\frac{dp}{dt} = -k_f [Tb] p - k_r^{\,E} p - k_-^{\,side} p + \left(k_f^{\,E} [TE] + k_{on} [E]\right)(1 - p) \tag{3-6}$$

The equations specific for solving the probability of EB1 binding to the plus-end and side of the protofilament are given by

$$\frac{dp_i}{dt} = k_{+,i}[E]_i c_i - k_{-,i} p_i + \left(k_f[Tb] + k_f^{E}[TE]\right)(p_{i-1} - p_i) + \left(k_r^{E} p_1 + k_r c_1\right)(p_{i+1} - p_i) \quad (3\text{-}7)$$

$$\frac{dp_1}{dt} = k_{+,1}[E]_1 c_1 - k_{-,1} p_1 - p_1[Tb] + k_f^{E}[TE]c_1 + [T]_c k_f c_1 p_2 - \frac{[Tb]_c K_d k_f^{E} p_1 c_2}{K_1 \cdot f}, \quad (3\text{-}8)$$

respectively, where $c_i \equiv 1\text{-}p_i$ (see full derivation in Appendix A.2). Here, the index $i$ represents the subunit on the protofilament numbered from the plus-end. These two differential equations were numerically integrated (fourth-order Runge-Kutta method; Appendix B.3 contains the Matlab code) under set parameters in order to calculate the occupational probability ($p_i$) of EB1 along the length of a free protofilament (equivalent to the EB1 binding density).

### 3.1.3 Parameter Estimations

The key parameters in this model, which include [Tb], $[Tb]_c$, [MT], $[E]_0$, $f$, and the kinetic rate constants, were obtained from literature or calculated based on known values. The intracellular tubulin and microtubule concentration, [Tb] and [MT], was assumed to be 10 μM (Mitchison and Kirschner, 1987), the value of the plus-end critical concentration $[Tb]_c = 5$ μM was estimated by Walker et al. (Walker et al., 1988), and the total intracellular concentration of EB1 was estimated as 0.27 μM (Tirnauer et al., 2002b). Unless otherwise indicated, the value $f=10^3$ was chosen for the affinity modulation factor, which reflects 7 $k_BT$ of the available GTP hydrolysis energy captured for affinity modulation. (As shown below, many predicted properties because asymptotically independent of $f >> 1$). The rate constants, $k_f$ and $k_r$ were assumed to be the same for free MT elongation as from Eq. 1-1 and Eq. 1-2, respectively, assuming a maximum velocity $v$=170 nm/s (Piehl and Cassimeris, 2003). The dissociation constant for EB1 to the GDP-bound side ($K_d$) of protofilaments was taken as 0.5 μM, based on an *in vitro* study on EB1-

MT binding interactions (Tirnauer et al., 2002b). The rate equations for the on rates of EB1 to the MT plus-end and sides are assumed to be equal and are based on the observed decay rate constant of EB1 form MT sides determined in a study by Tirnauer et al (Tirnauer et al., 2002b). The off-rates for EB1 on both the sides and plus-end of the protofilament are a fraction, *f*, less than their on-rates. This on-rate constant of TE binding to plus ends is assumed equivalent to that for Tb, (i.e., $k_f^E = k_f$).

Experimental data has not validated a dissociation constant for the binding of EB1 and tubulin in solution, $K_1$, so its optimal value was determined from $p_{eq}$ (at steady-state, Eq. 3-9) and $p_{end}$ (from Eq. 3-8).

$$p_{eq} = \frac{1}{1 + \frac{K_d}{[E]}} \tag{3-9}$$

Assuming a value for *f*, $p_{end}$ was calculated for various values of $K_1$. The ratio of $p_{end}$ to $p_{eq}$ was determined at each chosen $K_1$ value to determine which $K_1$ resulted a $p_{end} : p_{eq}$ ratio of 4.2 at steady-state. This procedure was repeated for various values of *f*, and the resulting $K_1$ values are shown in Figure 3-3. When *f* is equal to one or two, the EB1 binding ratio remains below the expected 4.2 value at all values of $K_1$. This result suggests that EB1 must have a greater affinity for T-GTP than T-GDP (i.e., *f* must be greater than two) in order for EB1 to accumulate at the plus-ends of protofilaments as seen experimentally. The optimal value of $K_1$ (for *f* greater than two) increases with increasing values of *f*. At larger values of *f* (*f*=5 and *f*=10), the optimal value for $K_1$ is approximately 0.21 μM. Increasing *f* past 10 does not provide any additional effect on $K_1$. By increasing *f*, the binding reaction of EB1 (to either the plus-end or the side of the protofilament) is favored. Once *f* becomes greater than ~10, these forward reactions essentially become irreversible and the probability of EB1 binding to the protofilament end is no longer

dependent on $K_1$. Thus, further increasing $f$ has minimal effect on the net rate of tubulin addition. Assuming an affinity modulation factor of 1000, the optimal value for $K_1$ (0.21 μM) was determined from the results obtain in Figure 3-3.

### 3.1.4 Results

Figure 3-4 shows the steady-state EB1 binding density profiles for $f=1$ and $f=1000$. When $f$=1 the steady state occupational probability is uniform along the length of the protofilament. The slightly higher EB1 density at the plus-end reflects some benefit of copolymerization with tubulin. However, EB1 is predicted to have a much larger density at the plus-end when $f$ is large. The EB1 density decreases exponentially along the length of the protofilament, consistent with experimental observations (Figure 1-4). This finding supports our assertation EB1 must have a significantly higher affinity for GTP-bound tubulin in order to track on the GTP-rich protofilament plus-ends.

The effect of $K_1$ on the EB1, monovalent occupational probability profile is demonstrated in Figure 3-5. The model was simulated at $K_1$ values from 0.01 μM to 1 μM at $f$=1000. When $K_1$ is small (e.g., 0.01 μM), EB1 preferentially binds to tubulin protomers in solution, therefore EB1 has a high occupational probability at the plus-end of a protofilament, which decreases along the length of the protofilament. This decay profile flattens out as $K_1$ increases; at $K_1$ =1 μM the profile is similar to the profile of $f$=1 in Figure 3-4. This behavior is expected because at larger values of $K_1$, EB1 has a large off-rate from tubulin protomers in solution; therefore it can bind along the entire length of the protofilament.

## 3.2 Tethered Protofilament Growth

Similar to the above model of untethered protofilament, this model simulates the growth of microtubules that bind to monovalent EB1 motors, but also introduces a linking protein (e.g.,

APC) that tethers the protofilament via EB1 to a motile surface. Here, we assume reversible binding of the linking protein on the motile object to EB1 from solution or on the MT lattice. Otherwise, the assumptions and parameter values from the previous model were applied in this model.

This model has the similar pathways as seen in the non-tethered model (Figure 3-6). In Mechanism A, EB1 binds directly to the protofilament; in Mechanism B, EB1 copolymerizes with tubulin, and Mechanism C (not shown) is a combination of A and B, but it also allows EB1 to dissociate from the tethering protein. The terminal subunit of a protofilament is assumed not to dissociate when bound to an EB1 molecule.

Consider the initial configuration of each cycle as the state with the EB1 motor bound at the protofilament plus-end. When tubulin adds to the protofilament, hydrolysis of the penultimate subunit that is bound to the motor is induced, and the motor's reduced affinity for the protofilament causes EB1 to dissociate from either the protofilament (A and B) or the tethering protein (C). In mechanism A, the motor can directly rebind to the protofilament plus-end; whereas the motor in B has to copolymerize with tubulin in solution first, and the motor in C has to wait until EB1-binds to the protofilament before either of the two motors can attach to the protofilament plus end. In each of the mechanisms, once the motor rebinds, the surface advances. These motors can continue to act processively on the end of the microtubule to generate force and propel the surface forward.

### 3.2.2 Model

To simulate this monovalent EB1 molecular motor, a probabilistic model similar to the non-tethered monovalent end-tracking model was derived to simulate the EB1 fluorescence along a protofilament based on the probability of EB1 and the tethering protein (Tk) making transitions between different binding states. The relevant probabilities considered were:

- $p_i$ = probability of EB1 bound to the protofilament
- $q_i$ = probability of Tk-E bound to the protofilament
- $w$ = probability of Tk bound to TE in solution
- $v$ = probability of Tk bound to E in solution
- $y$ = probability of Tk being unbound

The probability of Tk being unbound, y, is represented by:

$$y = 1 - w - v - \sum q_i \tag{3-10}$$

Similar to the derivation of Equations 3-7 and 3-8, the transition probabilities between states can be obtained from reaction rate constants for each pathway (Figure 3-6). The resulting differential equations for the probabilities of EB1 and Tk-E binding to the protofilament (in terms of the kinetic rates) are given by Equations 3-11 and 3-12, respectively, where $u_i$=1- $q_i$- $p_i$, $k_T$ is on-rate of the linking protein binding to solution-phase EB1, and $C_{eff}$ is the effective local concentration of the linking protein near the protofilament.

$$\begin{aligned}\frac{dp_i}{dt} &= k_{on}[E]u_i - k_{-}p_i - k_{T,i}C_{eff,i}yp_i + k_{T,i}^{-}q_i \\ &+ (k_f[Tb] + k_f^{E}[TE] + k_f^{E}C_{eff,i}w)(p_{i-1} - p_i) + (k_r^{E}p_1 + k_r u_1 + k_r^{E}q_1)(p_{i+1} - p_i)\end{aligned} \tag{3-11}$$

$$\begin{aligned}\frac{dq_i}{dt} &= k_{T,i}C_{eff,i}yp_i - k_{T,i}^{-}q_i + k_{+}C_{eff,i}vu_i - k_{-}q_i \\ &+ (k_f[Tb] + k_f^{E}[TE] + k_f^{E}C_{eff,i}w)(q_{i-1} - q_i) + (k_r^{E}p_1 + k_r u_1 + k_r^{E}q_1)(q_{i+1} - q_i)\end{aligned} \tag{3-12}$$

The differential equations for the probability of the track binding to either TE (3-13) or EB1 (3-14) in solution were also determined by the reaction rates and corresponding probability for that reaction.

$$\frac{dw}{dt} = k_T[TE]y - k_T^{-}w + k_1[Tb]v - k_1^{-}w - k_f^{E}C_{eff,1}w + k_r^{E}q_1 \tag{3-13}$$

$$\frac{dv}{dt} = k_T[E]y - k_T^{-}v - k_1[Tb]v + k_1^{-}w - \sum_i k_{on,i}C_{eff,i}vu_i + \sum_i k_{-,i}q_i \tag{3-14}$$

These ordinary differential equations were solved using a fourth-order Runge-Kutta method in Matlab in order to determine the occupational probability of EB1 along the length of a protofilament, as well as the effect of force on the velocity of the filament. The velocity of the protofilament is obtained to the steady-state net rate of the tubulin addition and dissociation pathways:

$$V = \begin{pmatrix} k_f[Tb]\cdot\left(e^{-Fd} - \frac{[Tb]_c}{[Tb]}\cdot(1 - q_{end} - p_{end})\right) \\ + k_f{}^{E}\cdot\left(([TE] + C_T\cdot w)\cdot e^{-Fd} - [Tb]_c{}^{E}\cdot(q_{end} + p_{end})\right) \end{pmatrix} \tag{3-15}$$

There are two ways tubulin can add to the protofilament plus-end, directly with an on-rate of $k_f$ or copolymerizing with EB1 with an on-rate of $k_f^E$, hence, there are two rates of tubulin addition included in the equation. Assuming direct tubulin addition, the first term of the equation accounts for the effect of applied force on direct tubulin addition ($e^{-Fd}$) and the dependence of the forward rate on the critical concentration when the protofilament plus-end is not bound to EB1. The second term represents the case when tubulin copolymerizes with EB1. This part of the equation accounts for: the effect of applied force on both direct TE addition and Tk-TE addition, and the dependence of the forward rate on the critical concentration $[Tb]_c^E$ when the protofilament plus-end is bound to EB1. The probabilities, $q_{end}$ and $p_{end}$, were solved from Equations 3-11 and 3-12 for the protofilament plus end.

### 3.2.3 Parameter Estimations

The protein concentrations used for the simulations in this section are the same as those in the monovalent, non-tethered case. The kinetic rate constants were calculated from detailed balance. The on-rates for an EB1 subunit (or head) to the protofilament side ($k_{on}^{side}$) and to the

protofilament plus-end ($k_{on}$) were calculated based on the observed decay rate of an EB1 dimer from the MT side, $k_{off}$= 0.11 $s^{-1}$. EB1 in solution can bind one of its heads to the side of a protofilament with a rate of $k_{on}^{side}$·[E], and dissociates from the protofilament with a rate of $k_{-}^{side}$. At equilibrium, the decay rate of an EB1 dimer from the MT side, $k_{off}$, is equal to the sum of these two terms:

$$k_{off} = k_{on}^{side}[E] + k_{-}^{side} \tag{3-16}$$

Rearranging this equation gives

$$k_{on}^{side} = k_{on} = \frac{k_{off}}{[E] + K_d} \tag{3-17}$$

where $K_d \equiv k_{-}^{side}/k_{on}^{side}$. The off-rate constant for EB1 from the GDP-bound tubulin subunits, $k_{-}^{side}$, is calculated from $K_d$. The off-rate of EB1 from the protofilament plus-end, $k_{-}$, is the equal to the off-rate of EB1 from divided by a factor of $f$.

The linking protein was assumed to be a flexible, spring-like tethering region with position fluctuations ($\sigma$) of 10 nm. The resulting effective concentration of the linking protein near the protofilament is estimated like $C_{eff}$, for a 3-D normal distribution on a half-sphere. The normal Gaussian distribution of the spring is given by Equation 3-18, where $\gamma$ is the spring constant and is equal to $k_B T/\sigma^2$,

$$C_T = \frac{1}{\sqrt{2\pi}\sigma} \cdot \exp\left(\frac{-\gamma d^2}{2k_B T}\right) \cdot \frac{1}{A_s} \tag{3-18}$$

The surface area of the binding location, $A_s$, is estimated as half a sphere ($2\pi\sigma^2$) since the linking protein can only bind to the one half of the microtubule at a time. This value is analogous to $\rho^{-2}$ in the EB1 effective concentration calculated in Chapter 2.

### 3.2.4 Results

Figure 3-7A shows the predicted density of EB1 along the length of the protofilament (zero represents the plus-end). The protein species considered are the non-tethered EB1 protein in solution, the EB1 tethered to the protofilament, and the sum of the two species. The density of the tethered EB1 species shows a high concentration of EB1 at the protofilament plus-end which decreases along the length of the protofilament. This decay behavior is expected; it requires more energy for the linking protein (spring) to maintain attachment at distances from the protofilament plus-end, and EB1 is expected to have preferential binding to the protofilament plus-end due to its affinity modulation. The unattached EB1 protein does not seem to bind significantly at the protofilament plus end, most likely because the on-rate of linking protein to EB1 at this location is much greater than its dissociation rate. The non-tethered EB1 experiences a small peak in probability near the protofilament plus-end, likely because it was initially GTP-bound, and eventually dissociates from T-GDP.

The force-velocity profile for these mechanisms is shown in Figure 3-7B, which compares a protofilament whose driving force is the monovalent EB1 motor to where the driving force is solely free monomer addition. At an affinity modulation factor of 1000, the end-tracking model provides a higher maximum achievable force (~1.2 pN) demonstrating its advantage over the thermal ratchet model, whose stall force is 0.4 pN. However the advantage is modest because of the monovalent nature of this end-tracking motor requires it to detach from the protofilament during the cycle, thereby still permit tubulin dissociation, which is energetically favored while EB1 is unbound. However, it is known that EB1 is actually a dimer (Figure 3-8), with two MT binding domains, which may facilitate processivity by allowing one EB1 head to remain bound while the other head releases. EB1 may therefore behave as a divalent motor, which would provide the end-tracking model with the advantage to allow rapid MT polymerization while

maintaining a persistent attachment between the MT and the motile surface. This idea is explored in Chapter 4.

## 3.3 Summary

This chapter described two models that simulate the growth of a single protofilament in the presence of a monovalent EB1 protein to determine the advantages of the mechanochemical process over a simple monomer addition-driven (Brownian ratchet) mechanism. They key characteristic of these models is that they account for the reaction between solution phase EB1 and tubulin protomers. In the previous chapter, it was assumed that the EB1 protein behaves as an end-tracking motor, with preferential binding to T-GTP over T-GDP, and an affinity modulation factor greater than one. In this chapter, this assumption is supported by our finding that affinity modulation is necessary to achieve the observed high density of EB1 at filament ends relative to filament sides.

### 3.3.1 Non-Tethered Protofilaments

The first model presented eliminates any force effects by allowing free filament growth and EB1 binding, and assumes that neither the EB1 nor the protofilament are tethered to a motile surface. Although experimental results are not conclusive as to whether EB1 binds to T-GTP in solution, this model accounts for several reaction pathways to allow EB1 to bind with tubulin in solution as well as filament-bound tubulin. The dissociation constant for EB1 and free T-GTP was taken as that need to provide a 4.2 ratio of EB1-bound subunits at the protofilament plus-end versus protofilament sides, which would correlate well with experimental results. Large affinity modulation factors resulted in an equilibrium value for the tubulin-EB1 dissociation constant, and are therefore optimal for simulation purposes. Regardless of the value for other key kinetic rates (i.e., on-rate of tubulin, $k_f$, or on-rate of EB1 on protofilament sides, $k_+$), it is required for EB1 to have a larger affinity for T-GTP rather T-GDP ($f>1$) in order to achieve the 4.2 ratio.

This result supports the assertation that EB1 has an affinity-modulated interaction with tubulin, which is not accounted for in the Brownian ratchet mechanisms, but is the key characteristic of the end-tracking model.

This model predicts the density of EB1 bound along the length of a protofilament, and compares the results from affinity modulation to a mechanism with no affinity modulation. The optimal, equilibrium EB1-tubulin dissociation constant was used to calculate the binding probability of EB1 to the plus-end and sides of a microtubule protofilament. The results of the model demonstrate that the mechanism with no affinity modulation results in a near-uniform EB1 density along the entire length of the protofilament. However, large affinity modulation results in a greater EB1 binding at the protofilament plus-end that decays along the length of the protofilament, a prediction which agrees to experimental results showing the decay of fluorescent EB1 on a non-tethered microtubule.

To simplify this complex model, several assumptions were made. First, tubulin addition induces filament-bound hydrolysis at the protofilament plus-end. The affinity modulation is assumed to affect only the off-rates of the protein interactions and not the on-rates. Because EB1 stabilizes the protofilament end, it is assumed that the terminal subunit of a protofilament cannot dissociate if bound to an EB1 molecule. All protein concentrations are considered to be constant.

### 3.3.2 Tethered Protofilaments

We have previously proposed a potential role of EB1 acting as a co-factor protein in end-tracking mechanisms (Dickinson et al., 2004). Consistent with this proposition, the second model allows EB1 binding to be translated to MT force generation by introducing a linking protein that attaches the monovalent EB1 protein to a motile surface. To simulate this monovalent EB1 molecular motor, a model similar to the non-tethered, monovalent end-tracking

model was used. The reaction mechanisms considered were the same with exception of association and dissociation of EB1 from the surface linking protein. As a result, these motors act processively on the end of the microtubule to generate force and propel the surface forward.

The occupational probability of all EB1 species (tethered and non-tethered) demonstrates that at large affinity modulation factors there is a high occupation of total EB1 at the protofilament plus-end, which decays along the length of the protofilament. This decayed concentration of EB1 along the protofilament is comparable to the decay profile shown by Tirnauer et al. (Tirnauer et al., 2002b) for EB1 on free-growing protofilaments. More importantly was the effect of force on the end-tracking model. This model demonstrates the potential of the monovalent end-tracking motor to provide a higher maximum achievable force (~1.2 pN) than the thermal ratchet model (0.4 pN). However, the advantage is not that significant because it was assumed that EB1 is a monovalent protein instead of its true configuration as a divalent protein.

For simplification, this modeling approach neglected the potential energy exerted by compression and extension of the spring-like linking protein, particularly when a load is applied to the motile surface. When a load is introduced, there is an associated change in the kinetic reactions between the end-tracking complex and the protofilament that would affect the occupational probability of EB1 and the force-velocity profile. The subsequent tethered protofilament growth model with divalent end-tracking EB1 motors will account for the force effects on the linking protein.

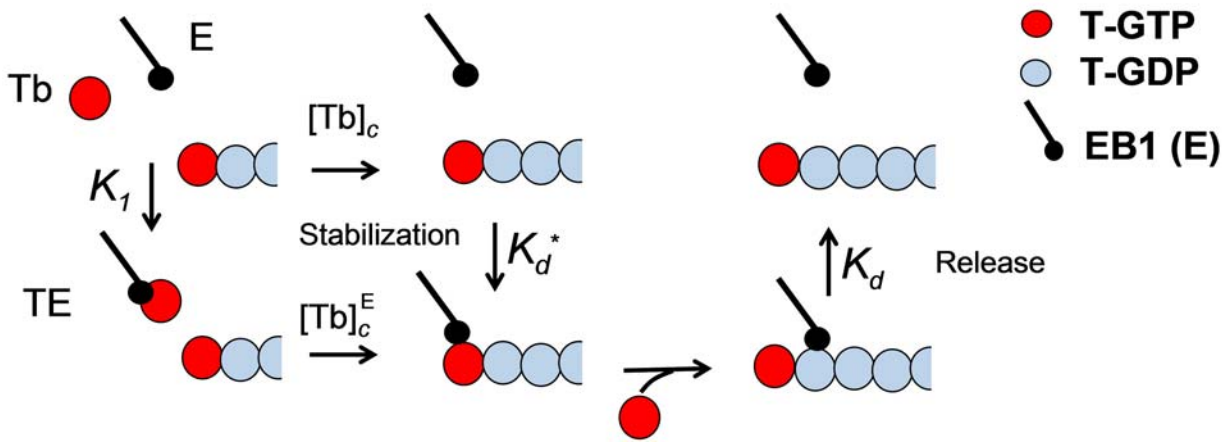


Figure 3-1. Schematic of non-tethered, monovalent EB1 end-tracking motor mechanisms. Tubulin protomers (Tb) can add directly to filament ends with an equilibrium dissociation constant $[Tb]_c$, or they can first bind to EB1 (E) in solution (with dissociation constant $K_1$) then add as an EB1-tubulin complex ($[Tb]_c^E$). GTP hydrolysis on the penultimate subunit occurs upon tubulin addition to the protofilament plus-end. $K_d$ is the EB1 dissociation from the protofilament plus-end and $K_d^*$ is the dissociation constant for EB1 from T-GDP, where $f = K_d/K_d^*$.

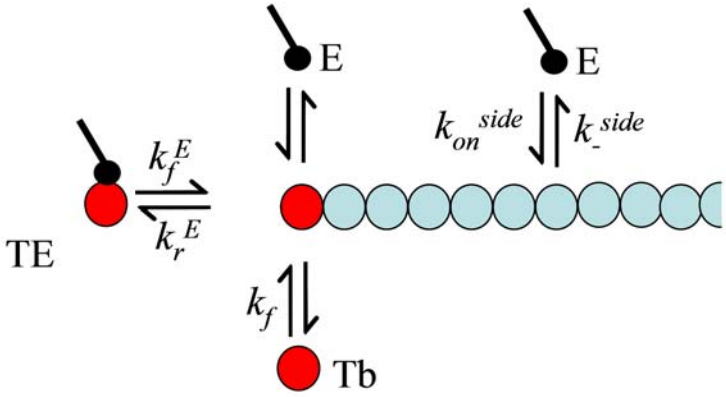


Figure 3-2. Various pathways of non-tethered monovalent EB1 binding to protofilament. EB1 can bind directly to the GTP-rich protofilament plus-end, or EB1 can associate with T-GDP on the side of the protofilament, or EB1 can copolymerize with tubulin in solution.

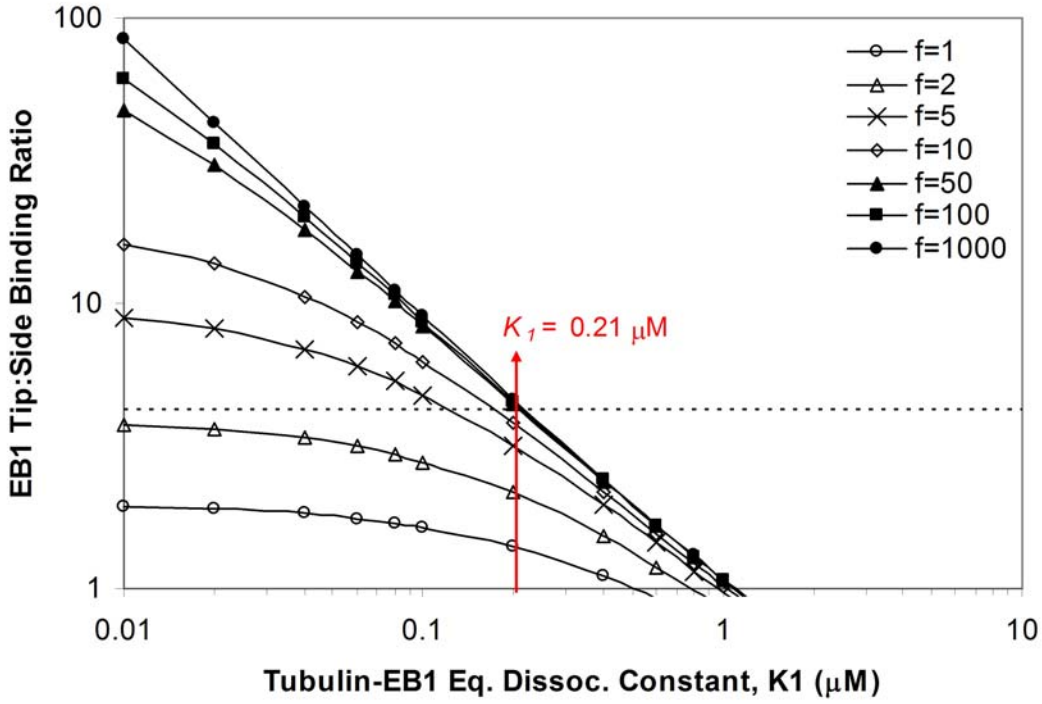


Figure 3-3. Choosing an optimal $K_1$ value for monovalent EB1. The experimentally determined ratio of EB1 binding to the tip versus the side of a protofilament (4.2) is represented by the dotted line. Each curve represents a different affinity modulation factor value, $f$, and the data points correspond to the EB1 binding ratio at various values of $K_1$ and a $k_{on}$ of 2.1 $\mu M^{-1}s^{-1}$. The value of $K_1$ required to achieve a tip-to-side binding ratio of 4.2 for $f < 50$ increases with increasing $f$. The optimal value of $K_1$ chosen was 0.21 μM where $f > 10$. The simulation time was 1000 seconds.

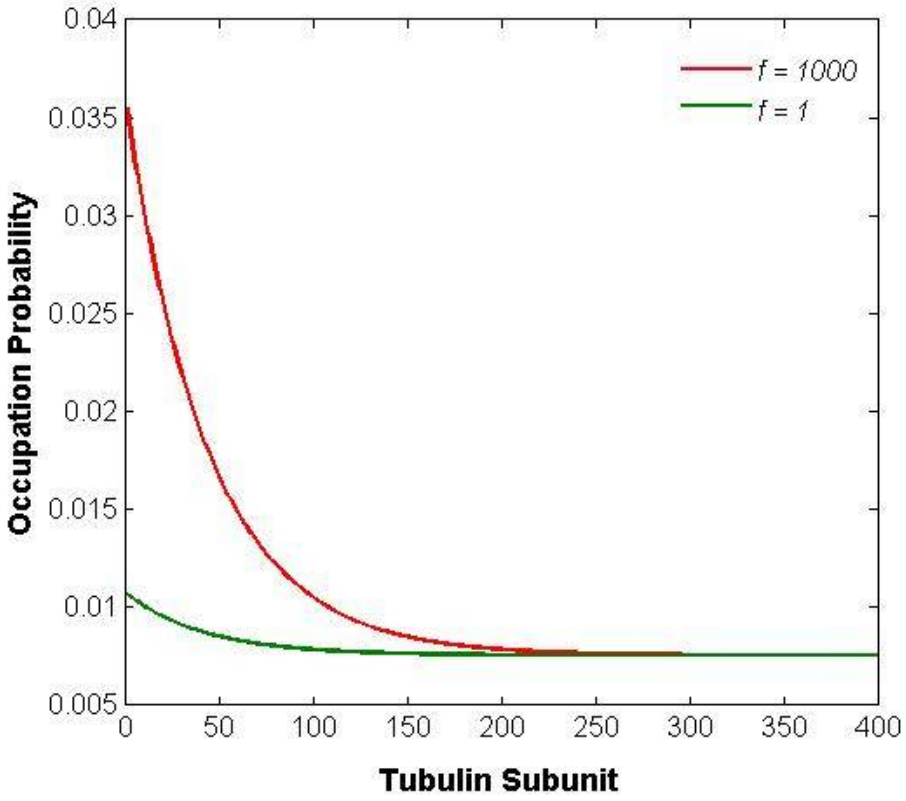


Figure 3-4. EB1 density profile on a non-tethered microtubule protofilament with monovalent EB1. Considering the various mechanisms of EB1 binding, the occupation probability for both $f$=1 and $f$=1000 are shown. At $f$=1 the steady state occupational probability is uniform along the length of the protofilament. When $f$=1000, EB1 has a high occupational probability at the plus-end, which decreases along the length of the protofilament.

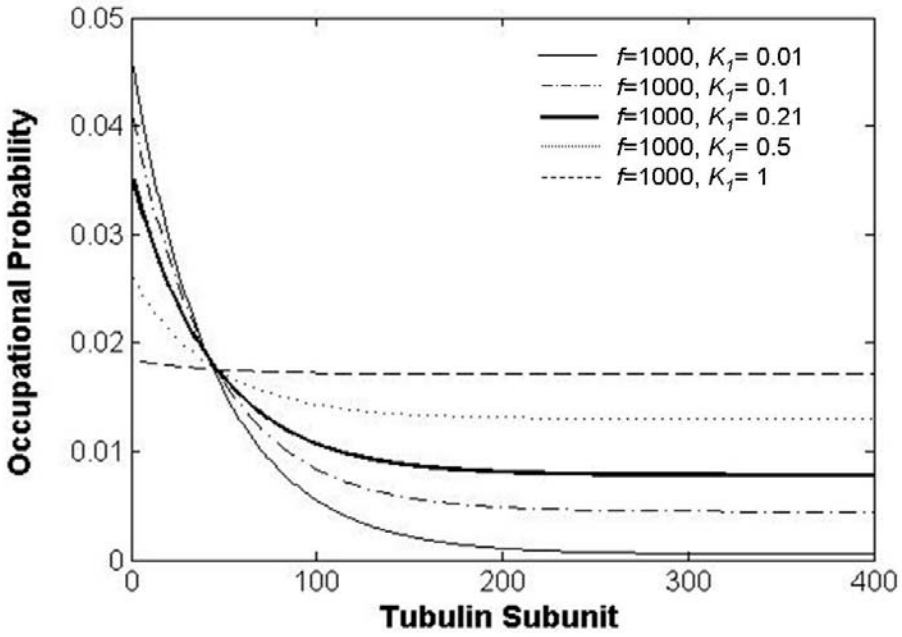


Figure 3-5. Effect of $K_1$ on profile of monovalent EB1 occupational probability. Considering the various mechanisms of EB1 binding, the occupation probability for $K_1$ from 0.01 to 1 μM at $f$=1000 is shown. When $K_1$ is 0.01 μM, EB1 has a high occupational probability at the plus-end, which decreases along the length of the protofilament. This decay profile flattens out as $K_1$ increases; at $K_1$ =1 μM the profile is similar to the profile of $f$=1 in Figure 3-4.

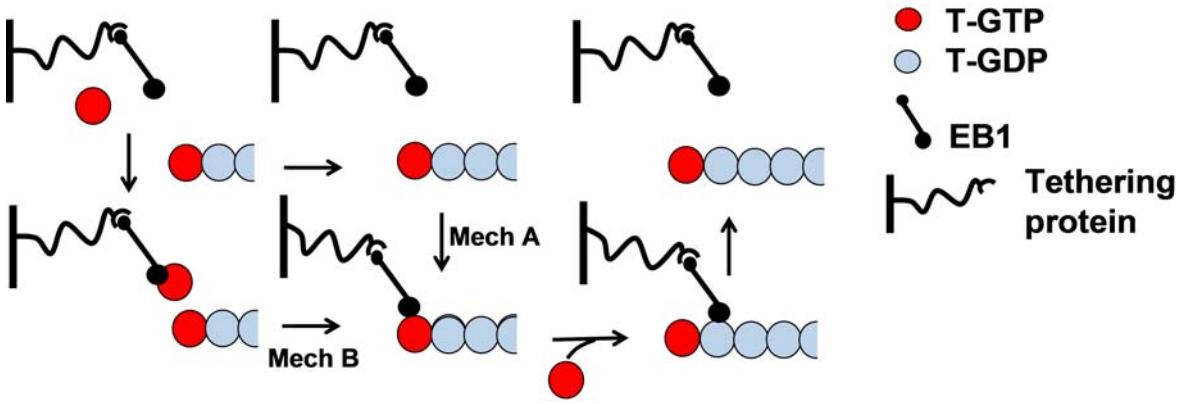


Figure 3-6. Schematic of tethered, monovalent EB1 end-tracking motor mechanisms. Tubulin protomers can add directly to filament ends, or they can first bind to surface-tethered EB1 in solution then add as an EB1-tubulin complex. GTP hydrolysis on the penultimate subunit occurs upon tubulin addition to the protofilament plus-end. EB1 is allowed to dissociate from surface linking protein (pathway not shown here).

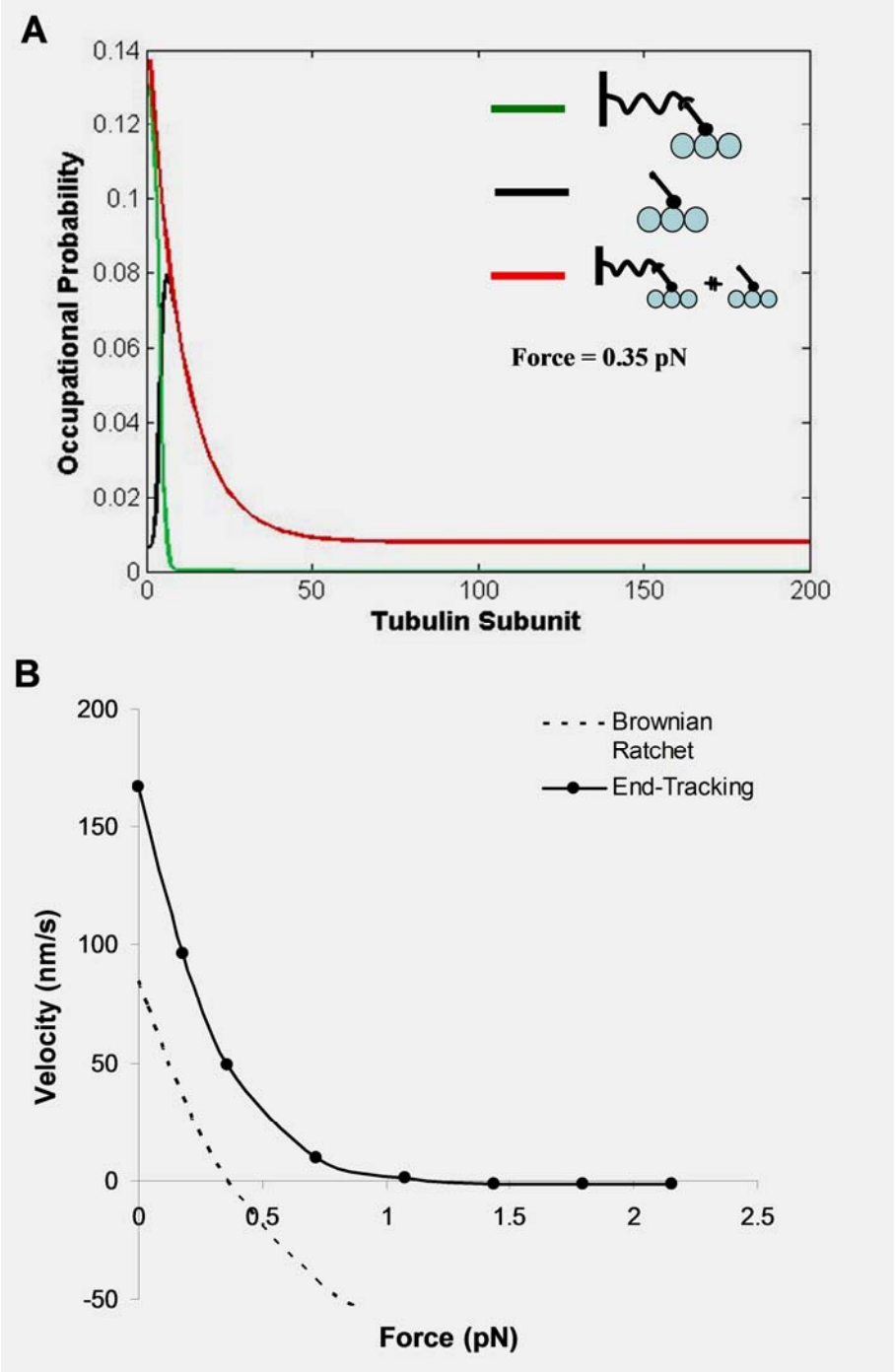


Figure 3-7. Force effects on a tethered protofilament with monovalent EB1. A) Occupational probability of EB1 along length of protofilament (zero represents plus-end) at $f$=1000. Two protein species considered: un-tethered EB1 and tethered EB1 on protofilament. Occupation of EB1 for each species decreases along length of protofilament. B) Force-Velocity profile. Maximum achievable force for end-tracking model at $f$=1000 (~1.2 pN) exceeds that of Brownian Ratchet model (0.4 pN)

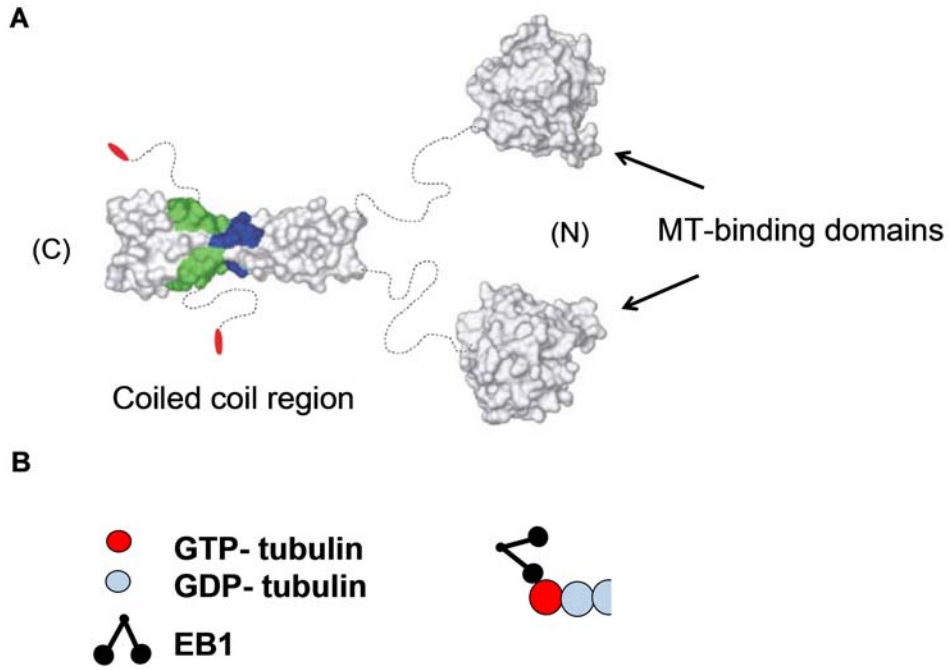


Figure 3-8. Divalent EB1 represented as divalent end-tracking motor. A) Depiction of EB1 structure characterized from crystal structures. The C-terminus is represented by (C) and the N-terminus is represented by (N). Reprinted by permission from Macmillan Publishers Ltd: [Nature] (Honnappa et al., 2005) , copyright (2005). B) Schematic of end-tracking motor complex comparable to crystal structure of EB1.

# CHAPTER 4
# PROTOFILAMENT END-TRACKING MODEL WITH DIVALENT EB1

The protofilament end-tracking model described in Chapter 3 is a simplified model that does not account for the divalent structure of EB1. This chapter discusses the more realistic models developed that simulate the growth of a protofilament in the presence of divalent EB1 end-tracking motors. Similar to Chapter 3, we first model the growth of an untethered protofilament in the presence of solution-phase EB1 end-tracking motors. The model accounts for the solution binding of tubulin and EB1, and predicts the EB1 density along a polymerizing protofilament, with a 4.2 tip-to-side ratio of EB1. The second model allows EB1 to bind to a motile surface via a tethering protein. The resulting protofilament dynamics were analyzed, and the force-dependent velocity was compared to that of the Brownian Ratchet mechanism.

## 4.1 Non-Tethered Protofilament Growth

As in the models from previous chapters, EB1 is assumed to preferentially binds to T-GTP rather than T-GDP. For simplicity, we assume that if one subunit ("head") is bound to the protofilament, the remaining unbound head can only bind to an adjacent tubulin subunit.

### 4.1.1 Kinetics of EB1-Tubulin Interactions

The reactions considered in this protofilament model are shown in Figures 4-1 and 4-2. We assume for all pathways that GTP hydrolysis of the penultimate subunit occurs immediately after tubulin addition (O'Brien et al., 1987; Schilstra et al., 1987; Stewart et al., 1990) and that solution-phase EB1 can exist in three forms: unbound (E), bound to one tubulin protomer (TE), or bound to two tubulin protomers (TTE). To determine the concentrations of these three species, we determined [E] by assuming equilibrium binding with Tb and microtubule sides, and equilibrium binding of TE and Tb. EB1 is a homodimer, so it is assumed that both tubulin binding domains ("heads") are identical and non-cooperative; this property allows EB1 to bind to

its first or second tubulin protomer with an equilibrium dissociation constant, $K_1$. As derived in Appendix A.1, these assumptions results in the following concentrations:

$$[E] = \frac{[E]_0}{\left(1 + \frac{[Tb]}{K_1}\right)^2 + \frac{[MT]}{K_d}} \tag{4-1}$$

$$[TE] = \frac{2[E][Tb]}{K_1} \tag{4-2}$$

$$[TTE] = \frac{[E][Tb]^2}{K_1^2} \tag{4-3}$$

Figure 4-1A shows the two methods in which unbound EB1 in solution can bind to a protofilament, by adding directly to filament ends ($k_{on}$) after tubulin addition ($k_f$), or by first binding to tubulin in solution ($k_1$) then adding as an EB1-tubulin complex ($k_f^E$). Since unbound EB1 can bind to Tb in two identical ways, the on-rate for these binding steps is doubled ($2k_1$ or $2k_{on}$). Once EB1 is bound, there are two pathways that result in attachment of EB1's second head to the protofilament plus-end (Figure 4-1B). One pathway involves direct binding of the EB1 head to the terminal, GTP-bound subunit ($k_+$) after tubulin addition ($k_f$). The other pathway allows the EB1 head to bind to solution-phase Tb ($k_1$) and facilitate tubulin addition by shuttling it to the protofilament plus-end ($k_f^{E'''}$). The value for $k_f^{E'''}$ accounts for the on-rate of TE and the local, effective concentration of the unbound EB1 head ($C_{eff}$), which is represented by Equation 4-4.

$$k_f^{E'''} = k_f^E C_{eff} \tag{4-4}$$

The terminal two subunits at this stage are both bound to the same EB1 protein. The state of the terminal subunit is referred to as $dbE^+$ (double-bound to EB1 on plus-end) and the penultimate subunit is in state $dbE^-$ (double-bound to EB1 on minus-end). Figure 4-1C shows how TE in

solution can bind the protofilament: binding directly to the protofilament plus-end ($k_{on}$) after tubulin addition ($k_f$), or by first binding to tubulin in solution ($k_1$) then adding as an EB1-tubulin complex ($2k_f^E$).

Figure 4-2 shows the various mechanisms by which EB1 can bind to the GDP-rich protofilament side. As shown in the figure, free EB1 can bind directly from solution to a T-GDP subunit (pathway A), and subsequently bind its unbound head the neighboring subunit (pathway E). Additionally, TE can bind to the side of a protofilament with an on-rate of $k_{on}^{side}$ (pathway C).

### 4.1.2 EB1 Occupational Probability Model

A probabilistic model similar to the tethered, divalent end-tracking model (Chapter 3) was developed to simulate the pathways shown in Figure 4-1. This model determines the EB1 density along a protofilament based on the probability of each tubulin subunit being in a specific EB1 binding state. The relevant probabilities considered were:

- $p_i$ : probability of subunit $i$ bound to EB1 head (other head unbound)
- $w_i$ : probability of subunit $i$ bound to TE
- $q_i^+$: probability of subunit $i$ in state $dbE^+$
- $q_i^-$ : probability of subunit $i$ in state $dbE^-$
- $u_i$ : probability of subunit $i$ being unbound

The probability of the subunit being unbound, $u_i$, is represented by Equation 4-5.

$$u_i = 1 - q_i^+ + q_i^- - p_i - w_i \tag{4-5}$$

The probability of Tb being in any one of these binding states is based on its reaction for that pathway, the probability of the reaction, and the corresponding protein concentrations. The probabilities are defined by a set of ordinary differential equations (in terms of the kinetic rates),

and are represented by Equations 4-6 through 4-10 (Appendix A.3), where $R_+$ and $R_-$ are defined by Equations 4-11 and 4-12.

$$\frac{dp_i}{dt} = 2k_{on}[E]u_i - k_- p_i + k_1^- w_i - k_1^+ [Tb]p_i + k_- q_{i-1}^+ - k_+ p_i u_{i+1} + k_{-,i+1} q_{i+1}^- - k_+ p_i u_{i-1} + R_+(p_{i-1} - p_i) + R_-(p_{i+1} - p_i) \quad (4\text{-}6)$$

$$\frac{dw_i}{dt} = k_{on}[TE]u_i - k_- w_i + k_1^+ [Tb]p_i - k_1^- w_i + R_+(w_{i-1} - w_i) + R_-(w_{i+1} - w_i) \quad (4\text{-}7)$$

$$\frac{dq_i^+}{dt} = -k_{-.i+1} q_{i+1}^- - k_{-.i} q_i^+ + k_{+,i} p_{i+1} u_i + k_{+.i+1} p_i u_{i+1} + R_+(q_{i-1}^+ - q_i^+) + R_-(q_{i+1}^+ - q_i^+) \quad (4\text{-}8)$$

$$\frac{dq_i^-}{dt} = -k_{-,i} q_i^- - k_{-,i-1} q_{i-1}^+ + k_{+,i} p_{i-1} u_i + k_{+,i-1} p_i u_{i-1} + R_+(q_{i-1}^- - q_i^-) + R_-(q_{i+1}^- - q_i^-) \quad (4\text{-}9)$$

$$\frac{du_i}{dt} = k_- p_i + k_- w_i + k_- q_i^+ + k_- q_i^- - k_{+,i} p_{i+1} u_i - k_{+,i} p_{i-1} u_i - 2k_{on}[E]u_i - k_{on}[TE]u_i + R_+(u_{i-1} - u_i) + R_-(u_{i+1} - u_i) \quad (4\text{-}10)$$

$$R_+ = k_f [Tb] + k_f^E([TE] + [TTE]) + k_f^E C_{eff} w_1 \quad (4\text{-}11)$$

$$R_- = k_r u_1 + k_r^E(w_1 + p_1 + q_1^+) \quad (4\text{-}12)$$

At equilibrium, these probabilities reduce to Equations 4-13 through 4-16, where $q_{eq} \equiv q_{eq}^+ + q_{eq}^-$ and $K \equiv k_+^{side}/k_-^{side}$.

$$p_{eq} = \frac{2k_{on}[E]}{k_-} u_{eq} \quad (4\text{-}13)$$

$$w_{eq} = \frac{[Tb]}{K_1} p_{eq} \quad (4\text{-}14)$$

$$q_{eq} = 2 \cdot K \cdot p_{eq} u_{eq} \quad (4\text{-}15)$$

$$u_{eq} = \frac{-\left\{\left(\frac{[T]}{K_1}+1\right)\frac{2k_{on}^{\ side}[E]}{k_{-}^{\ side}}+1\right\}+\sqrt{\left\{\left(\frac{[T]}{K_1}+1\right)\frac{2k_{on}^{\ side}[E]}{k_{-}^{\ side}}+1\right\}^2+16\cdot K\frac{k_{on}^{\ side}[E]}{k_{-}^{\ side}}}}{8\cdot K\frac{k_{on}^{\ side}[E]}{k_{-}^{\ side}}} \quad (4\text{-}16)$$

The results of these equations were used to analyze the distribution of the divalent, EB1 end-tracking motors on the non-tethered protofilament, and determine the equilibrium EB1 concentration along the protofilament, $P_{eq}$.

$$P_{eq} = p_{eq} + w_{eq} + q_{eq}/2 \quad (4\text{-}17)$$

### 4.1.3 Average Fraction of EB1-bound Subunits at Equilibrium

A stochastic model was developed that determines the average binding fraction of EB1 along a non-growing protofilament in order to test the previous probabilistic model and compare the results. The pathways considered for this model are those where EB1 binds to the side of the protofilament and not the plus-end, which are shown in Figure 4-2. To model these pathways, the state of each tubulin subunit was analyzed. During the simulation, the state of each subunit in the protofilament was initially unbound from EB1. (The Matlab code can be found in Appendix B.3.2). The transition probability in time $\Delta t$ for each pathway reaction was analyzed; if that reaction occurred, then the state of the tubulin subunit would change to its new state. The EB1-binding state of each subunit was used to determine the fraction of EB1-bound subunits in the protofilament; this fraction was averaged over time for a total simulation time of 40 seconds.

### 4.1.4 Average Fraction of EB1-bound subunits during protofilament growth

A stochastic model was also used to calculate the time-averaged fraction of EB1-bound subunits during protofilament growth. The pathways considered in this model are those shown in Figure 4-2., as well as the association and dissociation of tubulin from the protofilament plus-end (Figure 4-1). The stochastic model used to simulate these pathways is very similar to

the previous model; it utilizes the same kinetic parameters, and the state of the tubulin subunits was determined from reaction rate for each pathway. (Appendix B.3.3 contains the Matlab code for this model.) The EB1-binding state of each subunit was determined for each time step and the fraction of EB1-bound subunits in the protofilament was averaged over time for a total simulation time of 40 seconds.

### 4.1.5 Parameter Estimations

Several key kinetic parameters listed in Figures 4-1 and 4-2 have not yet been determined experimentally, including the dissociation constant for Tb and EB1 in solution ($K_1$) the EB1 on-rate for protofilament-bound T-GTP ($k_{on}$), the EB1 off-rate from protofilament-bound T-GDP ($k_-^{side}$), and the value of $K$. To solve for these parameters, it was first assumed the protofilament was at equilibrium (i.e., it does not polymerize). At equilibrium, the fraction of filament-bound subunits attached to EB1 is given by Equation 4-18 (see appendix A.3 for full derivation).

$$\rho \equiv \frac{[E]_0 - [E]}{[E]_0} \equiv \frac{1}{\frac{K_{d,eff}}{[MT]_{tot}} + 1} \tag{4-18}$$

When half of the protofilament is saturated with EB1, the effective equilibrium dissociation constant of EB1 and the protofilament ($K_{d,eff}$) is given by Equation 4-19, where $u_{1/2} \equiv u_{eq}$ ($[E]-[E]_0/2$).

$$K_{d,eff} = \frac{1}{\left(\frac{k_+^{side}}{k_-^{side}}_{1/2} + 1\right)\frac{2k_{on}^{side}}{k_-^{side}} u_{1/2}} \tag{4-19}$$

Under this constraint, $u_{1/2}$ is given by Equation 4-20, where $k_+^{side} = k_{on}^{side} C_{eff}$ for the protofilament plus end, and $k_-^{side} = k_+^{side}/K$.

$$u_{1/2} = \frac{-\left\{K \cdot \frac{[E]_0}{C_{eff}} + 1\right\} + \sqrt{\left\{K \cdot \frac{[E]_0}{C_{eff}} + 1\right\}^2 + 8K^2 \frac{[E]_0}{C_{eff}}}}{4K^2 \frac{[E]_0}{C_{eff}}} \tag{4-20}$$

Assuming [Tb]=0, $[E]_0$=0.27 μM, [E]=$[E]_0$/2, and $C_{eff}$=153 μM, Equations 4-19 and 4-20 and the experimentally determined value for $K_{d,eff}$ of 0.44 μM (Tirnauer et al., 2002b) where used to determine the value of $K$ as 37. With this known value of $K$, $k_-^{side}$ can be represented as a function of $K_1$ from Equation 4-21, where $k_{off}$ is the known off-rate of dimeric EB1 from a protofilament ($k_{off}$=0.26 $s^{-1}$, (Tirnauer et al., 2002b)). Appendix A.3 contains the derivations for these equations and parameter calculations.

$$k_-^{side}(K_1) = k_{off}\left\{1 + \frac{K \cdot u_{eq}}{\left(1 + \frac{[Tb]}{K_1}\right)}\right\} \tag{4-21}$$

To determined the optimal value of $K_1$ (that provides a 4.2 tip-to-side EB1 binding ratio), the probabilistic model discussed in section 4.1.2 was simulated under different values of $f$ and $K_1$ (Appendix B.3.1 contains the Matlab code). Figure 4-3 shows the results of these simulations. When $f$ is equal to one, the EB1 binding ratio remains below the expected 4.2 value at all values of $K_1$. This result suggests that EB1 must have a greater affinity for T-GTP than T-GDP (i.e., $f$ must be greater than one) in order for EB1 to accumulate at the plus-ends of protofilaments as seen experimentally. The optimal value of $K_1$ for $f$ greater than one increases with increasing values of $f$. At larger values of $f$ (50 and 500), the optimal value for $K_1$ is approximately 0.65 μM. Increasing $f$ past 50 does not provide any additional effect on $K_1$. The reasoning behind the trends in these results lies in the reaction rates. Both $k_r^E$ and $k_-$ are inversely proportional to $f$, so an increase in $f$ causes the forward reactions to be favored in the mechanisms corresponding to

these rates (EB1 binding to the protofilament plus-end). But, as $f$ approaches infinity, it reaches a point in which the $k_r^E$ and $k_-$ become zero and no increase in $f$ will favor the forward reaction further. The optimal values of $K_1$ and $f$ chosen for all simulations used in this chapter were: $K_1$ = 0.65 μM and $f \geq 50$.

The value of $k_{on}$ used to determine $K_1$ in the previous analysis was estimated as 1 $\mu M^{-1}s^{-1}$, but this value has not been experimentally determined. To ensure that the value of $k_{on}$ chosen does not affect the binding ratio of EB1 (or $K_1$), we analyzed the effect of $k_{on}$ on $K_1$. The model from section 4.1.2 was simulated for affinity modulation factors from 1 and 50, and the value of $k_{on}$ was varied from 0.1 $\mu M^{-1}s^{-1}$ to 10 $\mu M^{-1}s^{-1}$. The resulting EB1 tip-to-side binding ratios for these conditions are shown in Figure 4-4. When $f$=1 and $K_1$ is less than 0.1 μM, there is no affect of $k_{on}$ on the binding ratio, and when $K_1$ is greater than 0.1 μM, there is a minimal effect of $k_{on}$. In either case, the binding ratio still fails to obtain the optimal value of 4.2. The optimal value of $K_1$ (0.65 μM) is not affected by the value of $k_{on}$ for $f$=50, therefore an average value of 5 $\mu M^{-1}s^{-1}$ for $k_{on}$ was chosen to be used for all further simulations.

The kinetic parameters used in this chapter that were also used in Chapter 3 were determined the same way. Additionally, the on-rate of EB1 and tubulin ($k_1$) was assumed to be a typical value for protein-protein binding interactions, 10 $\mu M^{-1}s^{-1}$. Consequently, the value of $k_1^-$ was determined from the optimal $K_1$ value ($K_1=k_1^-/k_1$). The on-rate constant for TE and TTE to the protofilament plus end, $k_f^E$, was assumed to be equal to the on-rate of tubulin addition, $k_f$. The off-rate constant of TE and TTE to the protofilament plus-end, $k_r^E$, was calculated based on detailed balance, and is represented by Equation 4-22.

$$k_r^E = \frac{k_f^E \cdot T_c}{K_1 \cdot k_- \cdot k_{on}} \tag{4-22}$$

### 4.1.6 Results

#### 4.1.6.1 Occupational probability

The ordinary differential equations that define the probabilities of EB1 binding (Eq 4-6 to Eq. 4-10) were solved to determine the expected equilibrium fraction of EB1-bound protomers in the protofilament (Figure 4-5). This fraction was evaluated by determining $P_{eq}$ from Equation 4-17 at various values of $K_1$. The percent of the protofilament bound to EB1 increases with increasing $K_1$. At large values of $K_1$ ($K_1 > 10$), the EB1 binding fraction reaches an equilibrium, with approximately 40% of the protofilament bound. The value of $K_1$ used for simulations (0.65 μM) corresponds to about 2.5% of EB1 bound to the protofilament at equilibrium. The data for this plot was recreated for $f$=1000; since the equilibrium binding probability of EB1 is not dependent on the affinity modulation factor, the results were the same as for $f$=1 (data not shown).

The set of ordinary differential equations in Equations 4-6 to 4-10 were numerically integrated and solved at a set value of $K$=37 and $K_1$=0.65 $\mu M^{-1}s^{-1}$ using a fourth-order Runge-Kutta method in Matlab. The occupational probability of EB1 along the length of the protofilament for $f$=1 and $f$=1000 is shown in Figure 4-6. When $f$=1, the EB1 density is nearly constant along the length of the protofilament at 2.5%. This behavior is expected since at $f$=1 EB1 does not have preferential binding to GTP or GDP-bound subunits, and this is the equilibrium EB1 binding fraction determined earlier (Figure 4-5). At $f$=1000, the probability at the protofilament end is 0.107, which decreases along the length of the protofilament to a value of 0.025. It is expected that there is a higher occupational probability at the protofilament plus end since EB1 has a higher affinity for T-GTP versus T-GDP when $f$=1000. This decay profile is comparable with the experimental results shown in Figure 1-4. The ratio of the occupational

probability at the plus and minus end of the protofilament for $f$=1000 is about 4.3, which is similar to the tip-to-side ratio of 4.2 observed in experiments. For both $f$=1 and $f$=1000. The occupational probability at the first tubulin subunit is significantly less than that of the rest of the filament because the value of $q_i^-$ is zero for the first subunit.

#### 4.1.6.2 Average fraction of EB1-bound subunits at equilibrium

The time averaged fraction of EB1-bound protomers at $f$=1 and $f$=1000 and optimal values for $K_1$ (0.65 μM) and $k_{on}$ (5 $\mu M^{-1}s^{-1}$) are displayed in Figure 4-7. The calculated equilibrium fraction of 0.024 from the probabilistic model is also shown on the plot for comparison with results from the stochastic model. Since this model only considers the binding of EB1 to filament-bound T-GDP, the time averaged fraction along the length of the protofilament is similar for $f$=1 and $f$=1000. In both cases, the fraction fluctuates around the equilibrium value of 0.024. Since it is assumed that the affinity modulation factor only affects the off-rates and not the on-rates on EB1, TE, or TTE to the protofilament plus-end, the only rates affected by $f$ are $k_-$ and $k_r^E$. These rates do not correspond to any of the pathways considered for this model; therefore, it is expected that there be a similarity between the two curves generated at $f$=1 and $f$=1000. The data for this plot was recreated for a simulation time of 20 seconds, which resulted in no noticeable difference in the plots (data not shown).

#### 4.1.6.3 Average fraction of EB1-bound subunits during protofilament growth

Figure 4-8 displays the average fraction of EB1-bound subunits on a protofilament when polymerization is allowed to occur, at affinity modulation factors $f$ = 1 and $f$ = 1000. The equilibrium percentage of EB1 bound (2.4%) for $K_1$=0.65 μM and $k_{on}$=5 $\mu M^{-1}s^{-1}$ is shown for comparison. The results show that the fraction corresponding to $f$=1 is overall slightly smaller than that of $f$=1000, but both results show a larger fraction of bound EB1 at the plus-end. This

result is expected since when $f$=1000 the rate of EB1 addition at the protofilament plus-end is increased. When $f$=1000, there is a sharp decrease in the EB1-bound fraction along the length of the protofilament. This behavior is due to the large affinity modulation factor, which results in a lower affinity for EB1 to GDP-bound tubulin subunits and hence significantly reduced off-rates from the protofilament plus-end ($k_r^E$ and $k_-$). Conversely, when $f$=1 the EB1-bound fraction of subunits along the side of the protofilament fluctuates around the equilibrium value; since EB1 has no preferential binding to GTP- or GDP-bound subunits, there are significant amounts of EB1 bound along the side of the protofilament.

## 4.2 Tethered Protofilament Growth Model

This model, similar to the tethered-protofilament model discussed in section 3.2, considers the growth of a single microtubule protofilament in the presence of solution-phase, divalent EB1. A flexible binding protein provides as a link between EB1 and a motile surface, allowing EB1 to behave as an end-tracking motor. The various reaction mechanisms considered for this tethered, protofilament model are those previously shown in Figures 4-1 and 4-2, and the binding pathways involving the surface-bound tethering protein (Figures 4-9 and 4-10). The tethering protein was modeled as a Hookean spring which exerts energy on the motile surface under a load. The spring is defined by its spring constant, $\gamma$, which is given by

$$\gamma = \frac{k_B T}{\sigma^2} \tag{4-23}$$

The thermal energy is given by $k_BT$, and $\sigma$ represents the variance in its position fluctuations. The effective concentration of the linking protein near the protofilament is obtained from normal Gaussian distribution of the spring given by Eq. 3-17 in section 3.2.3. The assumptions and parameter values used are the same as those in section 4.1.

### 4.2.1 Kinetics of EB1-Tubulin Interactions

Figures 4-9 A and B shows the two methods by which EB1 can bind to the surface-bound tethering protein, hereafter abbreviated Tk. Tk can associate with EB1 in solution (pathway A) or with protofilament-bound EB1 (pathway B). Although pathway A only shows the reaction between free EB1 and Tk, this reaction can occur with TE or TTE under the same on- and off-rates.

In pathway B, Tk binds to EB1 on the protofilament (this could also be filament-bound TE or doubly bound EB1). The forward kinetic rate of this reaction, $k_T$', is represented by Equation 4-24, and is proportional to the forward rate of Tk binding to EB1, $k_T$, the effective concentration of Tk at the protofilament plus-end, $C_T$, and the effects of the transition state and spring energies.

$$k_T' = k_T C_T e^{\gamma(n-1)d\Delta/2k_BT} e^{-\gamma((n-1)d)^2/2k_BT} \tag{4-24}$$

The $e^{\gamma(n-1)d\Delta/2k_BT}$ term represents the contribution of the transition state effects from force, where $\Delta$ is the transition state distance. The subunit position on the protofilament ($n$) is equal to one at the plus-end and increases toward the minus-end of the filament. The $e^{-\gamma((n-1)d)^2/2k_BT}$ term corresponds to the effect of stretching the tethering protein (or spring) from its initial position to its binding position on the protofilament. Since the tethering protein's unbound, equilibrium position is one, the number of subunits between an unbound, surface-tethered EB1 protein and its equilibrium binding position on the protofilament is $n$-1. Hence, the displacement distance of the spring is given by $(n-1) \cdot d$ where $d$ is the length of a subunit (8 nm).

The effects of the transition state energy is associated with a bond under tension; therefore it also affects the reverse rate constants. Since the dissociation pathway in 4-9 B allows the EB1 spring to return to its equilibrium position, the only energy associated with the reverse rate, $k_T^-$', is that of the transition state:

$$k_T^{-}{}' = k_T^{-} e^{\gamma(n-1)d\Delta/2k_BT} \quad (4\text{-}25)$$

The mechanisms by which surface-tethered EB1 can bind to the protofilament are shown in Figures 4-9 C and D. Surface-bound TE can attach to the protofilament with a forward rate of $k_{on}'$ and a reverse rate of $k_-'$ (pathway C), given by Equations 4-26 and 4-27, respectively.

$$k_{on}' = k_{on} C_T e^{\gamma(n-1)d\Delta/2k_BT} e^{-\gamma((n-1)d)^2/2k_BT} \quad (4\text{-}26)$$

$$k_-' = k_- e^{\gamma(n-1)d\Delta/2k_BT} \quad (4\text{-}27)$$

The contribution of the transition state and spring energies are equal to that in equations 4-24 and 4-25. If the surface is initially tethered to unbound EB1 (pathway D), the on-rate of EB1 to the filament is twice that of $k_{on}'$ since EB1 is a homodimer that can bind with either one of its heads equally. For either pathway, C or D, the on-rate of EB1 in solution to a protofilament-bound subunit changes depending on whether EB1 binds to the terminal tubulin subunit ($k_{on}$) or a subunit on the side of the filament ($k_{on}^{side}$).

EB1 bound to the protofilament by only one of its heads has the potential to "walk" along the protofilament toward the plus- or minus-end. These two potential pathways are shown in Figure 4-9 E and F. If the EB1 motor walks in the plus direction (pathway E), no energy is exerted on the spring and the rates of reaction are those for a single EB1 head binding to the protofilament subunit. However, these rates will depend on whether the EB1 head binds to the terminal subunit ($k_+$ and $k_-$) or to the side of the filament ($k_+^{side}$ and $k_-^{side}$). If the EB1 motor walks in the minus-direction (pathway F), the kinetic rates will be affected by the transition and spring energies. These rate equations are described in Equations 4-28 and 4-29.

$$k_+^{side}{}' = k_+^{side} e^{\gamma(n-1)d\Delta/2k_BT} e^{-\gamma((n-1/2)d)^2/2k_BT} \quad (4\text{-}28)$$

$$k_-^{side}{}' = k_-^{side} e^{\gamma(n-1)d\Delta/2k_BT} \quad (4\text{-}29)$$

Figure 4-10 shows the various ways tubulin can add to the protofilament plus-end that involve the linking protein. Tubulin can add directly to the plus-end of the surface-tethered protofilament (mechanism A), tubulin can be transferred to the protofilament plus-end by surface-tethered TE (Tk-TE) or TTE (Tk-TTE) as seen in pathways B and C, respectively, or the protofilament-tethered TE can shuttle tubulin to the protofilament end (mechanism D). Only the on-rates, not the reverse rates, for these reactions are affected by the interaction with the tethering protein. For all four pathways (A-D), when there is an applied force against the surface (in the opposite direction of protofilament growth), $F$, the tubulin on-rates are reduced by a factor of $e^{-Fd/k_BT}$.

For direct tubulin addition in pathway A, the forward rate, $k_f'$ is proportional to the on-rate of tubulin addition, $k_f$, and the effect of force, as shown in Equation 4-30. There is also an effect of the spring energy due to the insertion of tubulin and extension of the spring.

$$k_f' = k_f e^{-\gamma((n-1)d)^2/2k_BT} e^{-Fd/k_BT} \tag{4-30}$$

Tubulin transferred to the protofilament end by Tk-TE or Tk-TTE (pathways B and C) are both proportional to the on-rate of TE (or TTE) to the protofilament plus end, $k_f^E$, as seen in Equation 4-31. There is also an effect from $C_T$ and any load applied to the motile surface. The on-rate of tubulin in these pathways is twice that of $k_f^E$' because of EB1's dimeric structure.

$$k_f^E' = k_f^E C_T e^{-Fd/kT} \tag{4-31}$$

Tubulin shuttled to the protofilament plus-end by filament-bound EB1 (pathway D) has a corresponding on-rate of $k_f^E$''. This forward rate (Equation 4-32) has an effect from applied force, spring energy, and from the local effective concentration of the EB1 head, $C_{eff}$. This local concentration is estimated based on the 3-D normal distribution on a half-sphere (see section 4.2.3).

$$k_f^{E}'' = k_f^{E} C_{eff} e^{-\gamma((1/2)d)^2/2k_BT} e^{-Fd/k_BT} \quad (4\text{-}32)$$

### 4.2.2 Protofilament End-Tracking Model

Considering the above reactions, stochastic models were performed to analyze the behavior of divalent, EB1 end-tracking motors operating on a single, growing microtubule protofilament. The model used to simulate the various reaction pathways is very similar to the model in section 4.1.4, where the pathway taken by the EB1 motor was determined by the probability of the corresponding kinetic reaction occurring (Appendix B.3.4 contains Matlab code).

### 4.2.3 Parameter Estimations

The kinetic parameters used in this chapter section that were also used in section 4.1 were determined the same way. The on-rate of Tk and EB1 binding ($k_T$) was estimated as 5 $\mu M^{-1}s^{-1}$ and the off-rate, $k_T^-$ was calculated from the value of $K_T$ provided ($K_T=k_T^-/k_T$). The value for $v$ used to calculate the tubulin on-rate from Equation 1-1 was 170 nm/s (Piehl and Cassimeris, 2003), which was assumed to be the irreversible elongation at the protofilament plus-end. $C_T$ was estimated as 100μM. It was assumed that the bond between EB1 and the protofilament is a slip bond (i.e., tension force on the motile surface would increase the dissociate rate of EB1 to the microtubule). The transition state distance for this slip bond was estimated as 20 percent of a typical bond length, or 1 nm.

### 4.2.4 Results

In the presence of a force, $F$, the surface-tethered protofilament polymerized in the direction of the surface. The effect of force on the velocity of the protofilament was analyzed. The values for $F$ were varied, which consequently affected the kinetic rate equations and corresponding probability for the pathways that are dependent on force. The resultant protofilament velocity was determined by dividing the total length of tubulin dimers added to the protofilament

plus-end ($n_{add} \cdot d$) by the total simulation time, $t$. This model also provided the state of the terminal subunit, position of the linking protein, the time-averaged fluorescence along the protofilament, and time spent in each pathway.

Figure 4-11 shows the force-velocity profiles for a polymerizing protofilament with surface-tethered EB1 end-tracking motors. To analyze the effect of the affinity modulation factor n the velocity profile, several affinity modulation factors were considered (Figures 4-11 A-E). Regardless of the value of $f$, the velocity decreased as the force increased because the force is opposite the direction of growth. For $f$=1 and $f$=10, velocities at forces greater than the stall force (force at which the velocity is zero) were negative; at larger values of $f$ the velocity decayed slower and approached zero as the force increased.

These figures also show the effect of $K_T$ on the velocity profile. Since $K_T$ is the dissociation constant for EB1 and Tk, it represents the strength of the interaction between the protofilament and the motile surface, and the protofilament cannot attach to the surface if EB1 is not bound to Tk. For all values of $f$, a $K_T$ value of 10 μM resulted in a maximum velocity of approximately 80 nm/s. This value is similar to the expected reversible elongation speed of the protofilaments is 85 nm/s (Equation 1-3), based on the rates determined for tubulin polymerization and depolymerization.

At decreasing values of $K_T$, the velocity at $F$=0 decreased, which is possibly due to the tether between the protofilament and the motile surface. At lower values of $K_T$ this interaction is less likely to dissociate, therefore more energy is required to insert a tubulin at the plus-end. At all affinity modulation factors, the value of $K_T$ did not affect the stall forces. However, it is expected that as $K_T$ increases, the protofilament will spend less time attached to the surface and will not be able to generate significant forces against a load. At $K_T$=10 $\mu M^{-1}s^{-1}$, the stall force

increased with increasing values of $f$, from 0.37 pN (at $f$=1) to ~1.7 pN (at $f$=1000), as seen in Figure 4-11 F.

Figure 4-12 summarizes the effect of $K_T$ and $f$ on the stall force, with the corresponding data in Table 4-1. The thermodynamic stall forces are shown for comparison to the simulation results. It is clear from the diagram that $K_T$ has little effect on the stall forces. When $f$=1, there is no affinity modulation and EB1 binds to T-GTP and T-GDP with equal affinity, hence the model is comparable with the Brownian Ratchet Mechanism. Therefore, it is not surprising that the resulting maximum achievable force at $f$=1 correlates well with the thermodynamics values, and is equal to that of the Brownian Ratchet Model, 0.37 pN. For $f$ >1, the stall forces were lower than the predicted thermodynamic values. At increasing values of the affinity modulation factor, the simulated stall forces increasingly deviated from the thermodynamic values. The reason the reactions stalled at forces lower than the thermodynamic limit is that there are parallel pathways of tubulin addition/dissociation (i.e., the direct tubulin addition/dissociation pathway and the end-tracking pathway), and the net tubulin dissociation is favored thermodynamically for the direct pathway and at higher forces. Increasing $f$ past a value of 1000 did not provide any additional effect on the stall force. Both $k_r^E$ and $k_-$ are inversely proportional to $f$, so an increase in $f$ favors the forward reactions for the mechanisms corresponding to these rates. But, as $f$ approaches infinity, it reaches a point in which the $k_r^E$ and $k_-$ become zero and no increase in $f$ will favor the forward reaction further.

To determine how this end-tracking mechanism mediates tubulin addition and to understand the effects of $f$ and $K_T$ on the velocity profiles (Figures 4-11 and 4-12), the frequency of the different pathways possible for association or dissociation of tubulin were measured and the resulting percentages are displayed in Figure 4-13. For an affinity modulation factor of

1000, when the $F$=0 and $K_T$ =0.1 μM, the protofilament spent 47% of its time in free tubulin association at the protofilament plus-end. But, when the force was increased to 2.1 pN (near the stall force), the percentage in the forward and reverse pathways were equal (50%), which explains the zero velocity at this force (Figure 4-11 D). An increase in $K_T$ from 0.1 to 10 μM when $f$=1000 and $F$=0, resulted in a larger percentage of time spent associating tubulin (47% versus 58%, respectively), which explains why the initial velocity was slightly higher when $K_T$ =10 μM (Figure 4-11 D). The same result was found when $f$=1; at $F$=0 pN, the percentage spent in the forward pathway at $K_T$=10 μM (78%) was significantly greater than at $K_T$=0.1 μM (32%), and resulted in a higher initial velocity at $K_T$=10 μM (Figure 4-11 A). When comparing the two affinity modulation factors (at $K_T$=10 μM and $F$=2.1 pN) the time spent associating tubulin at $f$=1 was 93%, which was higher than when $f$=1000 (85%). This result explains why lower values of $f$ resulted in negative velocities at large forces (Figure 4-11 F).

The percent of time the protofilament spent bound and unbound to the motile surface is shown in Figure 4-14. The unbound percentage increased with larger values of $K_T$ or $F$. Also, when a protofilament was surface-tethered, it was usually bound at its terminal or penultimate subunit. The forward rate equation in Equation 4-33 shows that when the linking protein binds to EB1 on the terminal subunit ($n$=1), the on-rate is proportional to $k_T C_T$. But when $n$ is greater than one, the on-rate, $k_T'$, is reduced to nearly zero. Therefore, no matter what the value of $k_T$, the linking protein either binds to terminally bound EB1 or most likely it does not bind to any filament-bound EB1.

The state of the terminal subunit in the filament was determined for each simulation to analyze the effect of $f$ and $K_T$ on the EB1 binding behavior. The fraction of time spent in each state is shown in Figure 4-15, where states Tk2, Tk3, and Tk4 represent states in which the

linking protein is bound to EB1, TTE or $dbE_+$ on the protofilament, respectively. For all variations of $K_T$, $F$, and $f$, most of the time the terminal subunit was in the unbound state (state 1). When $f$=1, the terminal subunit was in state Tk3 or Tk4 a significant fraction of time; when $f$=1000, S1 was in state 4 and Tk4 a large amount of time. The most significant difference in the state of the filament is when $K_T$ is 0.1 versus when $K_T$ is 10 (for both values of $f$); the larger $K_T$ value resulted in more subunits being unbound from EB1.

A graphical representation of the bound versus unbound fraction of terminal subunits for each combination of $f$, $K_T$, and $F$ is shown in Figure 4-16. The most significant result is that when $f$=1000, the unbound fraction decreased with increasing force, but when $f$=1 the unbound fraction increased with increasing force. This result has a significant implication for the role of the motor. When the force was increased at $f$=1, the frequency EB1-bound tubulin addition decreased (Figure 4-13). However, with large affinity modulation ($f$=1000), the frequency of tubulin addition occurs increased. Therefore, at large forces, affinity modulation allows EB1 to facilitate tubulin addition and maintain a persistent attachment to the motile surface.

When the linking protein is unbound from the protofilament, the state of the linking protein varied depending on the force and the affinity modulation factor (Figure 4-17). When the force was zero the state of the linking protein was mostly either unbound or bound to E or TE, which makes it easier to bind to the protofilament. When the force increased to 2.1 pN and $f$=1000, most of the linking protein are mostly bound to TE. When $f$=1 and force is 2.1 pN, most of the linking proteins were unbound or bound to TTE, which makes it easier to bind to the protofilament.

## 4.3 Summary

To account for the dimeric structure of EB1, this chapter discusses the models we have developed that simulate the growth of one protofilament in the presence of either tethered or

non-tethered, divalent EB1 end-tracing motors that processively linking protein the plus-ends of protofilaments. Because EB1 is divalent, even if one of its heads dissociates upon hydrolysis of its bound tubulin, the other EB1 head can remain bound to the protofilament. Hence, the divalent end-tracking model has an advantage over the monovalent end-tricking model and the Brownian ratchet mechanisms by maintaining a high EB1 concentration at the protofilament plus-end and allowing rapid MT polymerization

### 4.3.1 Non-Tethered Protofilaments

This model assumes that EB1 is not tethered to a motile surface, but is allowed to bind to tubulin in solution. By allowing tubulin addition (to the protofilament plus-end or side) from solution or by copolymerization with EB1, protofilament-bound tubulin can be in various EB1-binding states. The probability of tubulin being in any one of these states was used to determine the optimal dissociation constant for EB1 and tubulin in solution ($K_1$) that would result in the 4.2 binding ratio. As in the monovalent case, the Brownian ratchet mechanism was not able to obtain the expected 4.2 EB1 binding ratio at any value of $K_1$. EB1-tubulin interactions with large affinity modulation resulted in an optimal value for $K_1$ of 0.65 μM, which was used to determine the occupational probability of EB1 along the length of the protofilament. The results of this analysis demonstrates the advantage of the end-tracking model over the Brownian ratchet mechanism to preferentially bind to the protofilament plus-end and provide a decay behavior as seen in experiments. In addition, the model is able to simulate the occupational probability providing a 4.2 ratio of EB1 binding at the plus-end versus the side of the protofilament.

We also created a model that analyzes the average, equilibrium fraction of EB1 bound to the protofilament. This model only allows EB1 to bind to the sides of a protofilament (rich in GDP-bound subunits) and prevented the protofilament from growing. The results of this model

show that the affinity modulation of EB1 does not affect this side-binding behavior. The resulting fraction of subunits bound to EB1 was 2.6%, which is close to the expected equilibrium value of 2.4%. The same analysis was performed for growing protofilaments. The resulting average EB1-bound fraction of subunits shows a slightly larger fraction of EB1 binding at the plus-end when the affinity modulation factor is greater.

### 4.3.2 Tethered Protofilaments

The tethered protofilament end-tracking model simulates EB1 end-tracking motors operating on a growing protofilament plus-end, and introduces a co-factor protein that tethers EB1 to a motile surface. Unlike the monovalent end-tracking model, this model allows association and dissociation of the tethering protein to the motile surface and of EB1 to the tethering protein. The tethering protein was modeled as a Hookean spring, which translates its potential energy from mechanical work at the protofilament plus-end. This model also accounts for any transition state effects on the on-and off-rates due to binding between surface-tethered EB1 and the protofilament.

The force-velocity relationships developed from this model were compared to the Brownian ratchet mechanism. Under no affinity modulation, the model predicts values consistent with the thermodynamics values and comparable to the Brownian Ratchet mechanism, with a resulting stall of 0.37 pN. The end-tracking model provides a stall force up to 5 times greater than that of the Brownian Ratchet mechanism. Depending on the affinity of the interaction between EB1 and tubulin, the resulting stall force in the end-tracking model can range from 0.72 pN to 1.95 pN. However, as affinity modulation increases, the resulting stall forces deviate from the stall forces predicted by thermodynamics because the net tubulin dissociation is favored thermodynamically for the direct pathway and at higher forces. The effect of the dissociation rate of EB1 from the linking protein does not affect the stall force of the

end-tracking model, but it does affect the maximum protofilament velocity. We show that an increase in $K_T$ results in an increase in the maximum velocity, and vice-versa. A $K_T$ value of 10 μM allows the protofilament to grow at a rate of 80 nm/s which is comparable to the calculated value of 85 nm/s for reversible elongation.

At large forces (2.1 pN), the end-tracking model is able to maintain a persistent attachment of the protofilament plus-end (specifically the terminal and penultimate subunits) to the motile surface (71% of time); whereas the protofilament in the Brownian ratchet model spends most of the time (36%) un-tethered. This result suggests that the EB1 end-tracking motors are able to maintain persistent attachment of the protofilament end to the motile surface, translating its filament-bound hydrolysis energy to mechanical work and allowing the protofilament to grow even under large loads.

Figure 4-1. Mechanisms of a non-tethered, divalent end-tracking motor. A) Top-left: EB1 and T-GTP free in solution. EB1 binds to the protofilament in two ways: after tubulin addition (clockwise) or copolymerizing with tubulin (counter-clockwise). Clockwise: T-GTP adds to the protofilament end ($k_f$) and induces hydrolysis of the penultimate tubulin subunit; EB1 binds to T-GTP at the protofilament end ($2k_{on}$). Counter-clockwise: EB1 and T-GTP bind in solution ($2k_1$); Together, EB1 and T-GTP add to the protofilament end ($k_f^E$). B) Top-left: EB1 initiates bound to the GTP-rich protofilament plus-end. Free tubulin in solution binds to the protofilament in two ways: directly from solution (clockwise) or facilitated by the EB1 motor (counter-clockwise). Clockwise: Tubulin in solution adds to the protofilament end ($k_f$), which induces hydrolysis of the EB1-bound, penultimate tubulin subunit. The unbound EB1 head binds to the GTP-bound protofilament end ($k_+$). Counter-clockwise: The free EB1 head binds to tubulin in solution ($k_1$) and shuttles the protomer to the protofilament end ($k_f^{E'''}$). C) Top-Left: TE and T-GTP free in solution. TE binds to the protofilament in two ways: after tubulin addition (clockwise) or copolymerize as TTE (counter-clockwise). Clockwise: T-GTP binds to protofilament end ($k_f$), inducing hydrolysis of the penultimate subunit. TE binds to the T-GTP protofilament end ($k_{on}$). Counter-clockwise: TE binds to T-GTP in solution ($k_1$). TTE binds to the protofilament end ($k_f^E$) and induces hydrolysis of the penultimate tubulin subunit.

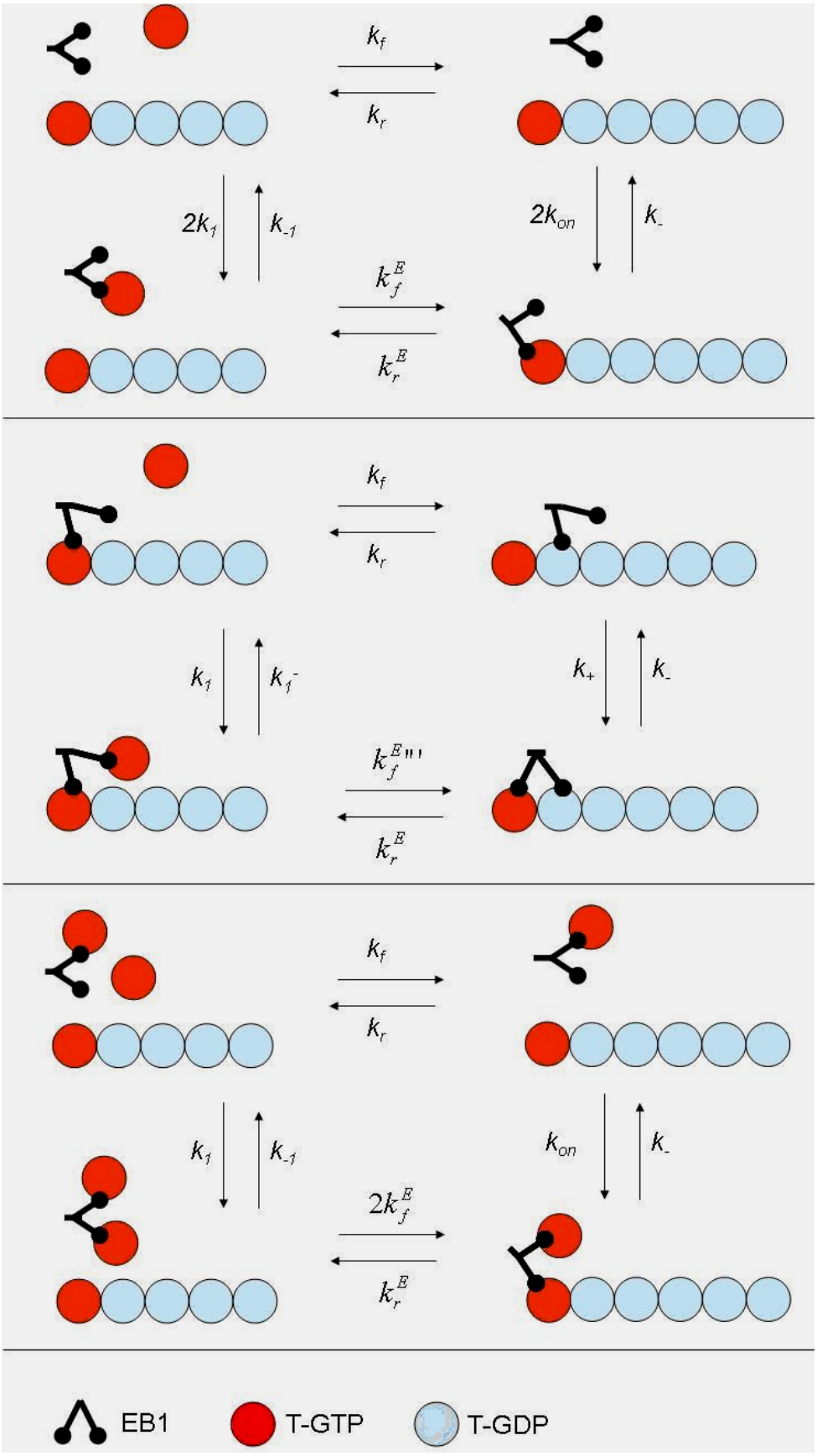
$k_f$
$k_r$
$2k_1$
$k_{-1}$
$2k_{on}$
$k_-$
$k_f^E$
$k_r^E$
$k_f$
$k_r$
$k_1$
$k_1^-$
$k_+$
$k_-$
$k_f^{E'''}$
$k_r^E$
$k_f$
$k_r$
$k_1$
$k_{-1}$
$k_{on}$
$k_-$
$2k_f^E$
$k_r^E$
EB1
T-GTP
T-GDP

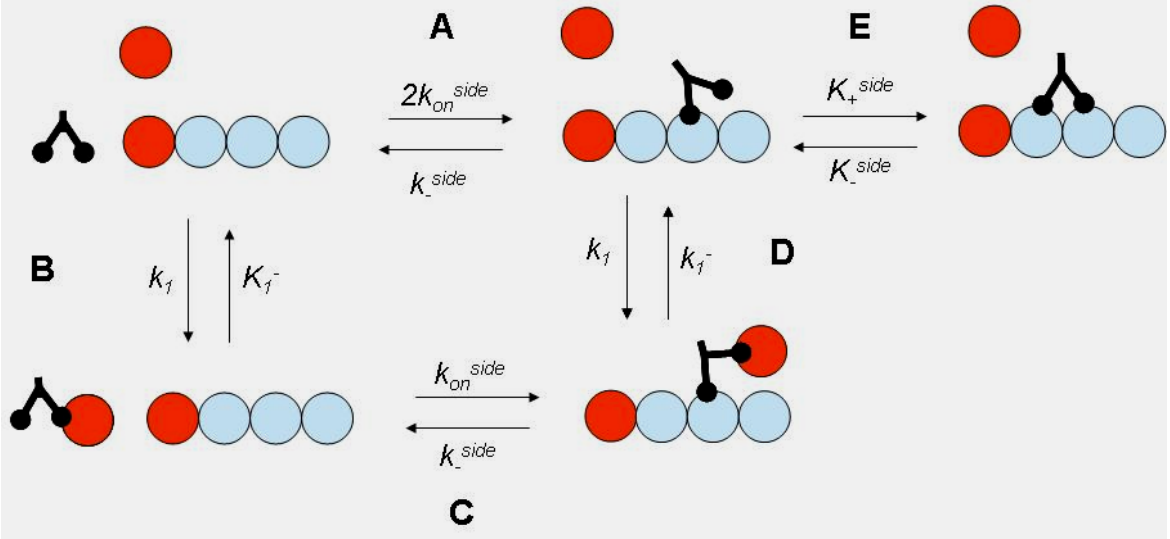


Figure 4-2. Mechanisms of equilibrium, side binding of EB1 to protofilament. Off-rates of EB1 binding to protofilament-bound GDP affected by affinity modulation factor. Tubulin addition and dissociation pathway neglected for this equilibrium mechanism.

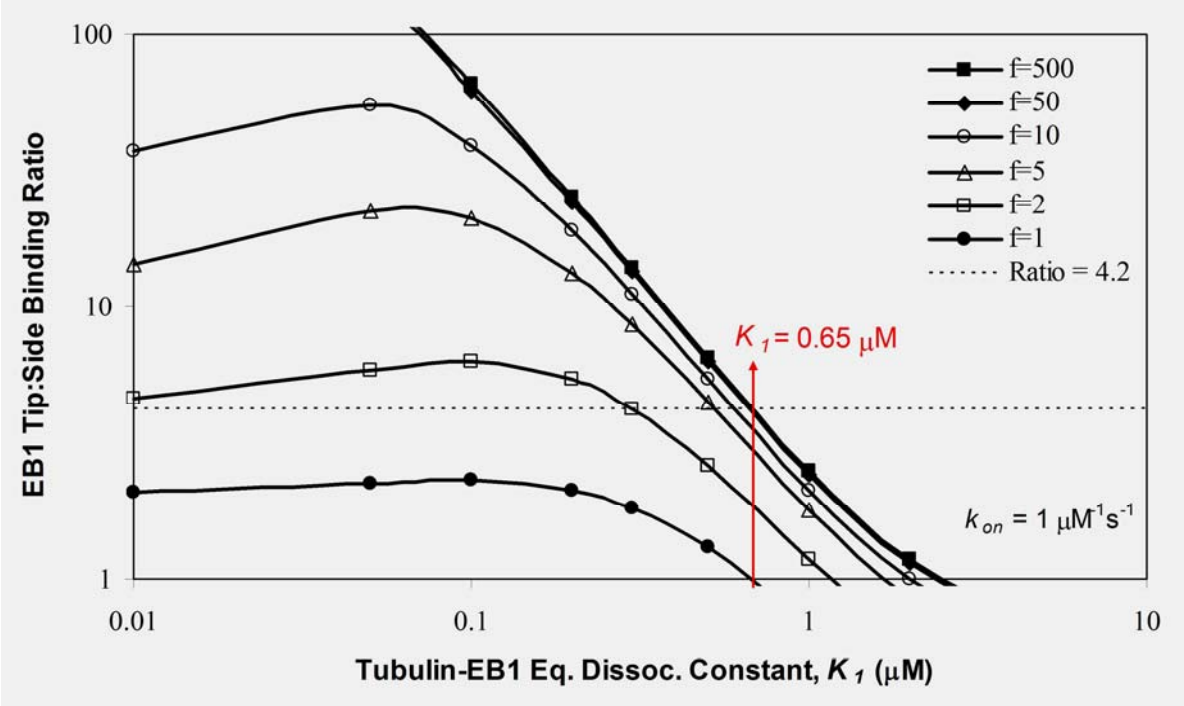


Figure 4-3. Choosing an optimal $K_1$ value for divalent EB1. The experimentally determined ratio of EB1 binding to the tip versus the side of a protofilament (4.2) is represented by the dotted line. Each curve represents a different affinity modulation factor value, $f$, and the data points correspond to the EB1 binding ratio at various values of $K_1$ and a $k_{on}$ of 1 $\mu M^{-1}s^{-1}$. The value of $K_1$ required to achieve a tip-to-side binding ratio of 4.2 for $50 > f > 1$ increases with increasing $f$. The optimal value of $K_1$ chosen was 0.65 μM where $f > 10$. The simulation time was 40 seconds.

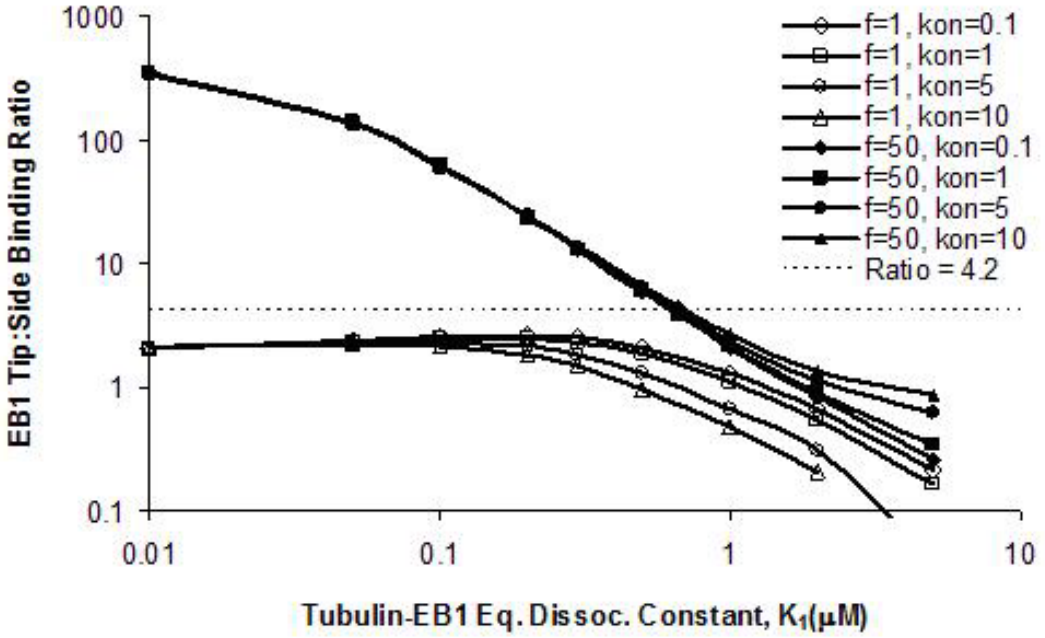


Figure 4-4. Effect of $k_{on}$ on optimal$K_1$. The experimentally determined ratio of EB1 binding to the tip versus the side of a protofilament (4.2) is represented by the dotted line. For affinity modulation factors of 1 and 50, the value of $k_{on}$ was varied from 0.1 to 10 $\mu M^{-1}s^{-1}$, and $K_1$ from 0.01 to 5 μM. The simulation time was 40 seconds. The optimal value of $K_1$ is not significantly affected by the value of $k_{on}$, and the optimal $K_1$ remains at 0.65 μM when $f$ =50.

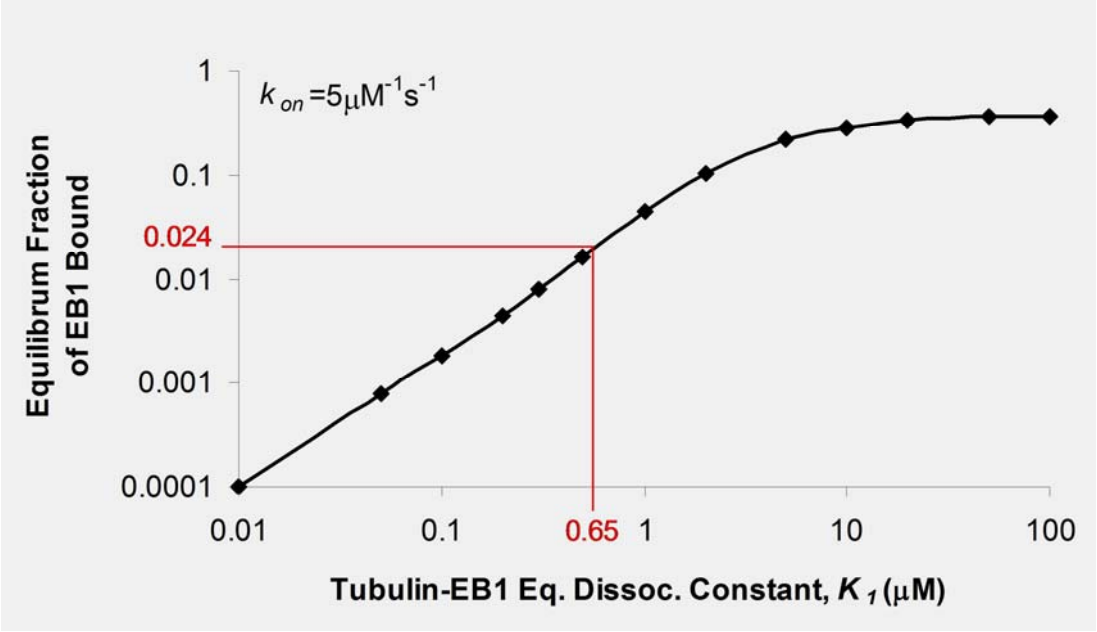


Figure 4-5. EB1 equilibrium binding. Data shown in figure is for a $k_{on}$ value of 5 μM$^{-1}$s$^{-1}$ and a simulation time of 40 seconds. At equilibrium, the percent of the protofilament bound to EB1 increases with increasing $K_1$. At large values of $K_1$ ($K_1$>10), the protofilament reaches an equilibrium with approximately 40% of EB1 bound. The value of $K_1$ used for simulations (0.65 μM) corresponds to an expected 2.4% of EB1 bound to the protofilament.

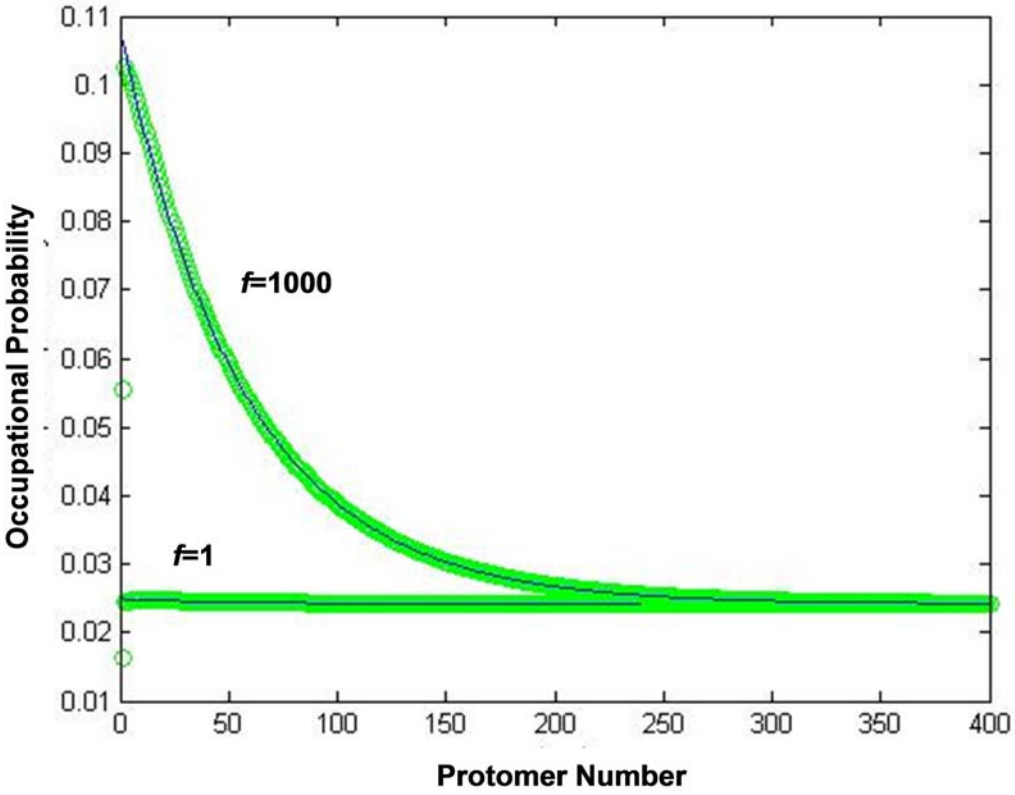


Figure 4-6. Occupational probability of EB1 along length of protofilament. Zero on the x-axis represents the protofilament plus (growing) end. Simulation time used was 40 seconds. Values for other variables: $K_1$=0.65 μM, $k_{on}$=5 $\mu M^{-1}s^{-1}$. Probability of EB1 when $f$=1 is nearly constant along the length of the protofilament. When $f$=1000, occupational probability at protofilament end (0.107) is ~4.2 times higher than $f$=1 (0.025); the probability decays along the length of the protofilament.

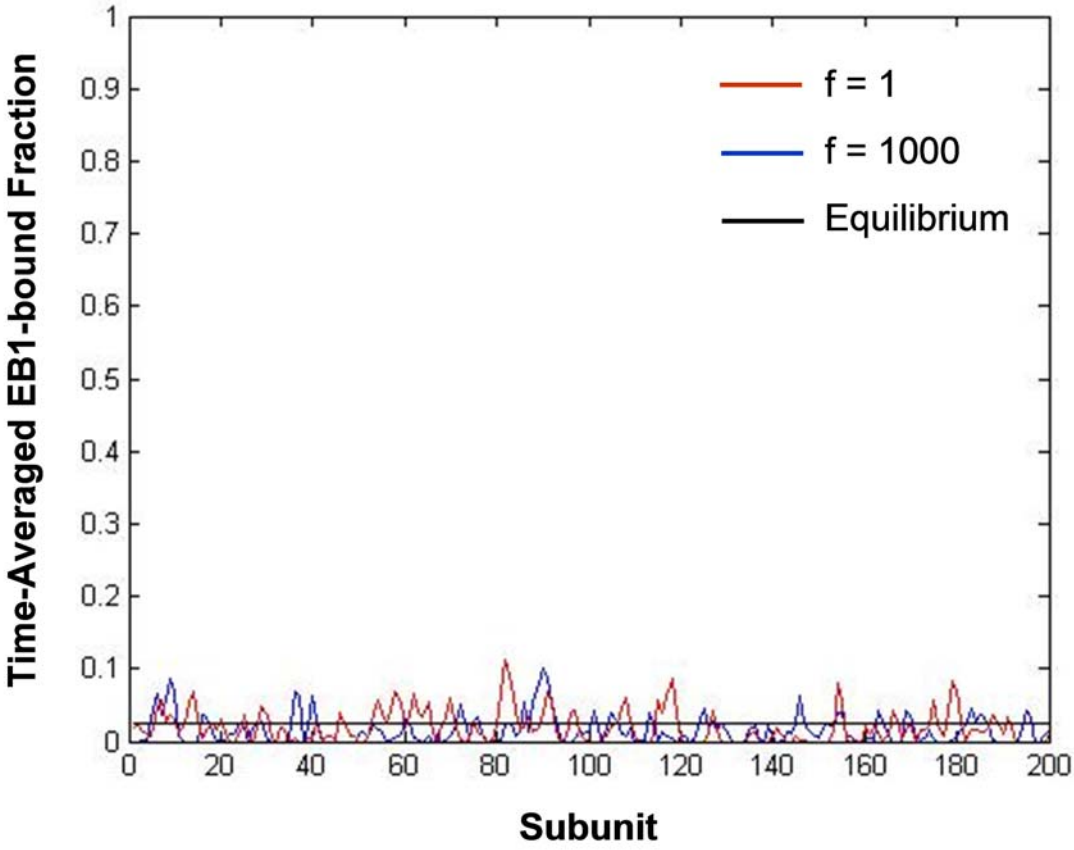


Figure 4-7. Time averaged EB1-bound tubulin fraction at equilibrium. Zero on the x-axis represents the protofilament plus (growing) end. Results for both $f$=1 and $f$=1000 shown. Values for other variables: $K_1$=0.65 μM, $k_{on}$=5 $\mu M^{-1}s^{-1}$. Equilibrium EB1-bound fraction represented by solid line at 0.024. Simulation time used was 80 seconds and $N$=200

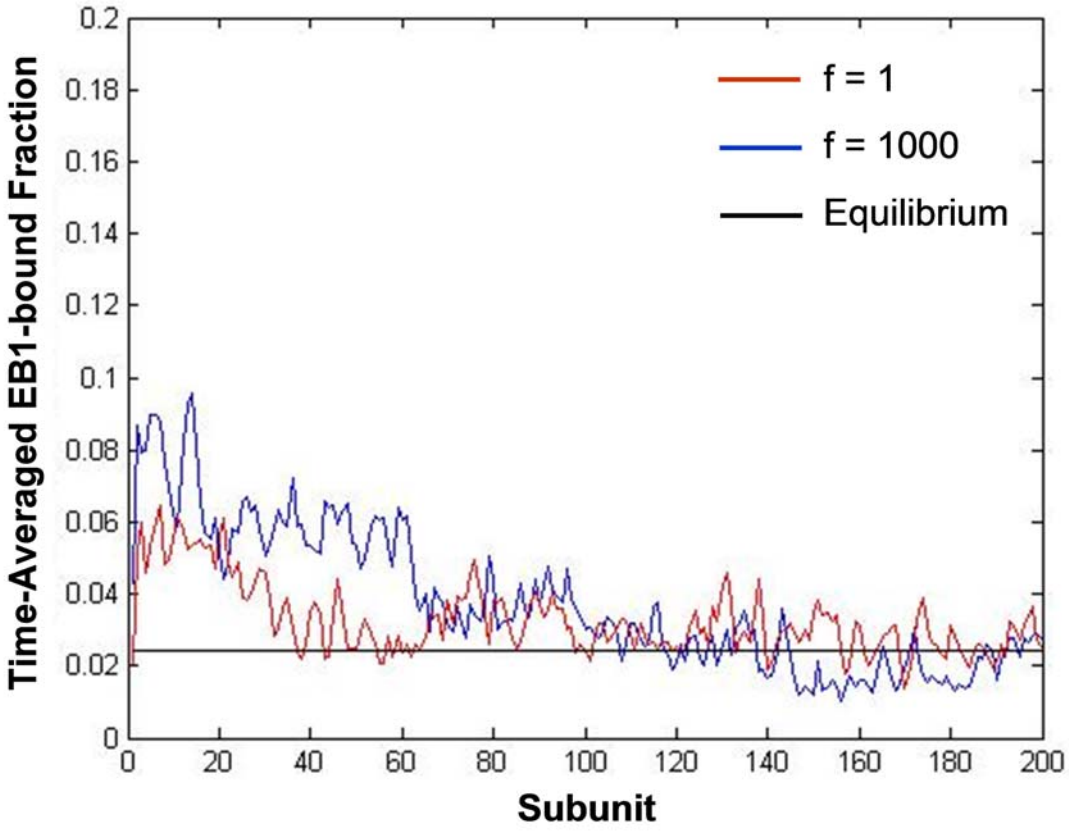


Figure 4-8. Time averaged fraction of EB1-bound subunits during protofilament growth. Zero on the x-axis represents the protofilament plus (growing) end. Results for both $f$=1 and $f$=1000 shown. Values for other variables: $K_1$=0.65 μM, $k_{on}$=5 $\mu M^{-1}s^{-1}$. Equilibrium EB1-bound fraction represented by solid line at 0.024. Simulation time used was 80 seconds and $N$=200.

Figure 4-9. Mechanisms of tethered, protofilament end-tracking model with divalent EB1. A) Pathway for tethering protein to bind to EB1 (or TE) in solution. B) Tethering protein binds to protofilament-bound EB1 (or TE). Energy is exerted by the spring, which is accounted for in the on- and off-rates ($k_T$' and $k_T$-'). C) Surface-tethered TE binds to protofilament plus-end with on rate of $k_{on}$'. D) Surface tethered EB1 has twice the on-rate due to EB1's dimeric structure. E) EB1 can "walk" along the protofilament in the plus direction (E) or minus direction (F). EB1 walking toward the minus-direction exerts no force on the spring, and has an on and off rate of $k_+^{side}$ and $k_-^{side}$, respectively. EB1 walking in the minus-direction exerts a force on the spring, which is accounted for in the on and off rates ($k_+^{side}$' and $k_-^{side}$')

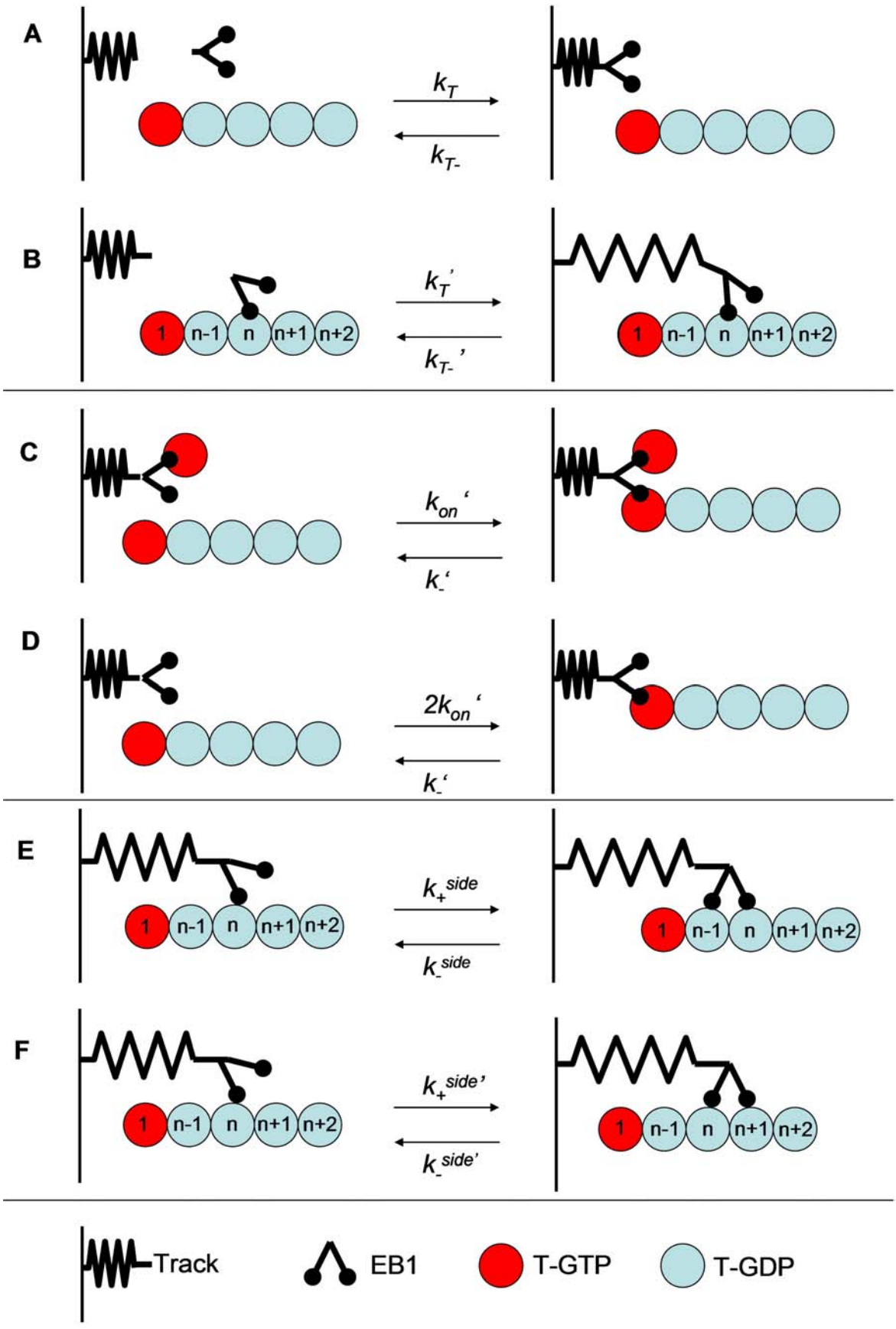
A
$k_T$
$k_{T-}$
B
$k_T'$
$k_{T-}'$
1
n-1
n
n+1
n+2
C
$k_{on}'$
$k_-'$
D
$2k_{on}'$
$k_-'$
E
$k_+^{side}$
$k_-^{side}$
F
$k_+^{side'}$
$k_-^{side'}$
Track
EB1
T-GTP
T-GDP

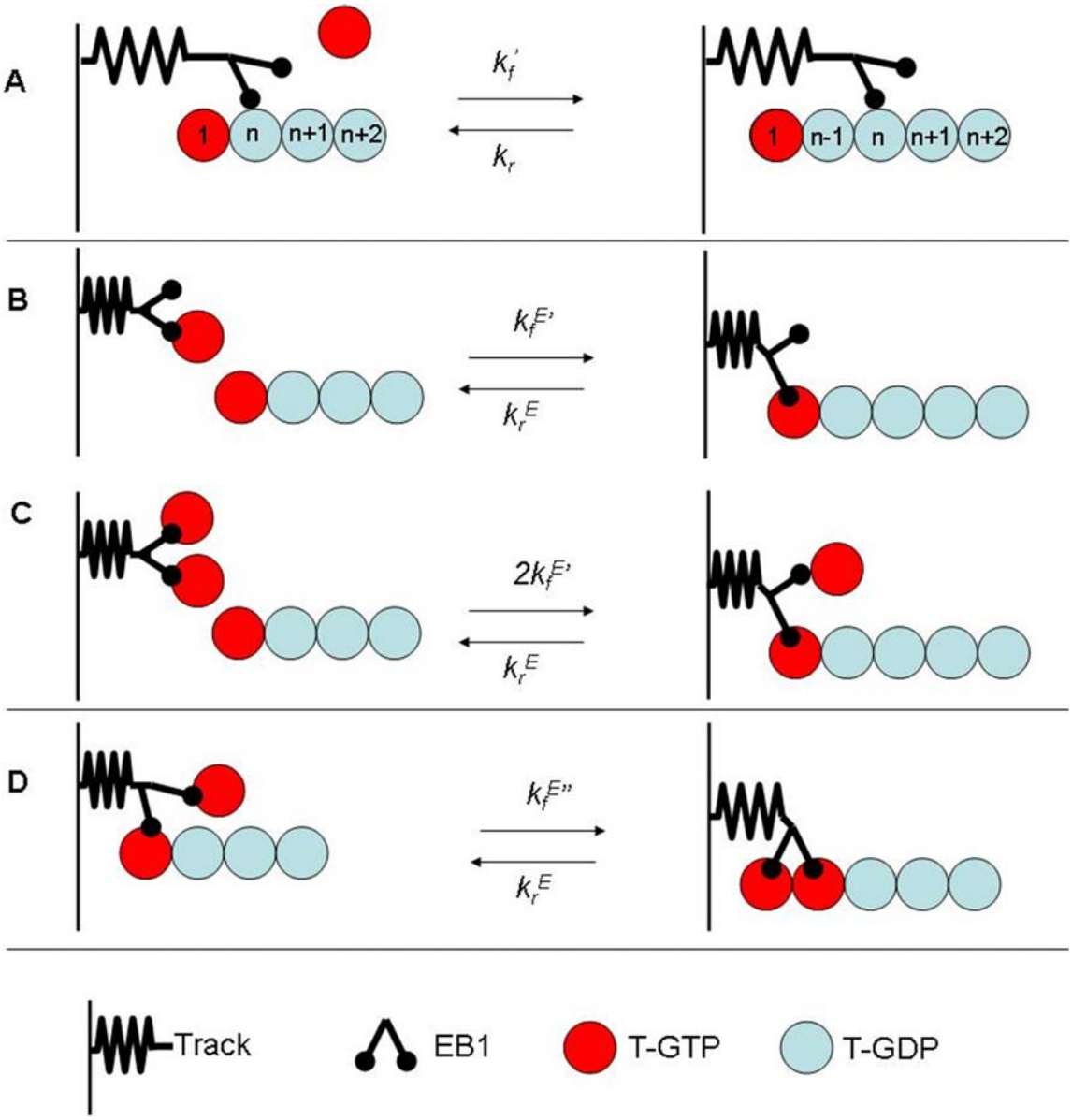


Figure 4-10. Mechanisms of tubulin addition to linking protein-bound protofilament. A) Tubulin can add to the plus-end of a surface-tethered protofilament. B, C) Tubulin bound to Tk-E or Tk-TE attaches to the protofilament end. Tubulin bound to Tk-TE has two configurations with which it can bind. D) Tubulin addition is facilitated by the filament-bound EB1 end-tracking motor. The forces exerted on the spring are accounted for in the forward rate constants for each mechanism.

Figure 4-11. Force-velocity profiles for tethered protofilaments bound to divalent EB1 end-tracking motors. The effect of force and velocity of both the Brownian Ratchet and End-Tracking models are shown. Simulation time used was 40 seconds. Values for other variables: $k_1$=10 $\mu M^{-1}s^{-1}$, $K_1$=0.65$\mu$M, $k_{on}$=5 $\mu M^{-1}s^{-1}$. $K_T$ values were varied (0.1, 1, 5, and 10 $\mu$M) in A – E to analyze the effects on the stall force. A) $f$=1 B) $f$=10 C) $f$=100 D) $f$=1000 E) $f$=10,000 F) Force-velocity profiles shown for varying values of $f$ (1,10,100,1000,10000) when $K_T$ =10 $\mu$M.

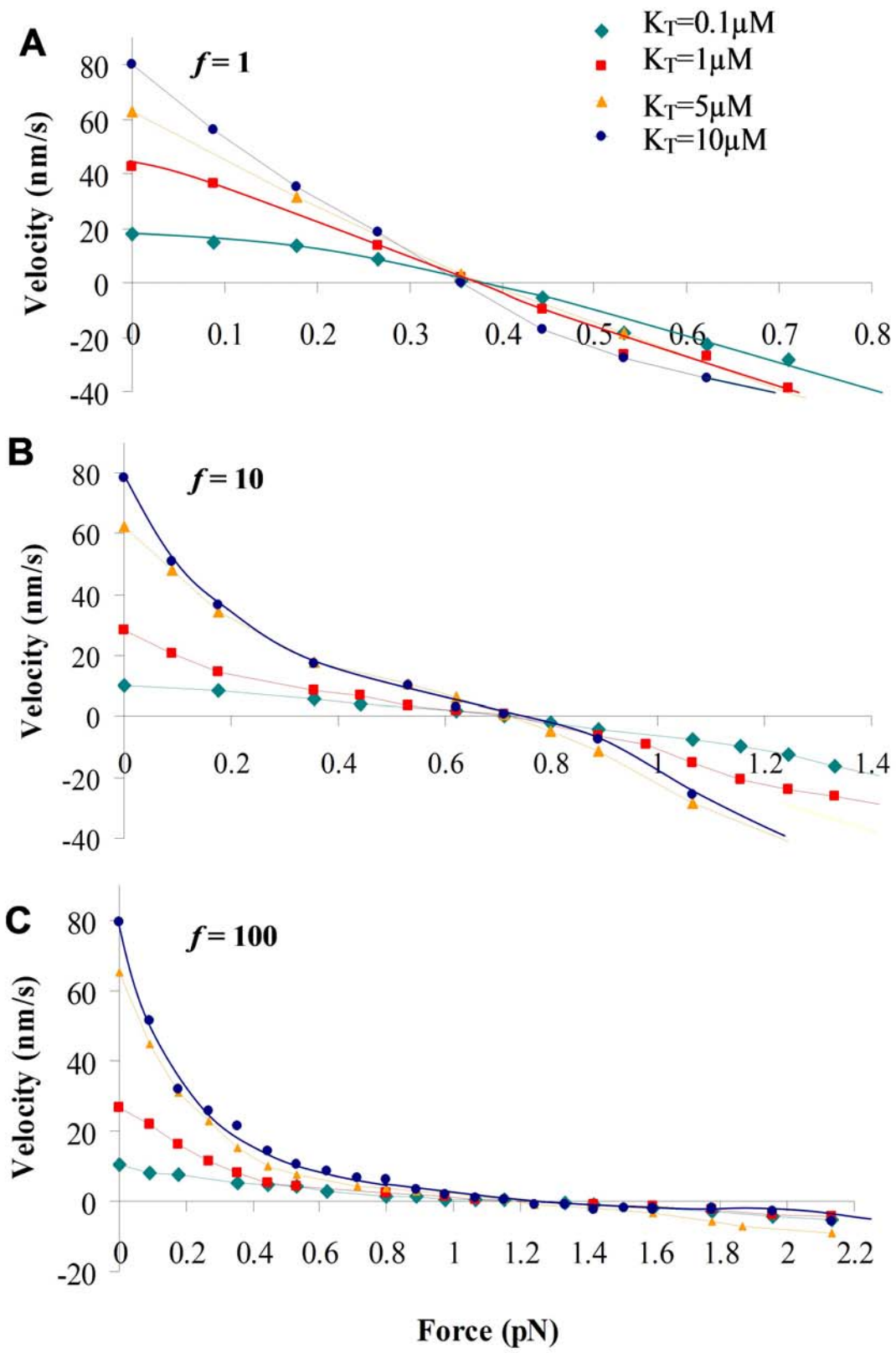
A
f = 1
K_T=0.1μM
K_T=1μM
K_T=5μM
K_T=10μM
Velocity (nm/s)
80
60
40
20
0
-20
-40
0
0.1
0.2
0.3
0.4
0.5
0.6
0.7
0.8
B
f = 10
Velocity (nm/s)
80
60
40
20
0
-20
-40
0
0.2
0.4
0.6
0.8
1
1.2
1.4
C
f = 100
Velocity (nm/s)
80
60
40
20
0
-20
0
0.2
0.4
0.6
0.8
1
1.2
1.4
1.6
1.8
2
2.2
Force (pN)

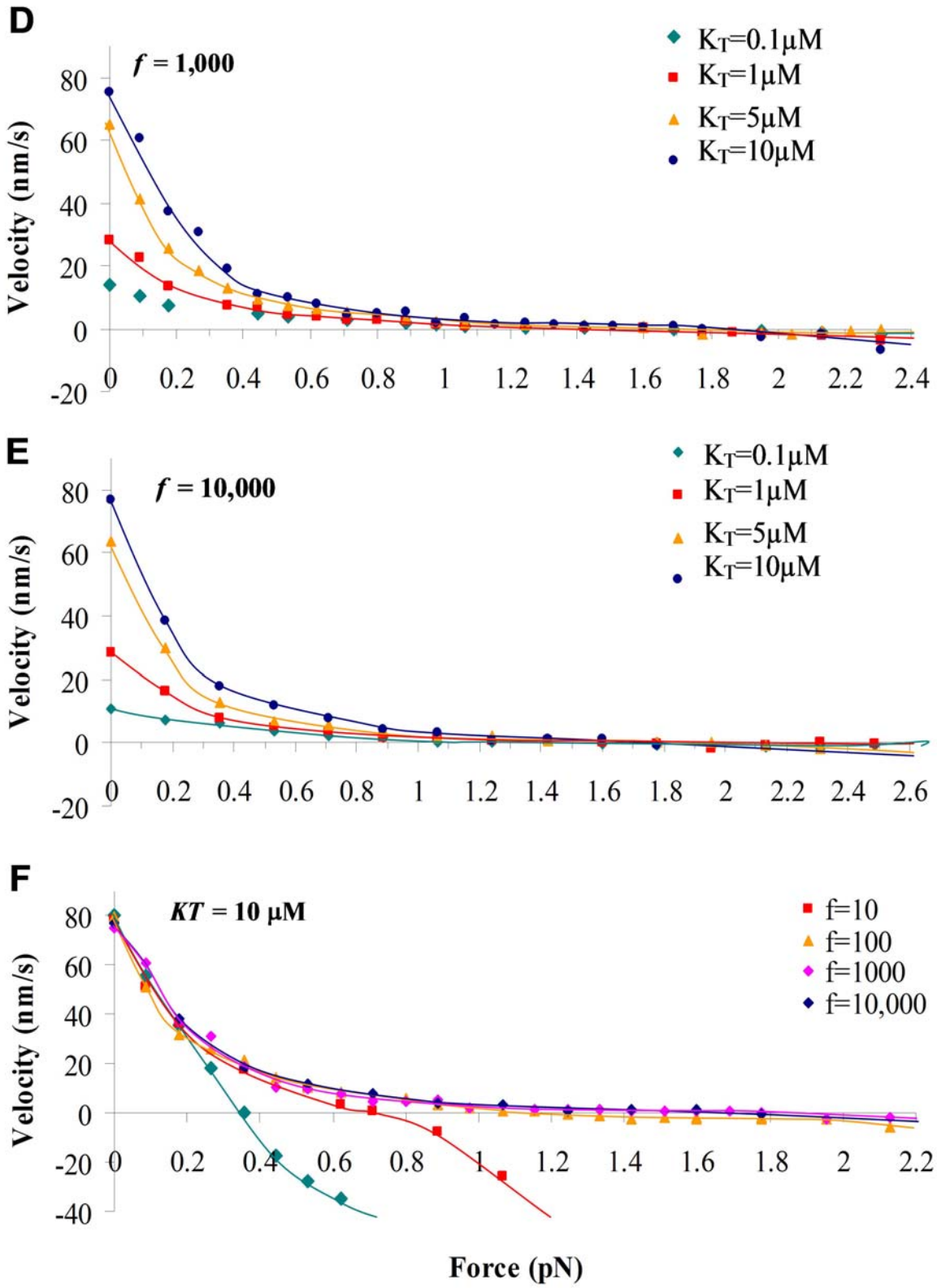
D
f = 1,000
Velocity (nm/s)
80
60
40
20
0
-20
0
0.2
0.4
0.6
0.8
1
1.2
1.4
1.6
1.8
2
2.2
2.4
KT=0.1μM
KT=1μM
KT=5μM
KT=10μM
E
f = 10,000
Velocity (nm/s)
80
60
40
20
0
-20
0
0.2
0.4
0.6
0.8
1
1.2
1.4
1.6
1.8
2
2.2
2.4
2.6
KT=0.1μM
KT=1μM
KT=5μM
KT=10μM
F
KT = 10 μM
Velocity (nm/s)
80
60
40
20
0
-20
-40
0
0.2
0.4
0.6
0.8
1
1.2
1.4
1.6
1.8
2
2.2
f=10
f=100
f=1000
f=10,000
Force (pN)

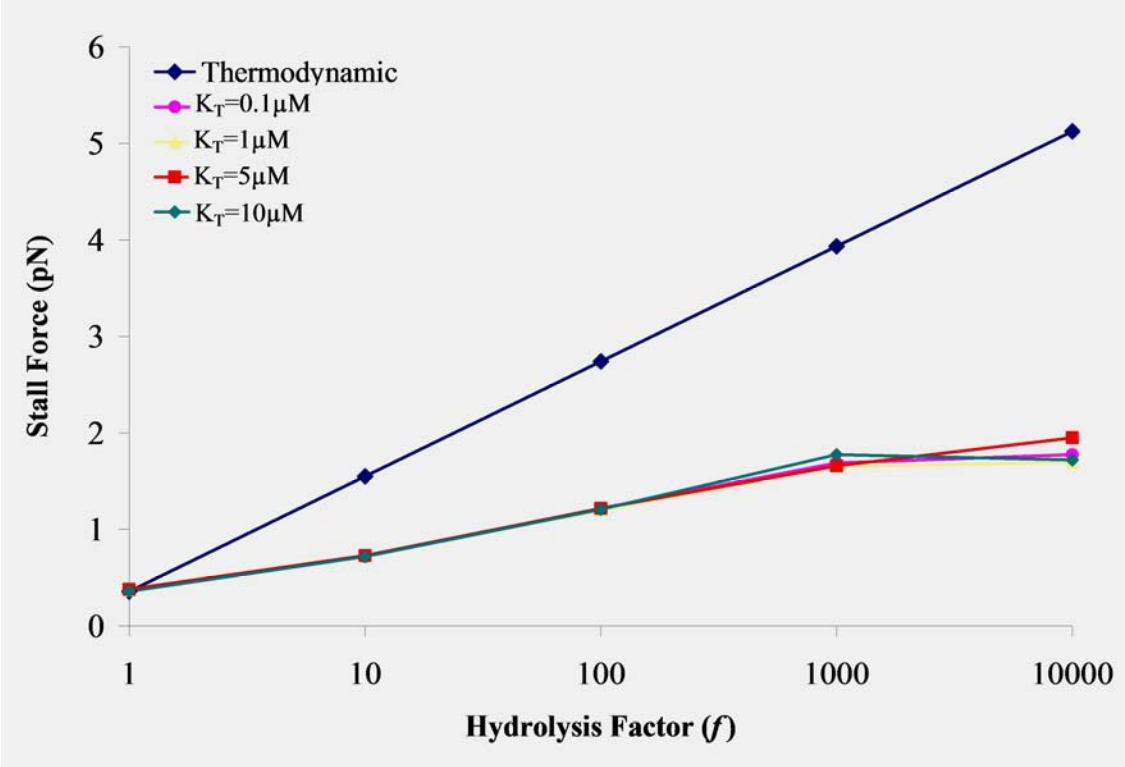


Figure 4-12. Stall forces versus affinity modulation factor at various $K_T$ values. Resulting stall forces for data in Figures 3-19 A-E. *Thermodynamic* represents the thermodynamic values at the various values of the affinity modulation factor, based on $k_BT$=4.14 pN-nm, $d$ = 8 nm, [Tb] = 10 μM, and $[Tb]_c$ = 5 μM. Data for this figure can be found in Table 4-1.

Table 4-1. Protofilament stall forces at varying values of $K_T$ and affinity modulation factors. Stall forces (in units of pN) correspond to the data represented in Figure 4-12.

| $f$ | Thermodynamic* | $K_T$ = 0.1 μM | $K_T$ = 1 μM | $K_T$ = 5 μM | $K_T$ = 10 μM |
|---|---|---|---|---|---|
| 1 | 0.36 | 0.37 | 0.37 | 0.38 | 0.36 |
| 10 | 1.55 | 0.72 | 0.73 | 0.73 | 0.72 |
| 100 | 2.74 | 1.22 | 1.2 | 1.22 | 1.21 |
| 1,000 | 3.93 | 1.69 | 1.65 | 1.66 | 1.78 |
| 10,000 | 5.13 | 1.78 | 1.7 | 1.95 | 1.72 |

*Thermodynamic values show the expected thermodynamic stall forces when $k_BT$ = 4.14 pN-nm, $d$ = 8 nm, [*Tb*] = 10 μM, and $[Tb]_c$ = 5 μM.

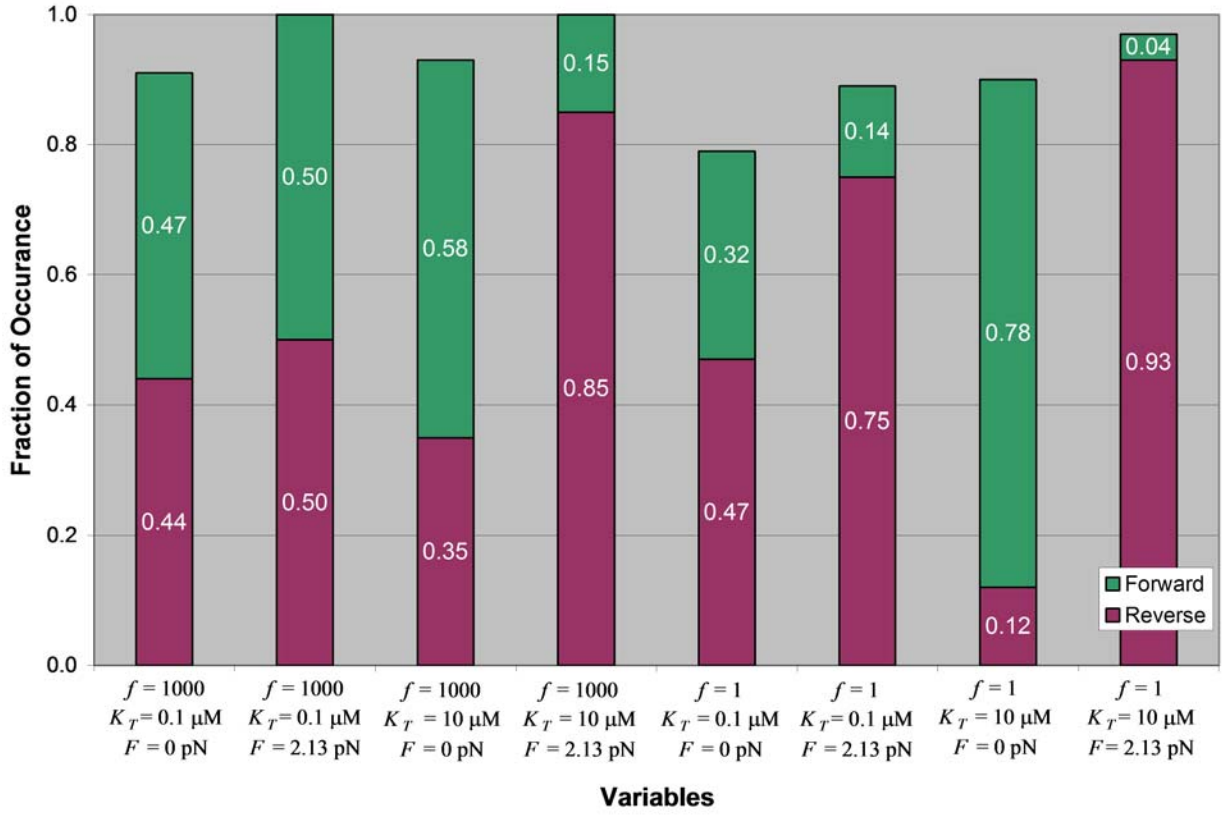


Figure 4-13. Effect of $f$, $K_T$, and $F$ on pathways taken. For each affinity modulation factor value (1 and 1000), forces of 0 and 2.13 pN were analyzed for both a $K_T$ value of 0.1 and 10 μM. For each $f$, $K_T$, $F$ combination, the percentage of time the protofilament advanced along a pathway that resulted in association or dissociation of a tubulin protomer is shown. Pathways occurring less than 5% of the time are not shown.

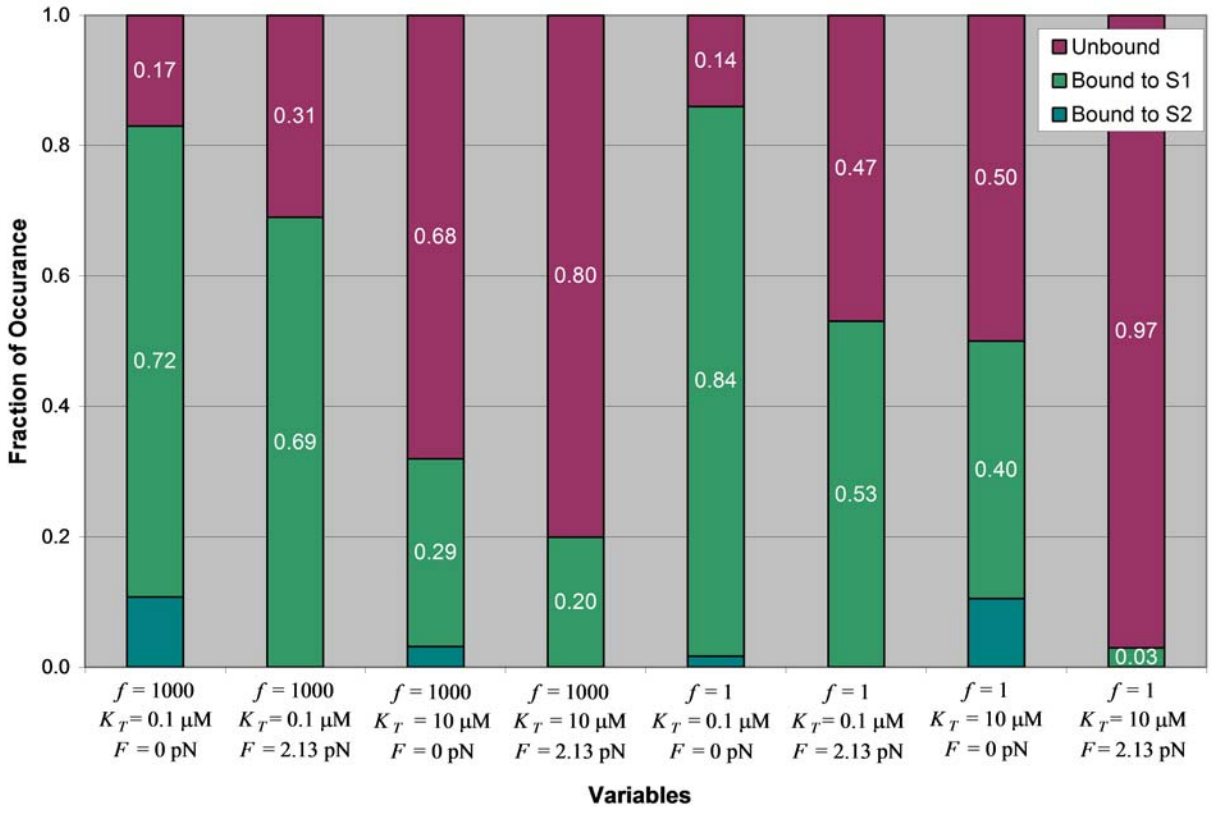


Figure 4-14. Percent of time protofilament bound and unbound to motile surface. The percentages listed are based on the same combinations of f, $K_T$, and F values considered in Figure 4-13. Protofilaments bound to the motile surface were consistently tethered at the terminal tubulin subunit (S1) or the second tubulin subunit (S2). Percentage of time bound protofilaments were tethered to either S1 or S2 shown for each combination of f, $K_T$, and F values.

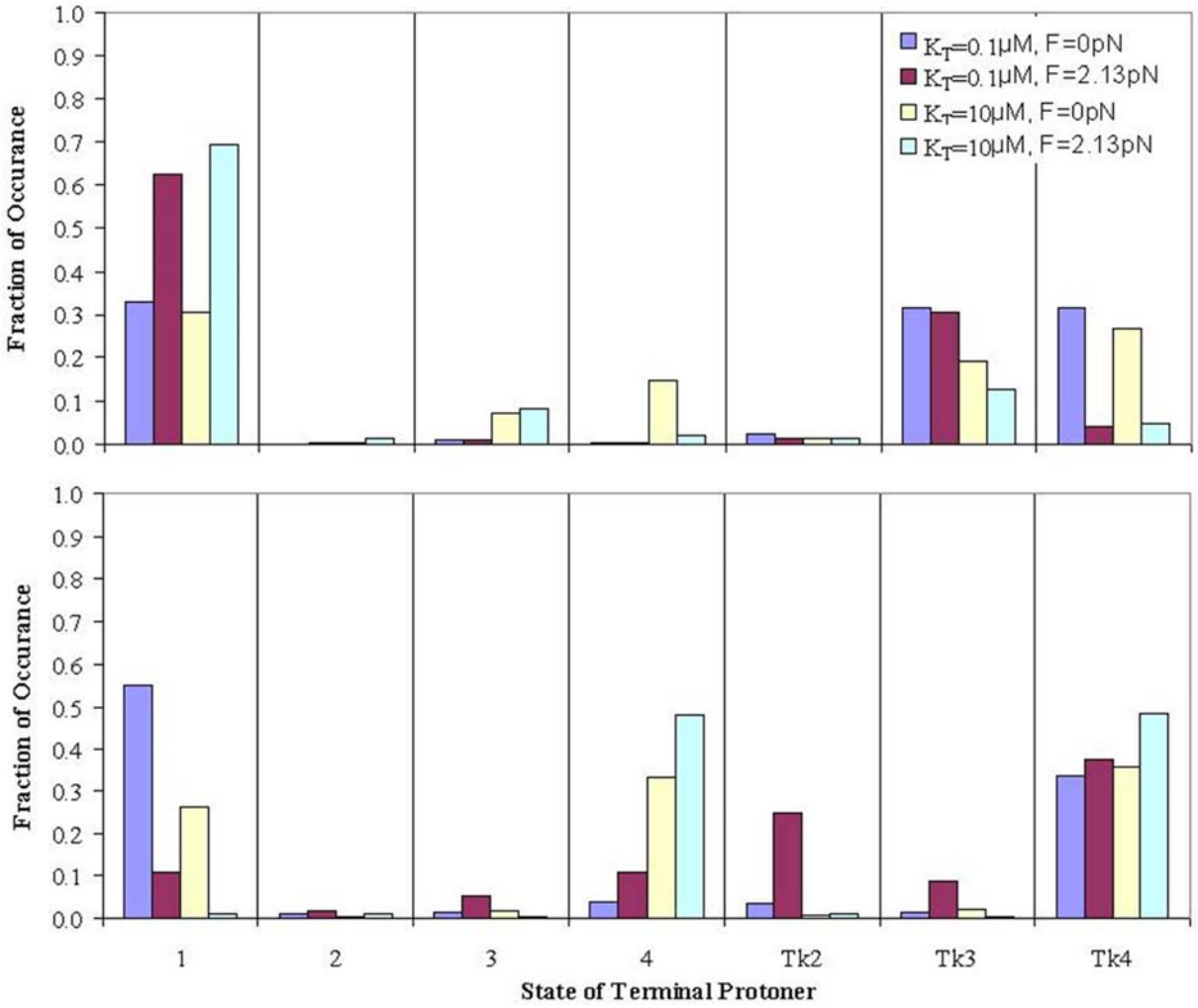


Figure 4-15. State of the terminal subunit (S1) when $f$=1 and $f$=1000. $K_T$ values of 0.1 and 10 μM and $F$ values of 0 and 2.1 pN were analyzed. The fraction of time the terminal tubulin subunit (S1) remained in each of each of the 7 different states is shown. The various states the protofilament subunits include: 1-unbound, 2-bound to E, 3-bound to TE, 4-bound to $dbE^+$, Tk2-bound to E tethered to linking protein, TK3-bound to TE tethered to linking protein, Tk4-bound to $dbE^+$ tethered to linking protein.

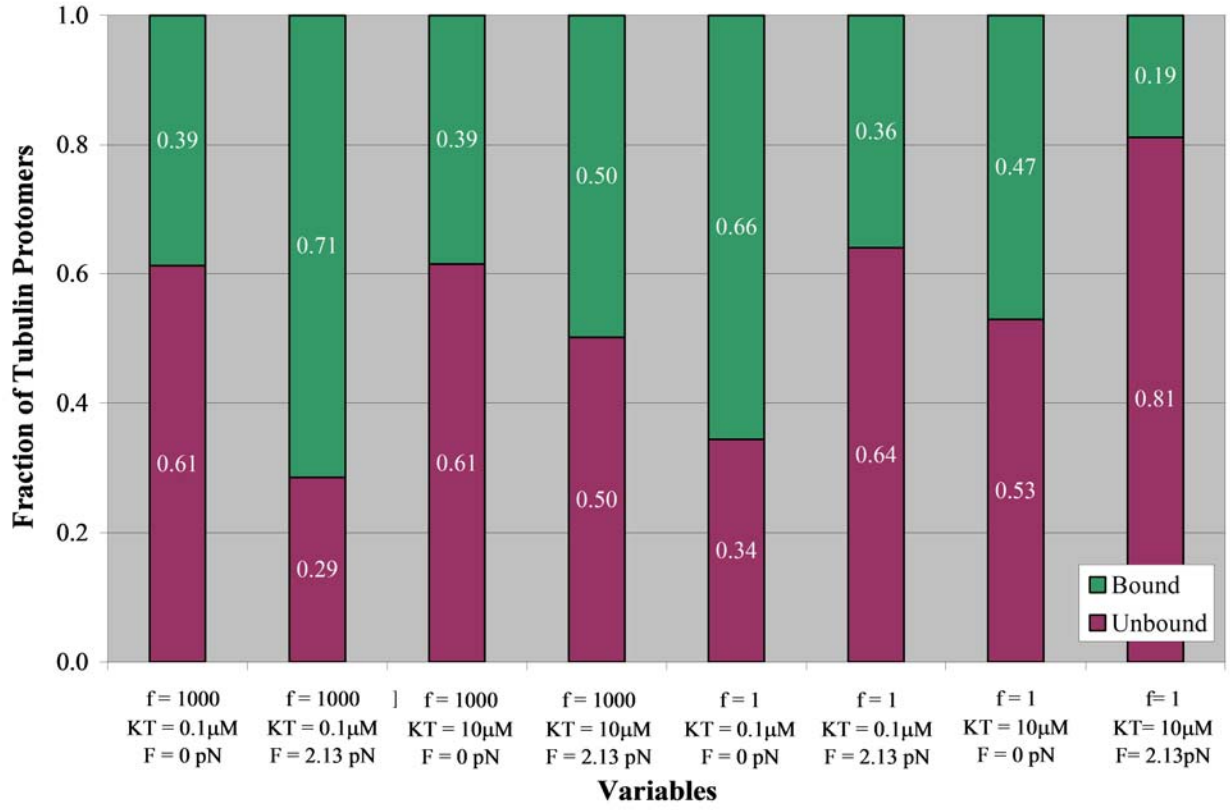


Figure 4-16. Fraction of S1 subunits bound and unbound from motile surface. Based on data presented in Figure 4-14, subunits in states 1-4 were considered unbound and subunits in states Tk2,Tk3, Tk4 were considered bound. All eight different variable combinations of $f$, $K_T$, and $F$ are presented.

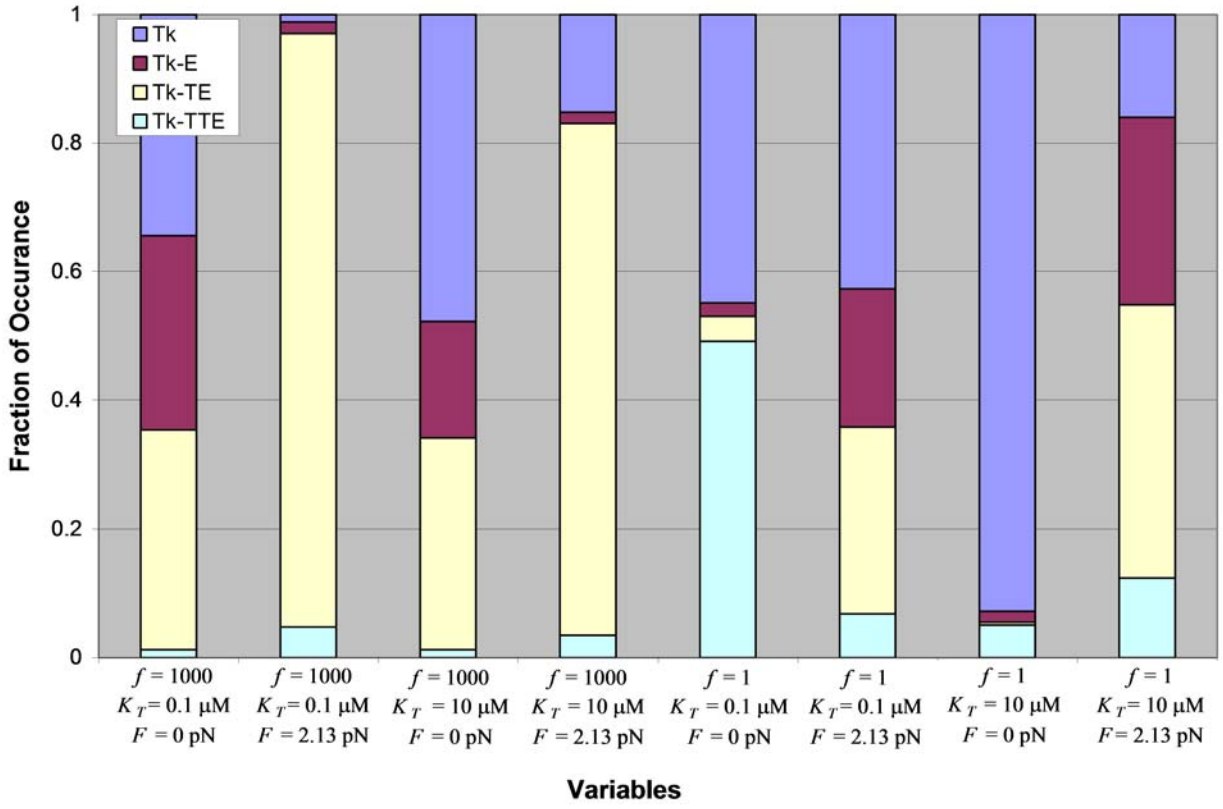


Figure 4-17. Average state of unbound linking protein. The fraction of time the linking protein spent in each of its unbound states is shown: Tk – unbound, Tk-E – linking protein bound to EB1, Tk-TE – linking protein bound to TE, Tk-TTE – linking protein bound to TTE. Each of the eight combinations of variables ($f$, $K_T$, $F$) was considered.

# CHAPTER 5
# CILIARY PLUG MODEL

Cilium is a motile organelle made up of an array of MTs. The plus-ends of ciliary MTs are attached to the cell membrane by MT-capping structures, which are located at the site of tubulin addition (Figure 5-1, (Suprenant and Dentler, 1988)). As the protofilaments polymerize, the cap remains tethered to the filament end and pushes the cell membrane forward. As mentioned earlier, EB1 has also been localized at the plus ends of ciliary microtubules. EB1 tends to localize at sites of MT force generation, therefore it was assumed that EB1 may be behaving end-tracking motor, similarly to the end-tracking motors in cell division and cellular growth.

This chapter discussed the EB1 end-tracking model developed for the ciliary plug. Essentially, the plug is the end-tracking motor, which is behaves similar to the Lock, Load and Fire Mechanism (Dickinson and Purich, 2002). The advancement of the plug at the microtubule plus-end occurs in three steps: tubulin addition, filament-bound GTP hydrolysis, and the shifting and rebinding of the ciliary plug (e.g., EB1) to the filament end. The key parameters used to simulate this model are the diffusivity of the microtubule in the medium, the length of the ciliary plug, the expected microtubule velocity, and the force applied against the plug. The force-velocity relationship for the microtubule is analyzed to determine the maximum achievable force the microtubule can withstand with the EB1 end-tracking motor.

## 5.1 Model

The physical characteristics of the plug make this model complex, but for simplification, the EB1 end-tracking motor is represented as a plug with multiple tubulin binding sites. The plug is inserted into the microtubule; hence, it was assumed that the plug creates a region where the protofilaments are separated from one another. The length of this region is labeled by a

distance $L$ (See Figure 5-2), where the 13 protofilaments are assumed to be independent of one another, and each of the motors operates on a single protofilament

The three steps of the end-tracking motor are represented in Figure 5-3. The first step in this end-tracking model is addition of tubulin to the filament end, which induces hydrolysis of the penultimate subunit. Because the EB1 plug has a low affinity for T-GDP, the motor rebinds to the GTP-rich, filament plus-end causing the plug to advance. This model is very similar to the Lock, Load and Fire Mechanism (LLF) proposed in 2002 (Dickinson and Purich, 2002).

The total time to complete one cycle is $T_m$ plus $\tau$. $T_m$ is the time it takes for the filament to add a dimer and undergo hydrolysis (Equation 5-1), $\tau$ time required for the plug to shift and relock to the new dimer following hydrolysis, and $d$ represents the length of a tubulin protomer. We anticipate that elongation of unloaded protofilaments is rate-limited by $T_{\mathrm{m}}$ (confirmed below), in which case $T_{\mathrm{m}}$ can again be estimated from $v_{max}$ (167 nm/s), i.e.,

$$T_m = \frac{d}{v_{\max}} = 0.05s \tag{5-1}$$

Following the approach of Dickinson & Purich (2002), the mean shift time $\tau$ is taken as the time required for the protofilament end to diffuse a distance $d$ and rebind and can be solved by the differential equation given by (Eq. 5-2) (Gardiner, 1986):

$$\frac{D_f}{k_B T} F \frac{d\tau}{dx'} + D_f \frac{d^2\tau}{dx'^2} = -1 \tag{5-2}$$

where $x$ is the protofilament end position, $F$ is the force subjected to the protofilament end, and the protofilaments fluctuate in position with a characteristic diffusivity, $D_f$. This diffusivity is dependent on the drag coefficient, $\delta$, and hence becomes a function of the length of the independent protofilament (Equation 5-3 and 5-4)

$$D_f = \frac{k_B T}{\delta} \tag{5-3}$$

$$\delta = \frac{4\pi\eta L}{\log(L/a)} \tag{5-4}$$

By varying the length of the protofilament, we can also analyze the dependence of $\tau$ and elongation rate on force. To determine the force dependence of $\tau$ on force, the differential equation in 5-2 was solved and is represented in Equation 5-5.

$$\tau(F)\big|_{x_1} = \frac{d^2}{D_f}\left[\left(\frac{k_B T}{dF}\right)^2 \exp\left(\frac{dF}{k_B T}\right) - \left(\frac{k_B T}{dF}\right)^2 - \left(\frac{k_B T}{dF}\right)\right] \tag{5-5}$$

With $\tau$ as a function of force, the equation that governs the velocity becomes a function of force, and is represented by Equation 5-6.

$$v(F) = \frac{d}{T_m + \tau(F)} \tag{5-6}$$

This equation was used to generate force-velocity profiles for the ciliary plug model.

Based on the compression stiffness of a protofilament, $\kappa$, and the thermal energy, $k_B T$, the stepwise motion of a microtubule with the ciliary end-tracking motor attached was also simulated. The filament end position, $x$, was governed by Equation 5-7.

$$x \propto \sqrt{k_B T/\kappa} \tag{5-7}$$

In the simulations for this model, the 13 protofilaments were initiated at different, random lengths. Prior to polymerization, the length of one of the protofilaments was set so that the initial, equilibrium force was balanced. For a protofilament to go through one cycle of tubulin addition, GTP hydrolysis, surface advancement, the probability of the cycle occurring was evaluated. This probability was determined based on the rate of the cycle reaction, $1/T_m\tau$. If any

of the protofilaments underwent shifting and rebinding, the new plug equilibrium position was determined by $z_{eq}=\kappa_i x/\Sigma\kappa_i$, where $\kappa_i$ is either the stretch of compression stiffness of each protofilament; the protofilament has a stretch stiffness if its length is less than the equilibrium value, and it is under compression when its length is greater than the equilibrium value. The resulting force on each filament is equal to its stiffness times the displacement of the protofilament from equilibrium, and the overall force on the ciliary plug is the sum of these individual forces.

## 5.2 Parameter Estimations

The key parameters used for this model were either based on literature values or estimated. The width of the protomer, $a$, was calculated as 5.15 nm from $a=2\pi R/N$ where $R$ is the radius of the protofilament and is equal to 11.48 nm for a 14-protofilmaent microtubule (Mickey and Howard, 1995). The length of the ciliary plug ($L$), or region where protofilaments are assumed to be independent, is estimated to be 75 nm from the EM image of the ciliary plug in Figure 5-1. The viscosity of the fluid used to calculate the drag coefficient was assumed to be that of water, $10^{-9}$ pN-s/nm$^2$ (Boal, 2002).

Assuming each of the protofilaments to be a semi-flexible rod, their filament compression ($\sigma$) and stretch stiffness ($\kappa$) were calculated. The compression stiffness is defined by the persistence length of the filament ($\lambda$), the thermal energy, and the length of the filament, and is represented by Equation 5-8 (Howard, 2001).

$$\sigma = \frac{k_B T \cdot \lambda^2}{L^4} \tag{5-8}$$

The persistence length is represented by Equation 5-9, where $B$ is the bending modulus of the filament ($B$ = 1.2 x $10^{-26}$ N-m$^2$, (Mickey and Howard, 1995)). The resulting value for the compression stiffness is 1.1 pN/nm.

$$\lambda = B / k_B T \tag{5-9}$$

The stretch stiffness is proportional to Young's modulus ($Y$=1.9 GPa, (Howard, 2001)), the cross sectional area of the microtubule ($A$=190 nm$^2$, (Gittes et al., 1993)), and the length of the rod being stretched, $L$:

$$\kappa = Y \cdot A / L \tag{5-10}$$

The resulting stretch stiffness for a protofilament was determined to be 370 pN/nm.

## 5.3 Results

Figure 5-4 shows the force effects on ciliary microtubules. In Figure 5-4A, the mean time to shift as a function of force is shown for various protofilament lengths. Regardless of the force, there is little effect of length on the cycle time. The time required for tubulin addition and filament-bound GTP hydrolysis remains constant and is force-independent, so the cycle time of the filaments is initially governed by $T_m$. As the load on the filament increases, the model is governed by the time it takes for the plug to advance ($\tau$). The effect of force and corresponding cycle time on the protofilament velocity is shown in Figure 5-4B. Again, the lengths of the protofilaments have little effect on the velocity of the microtubule. As the cycle time increases with increasing forces, the velocity exponentially decays to its maximum achievable force, or stall force ($F_{stall}$). The approximate stall for the microtubules simulated is approximately 12 pN.

The position versus time data is represented by Figure 5-5A, where the $x$-axis is representative of the end position of the ciliary plug. This figure shows how the ciliary plug advances as a steady rate for a short time then jumps to a new position. The size of this jump is

usually about 8nm, which is the size of the tubulin dimer. The reasoning for the step size is that the end-tracking motor for each protofilament must fill with tubulin before the ciliary plug can advance. The histogram in Figure 5-5B shows the number of protofilaments at each length greater than the equilibrium position. In this simulation, the protofilament end positions relative to the equilibrium position range from -5 to 55 nm after the simulation time of 1.6 s from Figure 5-5A.

## 5.4 Summary

The ciliary plug was simulated as an EB1 end-tracking motor similar to the end-tracking motors described in the Lock, Load and Fire Mechanism (Dickinson and Purich, 2002). The primary steps of this model are tubulin addition, filament-bound GTP hydrolysis and the shifting and rebinding of the ciliary plug (e.g., EB1) to the filament end. By analyzing the force-velocity profile of this mechanism, we found the stall force to be approximately 12 pN at various protofilament lengths, which is significantly greater than the stall force of 4.8 pN predicted by the Brownian ratchet mechanism. The results also shows the strong dependence of the stall force on the time for shift/rebinding of the ciliary plug to the filament end. The velocity profile shows the ability of the end-tracking motor to maintain fidelity of the microtubule by allowing the plug to advance only once all protofilaments are the same length.

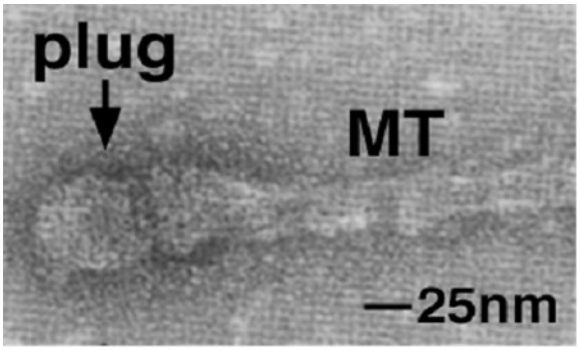


Figure 5-1. EM image of a ciliary plug at the end of a ciliary microtubule. The average length of the plug is approximately 75 nm. [Reproduced from **The Journal of Cell Biology, 1988, 107: 2259-2269**. Copyright 1988 The Rockefeller University Press]

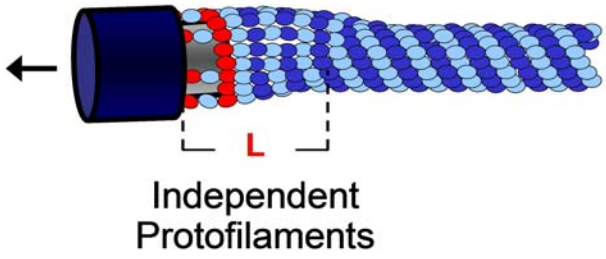


Figure 5-2. Schematic of ciliary plug inserted into the lumen of a cilia/flagella microtubule. The microtubules behave as independent protofilaments for a distance L from the MT plus-end. Red represents the GTP-bound tubulin subunits.

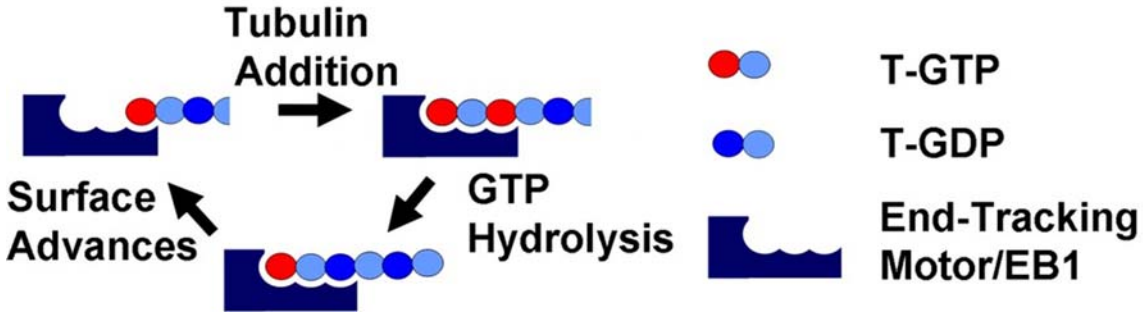


Figure 5-3. Mechanism of the ciliary/flagellar end-tracking motor. In the first step, tubulin adds to the MT plus-end into the end-tracking complex. This binding induces hydrolysis attenuating the affinity of the complex to the protofilament. The surface advances to the filament end.

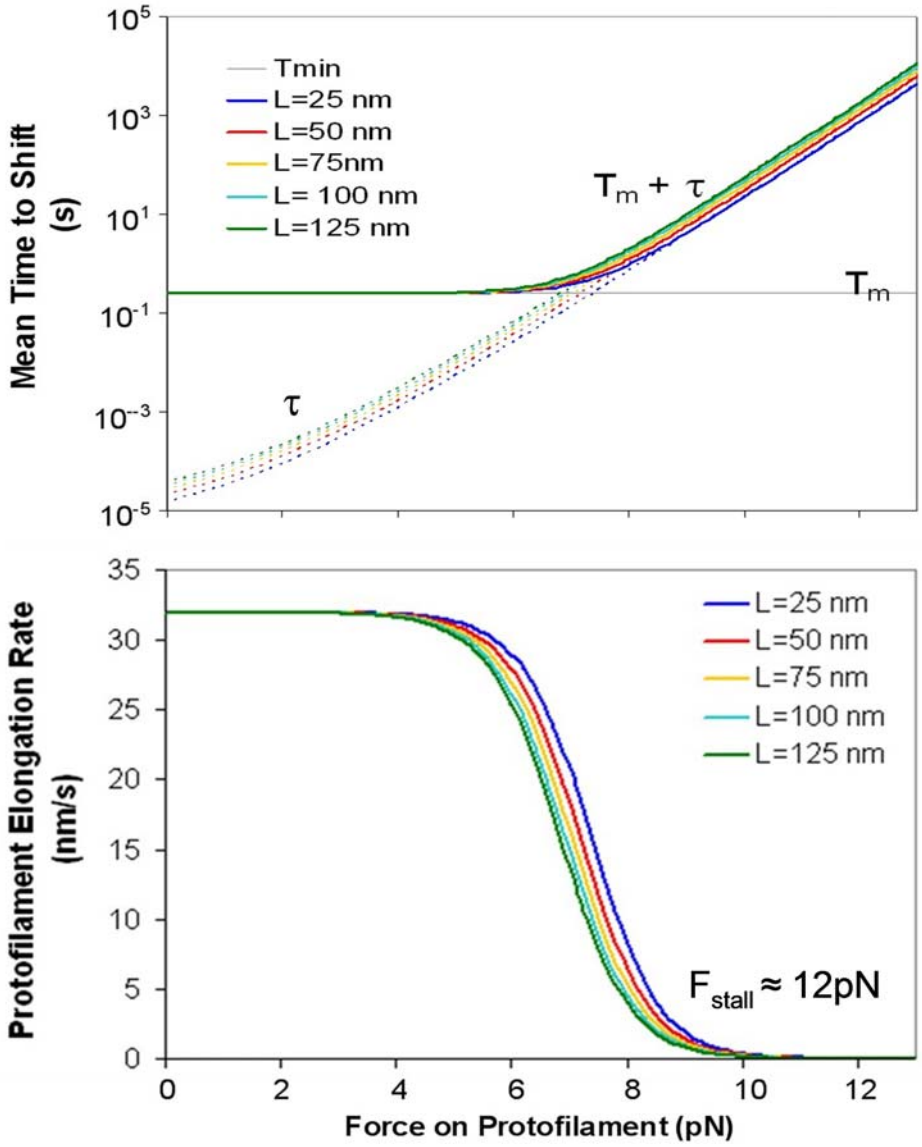


Figure 5-4. Force effects on ciliary microtubules. Initially the filament is governed by the time it takes for monomer addition & hydrolysis; however as the load on the filament increases, the model is governed by the time it takes for the plug to advance.

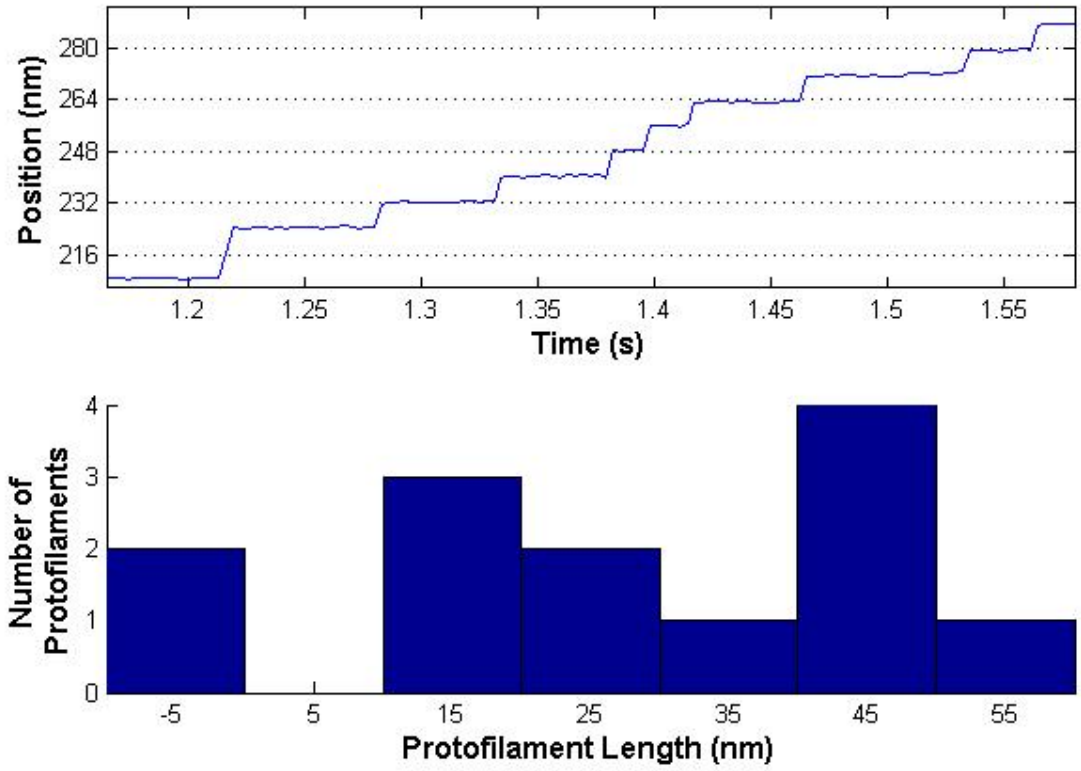


Figure 5-5. Ciliary plug movement. A) Position versus Time - Based on the compression stiffness $\kappa$, and the thermal energy $k_B T$, the stepwise motion of a ciliary plug with the end-tracking motor attached is shown. This motion shows how the ciliary plug advances as a steady rate for a short time then jumps to a new position. B) The histogram shows the length of the protofilaments.

# CHAPTER 6
# DISCUSSION

## 6.1 Possible Roles of End-Tracking Motors in Biology

The role of nucleotide hydrolysis in cytoskeletal molecular motor action is well-established for myosin, kinesin, and dynein. The affinity of a myosin head for the actin filament lattice is modulated by ATP hydrolysis, and dynein and kinesin act analogously in their binding and release from the microtubule lattice. In defining a new class of cytoskeletal filament end-tracking motors, we previously described how an microtubule filament end-tracking motors can exploit nucleotide hydrolysis to generate significantly greater force than that predicted by a free-filament thermal ratchet (i.e., the elastic Brownian ratchet mechanism), and these ideas were generalized based on thermodynamic considerations (Dickinson et al., 2004). In this report, we used known kinetic properties of EB1 binding and MT plus-end elongation to examine whether a hypothetical end-tracking motor consisting of affinity-modulated interactions of EB1 at MT and protofilament ends can propel objects (e.g., MT-attached kinetochores or MT-attached ciliary plugs) at typically observed velocities while operating against appreciable loads.

While there is no direct evidence that force production by polymerizing MT's is governed by an end-tracking motor mechanism, several experimental observations suggest that the properties and interactions of EB1 are compatible with such a model. Kinetochores, for example, are known to selectively bind EB1 by means of APC and/or other adapter proteins (Folker et al., 2005; Hayashi et al., 2005; Mimori-Kiyosue et al., 2005). Kinetochores also stabilize MTs against disassembly by preferentially attaching to GTP-containing β-subunits of tubulin subunits situated at or near MT plus-ends, and this property is likely to be the consequence of EB1's ability to attach to polymerizing GTP-rich MT subunits and to dissociate from GDP-containing subunits, thereby providing a thermodynamic driving force for localization at or near the MT

plus-end. Capture of EB1-rich MTs by kinetochores may allow those EB1 molecules combining with APC to self-assemble into an end-tracking motor unit that links force generation to MT polymerization and hydrolysis of MT-bound GTP. It is known that in the absence of the EB1/APC complex, chromosomes fail to align at the metaphase-plate, presumably due to disrupted MT polymerization and kinetochore attachment. The distal tips of ciliary/flagellar MTs are likewise decorated with EB1 proteins during formation and regeneration, suggesting EB1 may serve a similar role in forming an end-tracking motor there and playing a role in elongation-dependent force generation. In fact, it has previously been suggested that the plug-like structures found at the plus-ends of MTs in regenerating *Chlamydimonas* flagella appear to be "MT assembly machines". The analogous geometry of the ciliary/flagellar plug and the tubule-attachment complex in the kinetochore would allow plug- and kinetochore-bound EB1 to interact with their MT partners as an end-tracking motor. This proposal does not preclude the action of other ATP hydrolysis-dependent motors. For example, although the kinesin-like protein NOD lacks residues known to be critical for kinesin function, microtubule binding activates NOD's ATPase activity some 2000-fold, a property that (Matthies et al., 2001) suggested may allow chromosomes to be transiently attached to MTs without producing vectorial transport.

The Brownian Ratchet mechanism proposed for force generation by MTs in TAC models (Inoue and Salmon, 1995)) does not allow a strong association between the filaments and the motile object, and cannot predict substantial force generation at low protomer concentrations. End-Binding Protein 1 (EB1) has previously been shown to bind specifically to the polymerizing microtubule plus-end where the microtubule is tightly bound, suggesting a possible role in force generation at these sites. We propose that end-binding proteins (specifically EB1) behave as

molecular motors that modulate the interaction between MTs and the motile object, and generate the forces required for MT-based motility.

Although the importance of EB1 and its potential to behave as and end-tracking motors has been discussed thoroughly in this research study, the models developed can be used to understand force generating mechanisms involving other end-tracking proteins and their potential to act as motors (e.g., CLASPS, Clip-170). Adenomatous Polyposis Coli (or APC), which has an important role in preventing colon cancer, is like EB1 in that it is found at the tips of microtubules where microtubules bind to the chromosome at the kinetochore. It therefore also has the potential to behave like an end-tracking motor.

## 6.2 Microtubule End-Tracking Model

We developed and analyzed a preliminary EB1 filament end-tracking model for MTs to determine the advantages of the mechanochemical process over the monomer-driven ratchet mechanisms. The two important properties of this model are (a) maintenance of a tight, persistent (processive) attachment at elongating MT plus-ends by means of EB1's multivalent affinity-modulated interactions; and (b) a mechanism for the assembly of the MT end by EB1 dimers bound on the motile object, thus affording a high-fidelity pathway for assembling tethered MT's.

For simplicity, our model only considers simple reactions of the EB1 filament end-tracking motors. The details of the key assumptions applied to facilitate our analysis of this mechanism do not compromise key results of high force generation and processivity. For example, the effect of interactions among protofilaments on EB1-associated MT assembly was neglected. Although we accounted for EB1 flexibility, we neglected any contribution of the flexibility of the protofilaments themselves in net compliance of the EB1-protofilament interaction. We previously suggested that EB1 may be a polymerization cofactor acting together with APC to

end-track MT protofilaments (see Mechanism-C in (Dickinson et al., 2004). However, in view of the recent finding that EB1 is a stable, two-headed dimer (Honnappa et al., 2005), we now explain how such multivalency would allow EB1 alone to operate as the end-tracking motor (like Mechanism-A in Dickinson et al. (2004)). Either mechanism could capture energy from GTP hydrolysis and potentially translate it to mechanical work.

We simulated the kinetics of the latter mechanism by characterizing each reaction step based on its corresponding kinetic rate constant, with force-dependence of elongation arising from the dependence of probability of the flexible EB1 head binding at a specific MT lattice position. With hydrolysis-driven affinity-modulation factor $f$ greater than 10, our model recapitulates experimental, irreversible polymerization rates for free MTs of 170 nm/s. In the presence of an opposing force, the collective action of hydrolysis-mediated motors on an MT's thirteen protofilaments can yield kinetic stall forces of approximately 30 pN. This value is considerably larger than the ~7-pN achievable maximum force provided by the energy of monomer addition alone (i.e., without the benefit of GTP hydrolysis) in a Brownian Ratchet mechanism.

## 6.3 Protofilament End-Tracking Models

The microtubule end-tracking model developed neglected solution-phase End Binding protein 1 (EB1) and binding to microtubules and tubulin protomers. To account for binding solution-phase EB1, we developed simplified models that simulated the growth of a single protofilament in the presence of EB1 end-tracking motors. The properties of all protofilament the end-tracking models were compared to those of the simple Brownian Ratchet mechanism. Two of the models consider only free-protofilament growth operating with either monovalent or divalent EB1 proteins. The simulations for both models included a probabilistic analysis to determine the expected EB1 occupancy along the length of the protofilament. The results

confirm the assumption that GTP-driven affinity modulated binding of the EB1 end-tracking proteins is required in order to provide a 4.2 tip-to-side binding ratio as observed in experiments. We also developed two other protofilament models that allow EB1 to interact with a linker protein on a motile object (e.g., Adenomatous Polyposis Coli, APC), one model contained monovalent EB1 and the other had divalent EB1. By applying a load on the motile surface, we analyzed the resulting MT dynamics and force generation. The force-velocity profiles show that the divalent, EB1 end-tracking model provides an great advantage over the monovalent end-tracking model as well as a Brownian Ratchet mechanism. The divalent end-tracking motors are able to provide processive end-tracking and persistent attachment to the motile surface during protofilament polymerization. These divalent motor characteristics allow the protofilament to obtain much higher stall forces than predicted by the monovalent case or by a system with no affinity modulation (e.g., Brownian Ratchet model).

## 6.4 Future Work

Further analysis of a 13-protofilament, microtubule end-tracking model should be considered. It is suggested to develop a stochastic model that includes all mechanisms discussed in the tethered-protofilament model with divalent EB1. For simplifications it could be assumed that all protofilament behave independently, but whose individual EB1 end-tracking motors each contribute to the equilibrium position of the motile surface, much like the ciliary plug model. Based on results from the protofilament models, it is expected that the MT end-tracking model will predict greater stall forces than that of the Brownian ratchet model at large affinity modulation values.

Although much of the literature supports our proposed EB1 end-tracking mechanism, there remains definitive experimental literature that confirms this model. Future studies could clarify some of the assumptions made, and help to better characterize the mechanism by which EB1

associates with the MT plus-end. Of particular interest is whether EB1 together with growing MTs can generate the force predicted by our simulations while remaining persistently attached to the motile object. This hypothesis might be tested by adding EB1-coated beads to a solution of tubulin and MTs and with fluorescence microscopy determine if the MT binds to the beads and remains persistently attached as it polymerizes. Using optical trapping techniques, the velocity-force relationships could also be determined. This technique would provide more accurate stall force estimations for comparison with the simulated results.

APPENDIX A
PARAMETER ESTIMATIONS

## A.1 Concentrations of EB1 Species in Solution

**Monovalent EB1**: The reaction equations and corresponding equilibrium equations considered for monovalent EB1 binding to tubulin protomers (Tb) and microtubule sides (MT) in solution are:

$$E + Tb \overset{K_1}{\leftrightarrow} TE \qquad K_1 = [E][Tb]/[TE] \tag{A-1}$$

$$E + MT \overset{K_d}{\leftrightarrow} MT \cdot E \qquad K_d = [E][MT]/[MT{\cdot}E] \tag{A-2}$$

The total concentration of EB1 is represented in all states is

$$[E]_0 = [E] + [TE] + [MT{\cdot}E] \tag{A-3}$$

Substituting A-1 and A-2 into A-3 gives Equation A-4.

$$[E]_0 = [E] + [E][Tb]/K_1 + [E][MT]/K_d \tag{A-4}$$

such that solving for [E] yields.

$$[E] = \frac{[E]_0}{1 + \frac{[Tb]}{K_1} + \frac{[MT]}{K_d}} \tag{A-5}$$

**Divalent EB1**: For divalent EB1, two tubulin protomers can bind to each EB1 molecule (E) to form TE or TTE. The two binding sites are assumed identical and non-cooperative. Here, the relevant reaction and equilibrium equations are

$$E + Tb \leftrightarrow TE \qquad K_1 = 2{\cdot}\,[E][Tb]/[TE] \tag{A-6}$$

$$Tb + TE \leftrightarrow TTE \qquad K_1 = [Tb][TE]/(2{\cdot}\,[TTE]) \tag{A-7}$$

$$E + MT \overset{K_d}{\leftrightarrow} MT \cdot E \qquad K_d = [E][MT]/[MT{\cdot}E] \tag{A-8}$$

$$[E]_0 = [E] + [TE] + [TTE] + [MT{\cdot}E] \tag{A-9}$$

Combining A-6 and A-7 yields

$$[TTE] = \frac{[TE][Tb]}{2K_1} = \frac{[E][Tb]^2}{K_1^{\,2}} \tag{A-10}$$

Combining Eqs. A-9 and A-10 yields

$$[E]_0 = [E] + 2[E][Tb]/K_1 + [E][Tb]^2/K_1^{\,2} + [E][MT]/K_d \tag{A-11}$$

hence

$$[E] = \frac{[E]_0}{\left(1 + \frac{[Tb]}{K_1}\right)^2 + \frac{[MT]}{K_d}} \tag{A-12}$$

from which [TE] and [TTE] can be calculated using Eqs. A-6 and A-7.

## A.2 Occupation Probability of Monovalent EB1 Binding to Non-Tethered Protofilament

The probability of tubulin being bound to EB1 is given by the following:

$$\frac{dp_1}{d\tau} = k_+[EB1]_i u_i - k_{-,i} p_i + \left(k_f[Tb] + k_f^{\,E}[TE]u_i\right)(p_{i-1} - p_i) + \left(k_r u_1 + k_r^{\,E} p_1\right)(p_{i+1} - p_i) \tag{A-13}$$

The dimensionless relationships in Equations A-14 to A-17 can be substituted into Equation A-13:

$$\phi_i \equiv \frac{k_{+,i}[E]_i}{k_f[T]} \tag{A-14}$$

$$\alpha_i \equiv \frac{k_{-,i}}{k_f[T]} \tag{A-15}$$

$$\beta \equiv \frac{k_f^{\,E}[T \cdot E]}{k_f[T]} \tag{A-16}$$

$$T_r^{\,-1} \equiv \frac{k_r^{\,E} p_1 + k_r c_1}{k_f[T]} = \frac{T_c}{[T]} c_1 + \frac{T_c}{[T]} \frac{k_f^{\,E}}{k_f} \frac{K_d}{K_1 f} p_1 \equiv T_{r,0}^{\,-1} c_1 + T_{r,1}^{\,-1} p_1 \tag{A-17}$$

The resulting equations represent the differential equation for the probability of EB1 binding to the protofilament side (A-18) and plus-end (A-19), where $u \equiv 1-p_i$.

$$\frac{dp_i}{d\tau_d} = \phi_i c_i - \alpha_i p_i + (1+\beta)\left(p_{i-1} - p_i\right) + T_r^{-1}\left(p_{i+1} - p_i\right) \tag{A-18}$$

$$\frac{dp_1}{dt}\tau_d = \phi_1 c_1 - \alpha_1 p_1 - p_1 + \beta c_1 + T_{r,0}{}^{-1} c_1 p_2 - T_{r,1}{}^{-1} p_1 c_2 \tag{A-19}$$

## A.3 Occupation Probability of Monovalent EB1 Binding to Tethered Protofilament

This model determines the EB1 fluorescence along the protofilament based on the probability of each tubulin protomer being in a specific EB1 binding state. The binding states considered were:

$p_i$ = probability of EB1 bound to tubulin protomer in protofilament

$q_i$ = probability of Tk-E bound to tubulin in protofilament

$w$ = probability of Tk bound to TE in solution

$v$ = probability of Tk bound to E in solution

$y$ = probability of Tk being unbound

The probability of Tk being unbound, y, is represented by Equation A-20.

$$y = 1 - w - v - \sum q_i \tag{A-20}$$

The differential equations for the probabilities of EB1 and Tk-E binding to the protofilament are

$$\begin{aligned}\frac{dp_i}{dt} &= k_{on}[E]u_i - k_{\_}p_i - k_{T,i}C_{eff,i}yp_i + k_{T,i}{}^{-}q_i \\ &+ \left(k_f[Tb] + k_f{}^{E}[TE] + k_f{}^{E}C_{eff,i}w\right)\left(p_{i-1} - p_i\right) + \left(k_r{}^{E}p_1 + k_r u_1 + k_r{}^{E}q_1\right)\left(p_{i+1} - p_i\right)\end{aligned} \tag{A-21}$$

$$\frac{dq_i}{dt} = k_{T,i}C_{eff,i}yp_i - k_{T,i}^{-}q_i + k_{on}C_{eff,i}vu_i - k_{-}q_i$$
$$+ (k_f[T] + k_f^{E}[TE] + k_f^{E}C_{eff,i}w)(q_{i-1} - q_i) + \left(k_r^{E}p_1 + k_r u_1 + k_r^{E}q_1\right)(q_{i+1} - q_i) \quad \text{(A-22)}$$

where $u_i$ =1- $q_i$- $p_i$,,. The differential equations for the probability of the track binding to either TE or EB1 are given below:

$$\frac{dw}{dt} = k_T[TE]y - k_T^{-}w + k_1[T]v - k_1^{-}w - k_f^{E}C_{eff,1}w + k_r^{E}q_1 \quad \text{(A-23)}$$

$$\frac{dv}{dt} = k_T[E]y - k_T^{-}v - k_1[T]v + k_1^{-}w - \sum_i k_{on,i}C_{eff,i}vu_i + \sum_i k_{-,i}q_i \quad \text{(A-24)}$$

To de-dimensionalize time in these differential equations, the variable $T_r^{-1}$ was introduced, which is defined by Equation A-25.

$$T_r^{-1} \equiv \frac{k_r^{E}p_1 + k_r u_1}{k_f[T]} \quad \text{(A-25)}$$

Setting $T_{r,0}^{-1} = \frac{T_c}{[T]}$ and $T_{r,1}^{-1} \equiv \frac{T_c}{[T]}\frac{k_f^{E}}{k_f}\frac{K_d}{K_1 f}$, Equation A-25 gets reduced to A-26.

$$T_r^{-1} \equiv T_{r,0}^{-1}u_1 + T_{r,1}^{-1}p_1 \quad \text{(A-26)}$$

Dividing Equations A-21 to A-24 by $k_f$[T], results in the following differential equations with dimensionless time:

$$\frac{dp_i}{d\tau} = \frac{k_+}{k_f}\frac{[E]}{[T]}u_i - \frac{k_+}{k_f}\frac{K_d}{[T]}p_i - \frac{k_{t,i}}{k_f}\left(\frac{C_{eff,i}}{[T]}\right)yp_i + \frac{k_{t,i}}{k_f}\frac{K_{t,i}}{[T]}q_i$$
$$+ (1 + \frac{k_f^{E}}{k_f}\frac{[T\cdot E]}{[T]} + \frac{k_f^{E}}{k_f}\frac{C_{eff,i}}{[T]}w)(p_{i-1} - p_i) + \left(T_{r,1}^{-1}p_1 + T_{r,0}^{-1}u_1 + T_{r,1}^{-1}q_1\right)(p_{i+1} - p_i) \quad \text{(A-27)}$$

$$\frac{dq_i}{d\tau} = \frac{k_{t,i}}{k_f}\frac{C_{eff,i}}{[T]} yp_i - \frac{k_{t,i}}{k_f}\frac{K_{t,i}}{[T]} q_i + \frac{k_+}{k_f}\frac{C_{eff,i}}{[T]} vu_i - \frac{k_+}{k_f}\frac{K_d}{[T]} q_i$$
$$+ (1 + \frac{k_f^{\,E}}{k_f}\frac{[T\cdot E]}{[T]} + \frac{k_f^{\,E}}{k_f}\frac{C_{eff,i}}{[T]} w)(q_{i-1} - q_i) + \left(T_{r,1}^{\;-1} p_1 + T_{r,0}^{\;-1} u_1 + T_{r,1}^{\;-1} q_1\right)(q_{i+1} - q_i) \quad \text{(A-28)}$$

$$\frac{dw}{d\tau} = \frac{k_t}{k_f}\frac{[T\cdot E]}{[T]} y - \frac{k_t}{k_f}\frac{K_t}{[T]} w + \frac{k_1}{k_f} v - \frac{k_1}{k_f}\frac{K_1}{[T]} w - \frac{k_f^{\,E}}{k_f}\left(\frac{C_{eff,1}}{[T]}\right) w + T_{r,1}^{\;-1} q_1 \quad \text{(A-29)}$$

$$\frac{dv}{d\tau} = \frac{k_t}{k_f}\frac{[E]}{[T]} y - \frac{k_t}{k_f}\frac{K_t}{[T]} v - \frac{k_1}{k_f} v + \frac{k_1}{k_f}\frac{K_1}{[T]} w - \sum_i \frac{k_{+,i}}{k_f}\frac{C_{eff,i}}{[T]} vu_i + \sum_i \frac{k_{+,i}}{k_f}\frac{K_{d,i}}{[T]} q_i \quad \text{(A-30)}$$

To evaluate the probabilities of E or Tk-TE binding to the terminal subunit in the protofilament, these probabilities were re-written for the case when $i \rightarrow 1$:

$$\frac{dp_1}{d\tau} = \frac{k_+^{\,*}}{k_f}\frac{[E]}{[T]} u_1 - \frac{k_+^{\,*}}{k_f}\frac{K_d^{\,*}}{[T]} p_1 - \frac{k_{t,1}}{k_f}\frac{C_{eff,1}}{[T]} yp_1 - p_1 - \frac{k_f^{\,E}}{k_f}\frac{C_{eff,1}}{[T]} wp_1$$
$$+ \frac{k_{t,1}}{k_f}\frac{K_{t,1}}{[T]} q_1 + \frac{k_f^{\,E}}{k_f}\frac{[T\cdot E]}{[T]}(1 - p_1) + \left(T_{r,0}^{\;-1} u_1 + T_{r,1}^{\;-1} q_1\right) p_2 - T_{r,1}^{\;-1} p_1 (1 - p_2) \quad \text{(A-31)}$$

$$\frac{dq_1}{d\tau} = \frac{k_{t,1}}{k_f}\frac{C_{eff,1}}{[T]} yp_1 + \frac{k_+^{\,*}}{k_f}\frac{C_{eff,1}}{[T]} vu_1 + \frac{k_f^{\,E}}{k_f}\frac{C_{eff,1}}{[T]} w(1 - q_1)$$
$$- \left(\frac{k_{t,1}}{k_f}\frac{K_{t,1}}{[T]} + \frac{k_+^{\,*}}{k_f}\frac{K_D^{\,*}}{[T]} + 1 + \frac{k_f^{\,E}}{k_f}\frac{[T\cdot E]}{[T]}\right) q_1 + \left(\frac{T_c}{[T]} u_1 + \frac{k_f^{\,E}}{k_f}\frac{T_c}{[T]}\frac{K_d}{K_1 f} p_1\right) q_2 \quad \text{(A-32)}$$
$$- \frac{k_f^{\,E}}{k_f}\frac{T_c}{[T]}\frac{K_{d,1}}{K_1 f} q_1 (1 - q_2)$$

To solve for the probabilities ($p_i$, $q_i$, $w$, $v$) from Equations A-27 to A7-30, the equations were de-dimensionalized by using the following dimensionless parameters:

$$\alpha \equiv \frac{k_+}{k_f} \qquad \beta \equiv \frac{K_t}{[T]} \qquad \eta \equiv \frac{k_1}{k_f}$$

$$\gamma \equiv \frac{k_t}{k_f} \qquad \delta \equiv \frac{k_f^{\,E}}{k_f} \qquad \varphi_i = e^{\Delta(id - z_m)/\sigma^2}$$

The resulting de-dimensionalized differential equations are:

$$\frac{dp_i}{d\tau} = \alpha \frac{[E]}{[T]} u_i - \alpha \frac{K_d}{[T]} p_i - \gamma \left( \frac{C_{eff,i}}{[T]} \right) \varphi_i y p_i + \gamma \frac{K_t}{[T]} \varphi_i q_i$$
$$+ (1 + \delta \frac{[T \cdot E]}{[T]} + \delta \frac{C_{eff,1}}{[T]} \varphi_1 w)(p_{i-1} - p_i) \tag{A-33}$$
$$+ \left( \delta \frac{T_c}{[T]} \frac{K_d}{K_1 f} p_1 + \frac{T_c}{[T]} u_1 + \delta \frac{T_c}{[T]} \frac{K_d}{K_1 f} \varphi_1 q_1 \right)(p_{i+1} - p_i)$$

$$\frac{dq_i}{d\tau} = \gamma \frac{C_{eff,i}}{[T]} \varphi_i y p_i - \gamma \frac{K_{t,i}}{[T]} \varphi_i q_i + \alpha \frac{C_{eff,i}}{[T]} \varphi_i v u_i - \alpha \frac{K_d}{[T]} \varphi_i q_i$$
$$+ (1 + \delta \frac{[T \cdot E]}{[T]} + \delta \frac{C_{eff,1}}{[T]} \varphi_1 w)(q_{i-1} - q_i) \tag{A-34}$$
$$+ \left( \delta \frac{T_c}{[T]} \frac{K_d}{K_1 f} p_1 + \frac{T_c}{[T]} u_1 + \delta \frac{T_c}{[T]} \frac{K_d}{K_1 f} \varphi_1 q_1 \right)(q_{i+1} - q_i)$$

$$\frac{dw}{dt} = \gamma \frac{[T \cdot E]}{[T]} y - \gamma \frac{K_t}{[T]} w + \eta v - \eta \frac{K_1}{[T]} w - \delta \left( \frac{C_{eff,1}}{[T]} \right) \varphi_1 w + T_{r,1}{}^{-1} q_1 \varphi_1 \tag{A-35}$$

$$\frac{dv}{d\tau} = \gamma \frac{[E]}{[T]} y - \gamma \frac{K_t}{[T]} v - \eta v + \eta \frac{K_1}{[T]} w - \beta \frac{C_{eff,1}}{[T]} \varphi_1 v u_i + \beta \frac{K_d}{[T] f} \varphi_i q_i$$
$$- \sum_{i>1} \alpha \frac{C_{eff,i}}{[T]} \varphi_i v u_i + \sum_{i>1} \alpha \frac{K_d}{[T]} \varphi_i q_i \tag{A-36}$$

$$\frac{dp_1}{d\tau} = \beta \frac{[E]}{[T]} u_1 - \beta \frac{K_d / f}{[T]} p_1 - \gamma \frac{C_{eff,1}}{[T]} \varphi_1 y p_1 - p_1 - \delta \frac{C_{eff,1}}{[T]} \varphi_1 w p_1$$
$$+ \gamma \frac{K_t}{[T]} \varphi_1 q_1 + \delta \frac{[T \cdot E]}{[T]} (1 - p_1) + \left( \frac{T_c}{[T]} u_1 + \delta \frac{T_c}{[T]} \frac{K_d}{K_1 f} \varphi_1 q_1 \right) p_2 - T_{r,1}{}^{-1} p_1 (1 - p_2) \tag{A-37}$$

$$\frac{dq_1}{d\tau} = \gamma \frac{C_{eff,1}}{[T]} \varphi_1 y p_1 + \beta \frac{C_{eff,1}}{[T]} \varphi_1 v u_1 + \delta \frac{C_{eff,1}}{[T]} \varphi_1 w (1 - q_1)$$
$$- \left( \gamma \frac{K_t}{[T]} \varphi_1 + \beta \frac{K_d / f}{[T]} \varphi_1 + 1 + \delta \frac{[T \cdot E]}{[T]} \right) q_1 + \left( \frac{T_c}{[T]} u_1 + \delta \frac{T_c}{[T]} \frac{K_d}{K_1 f} p_1 \right) q_2 \tag{A-38}$$
$$- \delta \frac{T_c}{[T]} \frac{K_d}{K_1 f} \varphi_1 q_1 (1 - q_2)$$

For further simplification, more dimensionless parameters were substituted into these differential equations:

$$\alpha^* \equiv \frac{k_+^*}{k_f} \qquad \varepsilon \equiv \frac{[E]}{[T]} \qquad \xi \equiv \frac{K_1}{[T]} \qquad \chi \equiv \frac{C_{eff,0}}{[T]}$$

$$\mu \equiv \frac{K_d}{[T]} \qquad \psi \equiv \frac{T_c}{[T]} \qquad \theta_i \equiv e^{-\kappa(id - z_m)/2\sigma^2}$$

Both $\varphi_i$ and $\theta_t$ represent the effect of force on the probabilities for binding, based on a normal Gaussian distribution with a variance, $\sigma^2$, and filament end position, $z_m$. The rewritten differential equations are as follows:

$$\begin{aligned}\frac{dp_i}{d\tau} &= \alpha\varepsilon u_i - \alpha\mu p_i - \gamma\chi\theta_i\varphi_i y p_i + \gamma\beta\varphi_i q_i \\ &+ (1 + \delta\frac{\varepsilon}{\xi} + \delta\chi\theta_0\varphi_0 w)(p_{i-1} - p_i) + \left(\delta\psi\frac{\mu}{\xi f}p_1 + \psi u_1 + \delta\psi\frac{\mu}{\xi f}\varphi_1 q_1\right)(p_{i+1} - p_i)\end{aligned} \tag{A-39}$$

$$\begin{aligned}\frac{dq_i}{d\tau} &= \gamma\chi\theta_i\varphi_i y p_i - \gamma\beta\varphi_i q_i + \alpha\chi\theta_i\varphi_i v u_i - \alpha\mu\varphi_i q_i \\ &+ (1 + \delta\frac{\varepsilon}{\xi} + \delta\chi\theta_0\varphi_0 w)(q_{i-1} - q_i) + \left(\delta\psi\frac{\mu}{\xi f}p_1 + \psi u_1 + \delta\psi\frac{\mu}{\xi f}\varphi_1 q_1\right)(q_{i+1} - q_i)\end{aligned} \tag{A-40}$$

$$\frac{dw}{dt} = \gamma\frac{\varepsilon}{\xi}y - \gamma\beta w + \eta v - \eta\xi w - \delta\chi\theta_0\varphi_0 w + \delta\psi\frac{\mu}{\xi f}\varphi_1 q_1 \tag{A-41}$$

$$\begin{aligned}\frac{dv}{d\tau} &= \gamma\varepsilon y - \gamma\beta v - \eta v + \eta\xi w - \alpha^*\chi\theta_1\varphi_1 v u_i + \alpha^*\frac{\mu}{f}\varphi_1 q_1 \\ &- \sum_{i>1}\alpha\chi\theta_i\varphi_i v u_i + \sum_{i>1}\alpha\mu\varphi_i q_i\end{aligned} \tag{A-42}$$

$$\begin{aligned}\frac{dp_1}{d\tau} &= \alpha^*\varepsilon u_1 - \alpha^*\frac{\mu}{f}p_1 - \gamma\chi\theta_1\varphi_1 y p_1 - p_1 - \delta\chi\theta_0\varphi_0 w p_1 \\ &+ \gamma\beta\varphi_1 q_1 + \delta\frac{\varepsilon}{\xi}(1 - p_1) + \left(\psi u_1 + \delta\psi\frac{\mu}{\xi f}\varphi_1 q_1\right)p_2 - \delta\psi\frac{\mu}{\xi f}p_1(1 - p_2)\end{aligned} \tag{A-43}$$

$$\frac{dq_1}{d\tau} = \gamma\chi\theta_1\varphi_1 y p_1 + \alpha^* \chi\theta_1\varphi_1 v u_1 + \delta\chi\theta_0\varphi_0 w(1-q_1)$$
$$-\left(\gamma\beta\varphi_1 + \alpha^* \frac{\mu}{f}\varphi_1 + 1 + \delta\frac{\varepsilon}{\xi}\right)q_1 + \left(\psi u_1 + \delta\psi\frac{\mu}{\xi f}p_1\right)q_2 - \delta\psi\frac{\mu}{\xi f}\varphi_1 q_1(1-q_2) \quad \text{(A-44)}$$

These differential equations (A-39 to A-44) were solved with given kinetic parameters in Matlab (Appendix B.2.2) to determine the probability of the various EB1 binding interactions with the protomers in a protofilament.

### A.4 Occupation Probability of Divalent EB1 Binding to Tethered Protofilament

This model determines the EB1 fluorescence along the protofilament based on the probability of each tubulin protomer being in a specific EB1 binding state. The binding states considered were:

- $p_i$ : probability of protomer $i$ bound to EB1 subunit (other subunit unbound)
- $w_i$ : probability of protomer $i$ bound to *TE*
- $q_i^+$: probability of protomer $i$ in state $dbE^+$
- $q_i^-$ : probability of protomer $i$ in state $dbE^-$
- $u_i$ : probability of protomer $i$ being unbound

The probability of the protomer being unbound, $u_i$, is represented by

$$u_i = 1 - q_i^+ + q_i^- - p_i - w_i \quad \text{(A-45)}$$

$$\frac{dp_i}{dt} = 2k_{on}[E]u_i - k_- p_i + k_1^- w_i - k_1^+[T]p_i + k_- q_{i-1}^+ - k_+ p_i u_{i+1}$$
$$+ k_{-,i+1} q_{i+1}^- - k_+ p_i u_{i-1} + R_+(p_{i-1} - p_i) + R_-(p_{i+1} - p_i) \quad \text{(A-46)}$$

$$\frac{dw_i}{dt} = k_{on}[T\cdot E]u_i - k_- w_i + k_1^+[T]p_i - k_1^- w_i + R_+(w_{i-1} - w_i) + R_-(w_{i+1} - w_i) \quad \text{(A-47)}$$

$$\frac{dq_i^{+}}{dt} = -k_{-,i+1}q_{i+1}^{-} - k_{-,i}q_i^{+} + k_{+,i}p_{i+1}u_i + k_{+,i+1}p_i u_{i+1} + R_+\left(q_{i-1}^{+} - q_i^{+}\right) + R_-\left(q_{i+1}^{+} - q_i^{+}\right) \tag{A-48}$$

$$\frac{dq_i^{-}}{dt} = -k_{-,i}q_i^{-} - k_{-,i-1}q_{i-1}^{+} + k_{+,i}p_{i-1}u_i + k_{+,i-1}p_i u_{i-1} + R_+\left(q_{i-1}^{-} - q_i^{-}\right) + R_-\left(q_{i+1}^{-} - q_i^{-}\right) \tag{A-49}$$

$$\frac{du_i}{dt} = k_- p_i + k_- w_i + k_- q_i^{+} + k_- q_i^{-} - k_{+,i}p_{i+1}u_i - k_{+,i}p_{i-1}u_i - 2k_{on}[E]u_i - k_{on}[T\cdot E]u_i + R_+\left(u_{i-1} - u_i\right) + R_-\left(u_{i+1} - u_i\right) \tag{A-50}$$

$$R_+ = k_f[T] + k_f^{E}([T\cdot E] + [T\cdot E\cdot T]) + k_f^{E}C_{eff}w_1 \tag{A-51}$$

$$R_- = k_r u_1 + k_r^{E}\left(w_1 + p_1 + q_1^{+}\right) \tag{A-52}$$

The probabilities for the terminal protomer subunit are listed below:

$$\frac{dp_1}{dt} = 2k_{on}^{*}[E]u_1 - k_-^{*}p_1 + k_1^{-}w_1 - k_1^{+}[T]p_1 + k_- q_2^{-} - k_+ p_1 u_2 + k_f^{E}[T\cdot E](1-p_1) - (k_f[T] + k_f^{E}[T\cdot E\cdot T])p_1 + \left\{k_r u_1 + k_r^{E}w_1\right\}p_2 - k_r^{E}p_1(1-p_2) \tag{A-53}$$

$$\frac{dw_1}{dt} = k_{on}^{*}[T\cdot E]u_1 - k_-^{*}w_1 + k_1^{+}[T]p_1 - k_1^{-}w_1 + k_f^{E}[T\cdot E\cdot T](1-w_1) - (k_f[T] + k_f^{E}[T\cdot E])w_1 - k_f^{E}C_{eff}w_1 + k_r^{E}q_1^{+} + \left\{k_r u_1 + k_r^{E}p_1\right\}w_2 - k_r^{E}w_1(1-\pi_2) \tag{A-54}$$

$$\frac{dq_1^{+}}{dt} = -k_{-2}q_2^{-} - k_{-1}q_1^{+} + k_{+,1}p_2 u_1 + k_{+2}p_1 u_2 - \left\{k_f[T] + k_f^{E}([T\cdot E] + {}^{E}[T\cdot E\cdot T])\right\}q_1^{+} + k_f^{E}C_{eff}w_1 - k_r^{E}q_1^{+} + \left\{k_r u_1 + k_r^{E}\left(w_1 + p_1\right)\right\}q_2^{+} \tag{A-55}$$

$$\frac{du_1}{dt} = k_{-,1}p_1 + k_{-,1}w_1 + k_{-,1}q_1^{+} - k_{+,1}p_2u_1 - 2k_{on}^{*}[E]u_1 - k_{on}^{*}[T\cdot E]u_1$$
$$+ k_f[T](1-u_1) - \left\{k_f^{E}([T\cdot E] + k_f^{E}[T\cdot E\cdot T])\right\}u_1$$
$$- k_r u_1(1-u_2) + k_r^{E}(w_1 + p_1)u_2 \qquad \text{(A-56)}$$

Since an EB1 bound to the protofilament plus-end cannot bind in the negative direction, $dq_1^{-}/dt = 0$. At equilibrium (the protofilament does not polymerize), when *i*=1, $q_{eq} \equiv q_{eq}^{+} + q_{eq}^{-}$, these differential equations reduce to:

$$0 = 2k_{on}[E]u_{eq} - k_{-}p_{eq} + k_1^{-}w_{eq} - k_1^{+}[T]p_{eq} + k_{-}q_{eq} - 2k_{+}p_{eq}u_{eq} \qquad \text{(A-57)}$$

$$0 = k_{on}[T\cdot E]u_{eq} - k_{-}w_{eq} + k_1^{+}[T]p_{eq} - k_1^{-}w_{eq} \qquad \text{(A-58)}$$

$$0 = -k_{-}q_{eq} + 2k_{+}p_{eq}u_{eq} \qquad \text{(A-59)}$$

$$0 = k_{-}p_{eq} + k_{-}w_{eq} + k_{-}q_{eq} - 2k_{+}p_{eq}u_{eq} - 2k_{on}[E]u_{eq} - k_{on}[T\cdot E]u_{eq} \qquad \text{(A-60)}$$

And the following holds true:

$$u_{eq} = 1 - q_{eq} - p_{eq} - w_{eq} \qquad \text{(A-61)}$$

Solving Equation A-59 gives:

$$k_{-}q_{eq} = 2k_{+}p_{eq}u_{eq} \qquad \text{(A-62)}$$

Substituting this relationship into the other three equilibrium equations results in:

$$0 = 2k_{on}[E]u_{eq} - \left(k_{-} + k_1^{+}[T]\right)p_{eq} + k_1^{-}w_{eq} \qquad \text{(A-63)}$$

$$0 = k_{-}p_{eq} + k_{-}w_{eq} - \left(2k_{on}[E] + k_{on}[T\cdot E]\right)u_{eq} \qquad \text{(A-64)}$$

$$0 = k_{on}[T\cdot E]u_{eq} - \left(k_{-} + k_1^{-}\right)w_{eq} + k_1^{+}[T]p_{eq} \qquad \text{(A-65)}$$

From these three relationships, the equations for $w_{eq}$, and $p_{eq}$ were solved for:

$$w_{eq} = -2\frac{k_{on}[E]}{k_1^-}u_{eq} + \frac{\left(k_- + k_1^+[T]\right)}{k_1^-}p_{eq} \tag{A-66}$$

$$p_{eq} = \frac{\left\{2k_{on}[E]\left(\frac{k_-}{k_1^-}+1\right) + k_{on}[T\cdot E]\right\}}{\left\{k_- + k_-\frac{\left(k_- + k_1^+[T]\right)}{k_1^-}\right\}}u_{eq} \tag{A-67}$$

At equilibrium, the following relationship is true:

$$[T\cdot E] = 2\frac{[T][E]}{K_1} \tag{A-68}$$

Plugging this into Equation A-67, gives:

$$p_{eq} = \frac{2k_{on}[E]}{k_-}\frac{\left\{\left(\frac{k_-}{k_1^-}+1\right) + \frac{k_1^+}{k_1^-}[T]\right\}}{\left\{1+\frac{\left(k_- + k_1^+[T]\right)}{k_1^-}\right\}}u_{eq} \tag{A-69}$$

The terms in brackets on the top and bottom are identical, therefore it A-69 reduces to:

$$p_{eq} = \frac{2k_{on}[E]}{k_-}u_{eq} \tag{A-70}$$

Consequently, $w_{eq}$ and $q_{eq}$ reduce to Equation A-71.

$$w_{eq} = \frac{[Tb]}{K_1}p_{eq} \tag{A-71}$$

$$q_{eq} = 2\frac{k_+}{k_-}p_{eq}u_{eq} \tag{A-72}$$

Substituting A-70, 71, 72 into Equation A-61 results in the following equation:

$$0 = -1 + \left(1 + \frac{2k_{on}[E]}{k_-}\left(1+\frac{[T]}{K_1}\right)\right)u_{eq} + 2\frac{k_+}{k_-}\frac{2k_{on}[E]}{k_-}u_{eq}^{\ 2} \tag{A-73}$$

Solving for $u_{eq}$ gives:

$$u_{eq} = \frac{-\left\{\left(\frac{[T]}{K_1}+1\right)\frac{2k_{on}[E]}{k_-}+1\right\}+\sqrt{\left\{\left(\frac{[T]}{K_1}+1\right)\frac{2k_{on}[E]}{k_-}+1\right\}^2+8\frac{k_+}{k_-}\frac{2k_{on}[E]}{k_-}}}{4\frac{k_+}{k_-}\frac{2k_{on}[E]}{k_-}} \tag{A-74}$$

To determine the value of K1, we first assume [Tb]=0, which reduces Eq. A-75 to:

$$u_{eq}([T]=0) = \frac{-\left\{\frac{2k_{on}[E]}{k_-}+1\right\}+\sqrt{\left\{\frac{2k_{on}[E]}{k_-}+1\right\}^2+8\frac{k_+}{k_-}\frac{2k_{on}[E]}{k_-}}}{4\frac{k_+}{k_-}\frac{2k_{on}[E]}{k_-}} \tag{A-75}$$

The fraction of filament-bound protomers attached to EB1 at equilibrium defined by total amount of EB1 minus the amount of EB1 in solution:

$$\rho \equiv \frac{E_0 - [E]}{E_0} \tag{A-76}$$

This is also equivalent to:

$$\begin{aligned}\rho &= \frac{[MT]_{tot}}{E_0}(q_{eq}/2 + p_{eq}) \\ &= [MT]_{tot}\left(\frac{k_+}{k_-}u_{eq}+1\right)\frac{2k_{on}(1-\rho)}{k_-}u_{eq}\end{aligned} \tag{A-77}$$

Solving for $\rho$ gives:

$$\rho = \frac{1}{\frac{1}{[MT]_{tot}\left(\frac{k_+}{k_-}u_{eq}+1\right)\frac{2k_{on}}{k_-}u_{eq}}+1} \tag{A-78}$$

The effective equilibrium dissociation constant of EB1 and the protofilament ($K_{d,eff}$) is defined as:

$$K_{d,eff} = \frac{1}{\left(\frac{k_+}{k_-}u_{eq} + 1\right)\frac{2k_{on}}{k_-}u_{eq}} \tag{A-79}$$

Simplifying Equation A-78 gives:

$$\rho \equiv \frac{1}{\frac{K_{d,eff}}{[MT]_{tot}} + 1} \tag{A-80}$$

When half of the protofilament is saturated ($\rho$=1/2), $K_{d,eff}$ is given by Equation A-81 and $u_{1/2} \equiv u_{eq}([E]-[E]_0/2)$.

$$K_{d,eff} = \frac{1}{\left(\frac{k_+}{k_{-\,1/2}} + 1\right)\frac{2k_{on}}{k_-}u_{1/2}} \tag{A-81}$$

Under this constraint, $u_{1/2}$ is given by Equation A-82,

$$u_{1/2} = u_{eq}([E] = E_0/2) = \frac{-\left\{\frac{k_{on}E_0}{k_-} + 1\right\} + \sqrt{\left\{\frac{k_{on}E_0}{k_-} + 1\right\}^2 + 8\frac{k_{on}}{k_-}\frac{k_{on}C_{eff}E_0}{k_-}}}{4\frac{k_{on}}{k_-}\frac{k_{on}C_{eff}E_0}{k_-}} \tag{A-82}$$

Since $k_+ = k_{on} * C_{eff}$ and $k_+^{side} = k_{on}^{side} * C_{eff}$ for the protofilament plus end, Equation A-83 can be rewritten as:

$$u_{1/2} = u_{eq}([E] = E_0/2) = \frac{-\left\{\frac{k_+E_0}{k_-C_{eff}} + 1\right\} + \sqrt{\left\{\frac{k_+E_0}{k_-C_{eff}} + 1\right\}^2 + 8\frac{k_+}{k_-}\frac{k_+E_0}{k_-C_{eff}}}}{4\frac{k_+}{k_-}\frac{k_+E_0}{k_-C_{eff}}} \tag{A-83}$$

Substituting the definition of $K$, where $K \equiv k_+ / k_-$ gives:

$$u_{1/2} = \frac{-\left\{K \cdot \frac{E_0}{C_{eff}} + 1\right\} + \sqrt{\left\{K \cdot \frac{E_0}{C_{eff}} + 1\right\}^2 + 8 \cdot K^2 \frac{E_0}{C_{eff}}}}{4 \cdot K^2 \frac{E_0}{C_{eff}}} \tag{A-84}$$

Assuming $[Tb]$=0, $[E]_0$=0.27μM, [E]=$[E]_0$/2, and $C_{eff}$=153 μM and the experimentally determined value for $K_{d,eff}$ of 0.44μM (Tirnauer et al., 2002b) where used to determine the value of $K$ as 37. With $K \equiv k_+ / k_-$, $u_{eq}$ can be calculated for a given $\frac{[T]}{K_1}$:

$$u_{eq} = \frac{-\left\{\frac{2KE_0}{C_{eff}\left(\frac{[T]}{K_1}+1\right)} + 1\right\} + \sqrt{\left\{\left(\frac{[T]}{K_1}+1\right)\frac{2KE_0}{C_{eff}\left(\frac{[T]}{K_1}+1\right)} + 1\right\}^2 + 16K^2 \frac{E_0}{C_{eff}\left(\frac{[T]}{K_1}+1\right)^2}}}{8K^2 \frac{E_0}{C_{eff}\left(\frac{[T]}{K_1}+1\right)^2}} \tag{A-85}$$

**Determination of *k*:** At steady-state, the measured off-rate $k_{off}$ = 0.26 $s^{-1}$ is related to the $k_-$ by:

$$k_{off} = \frac{k_-(p_{eq} + \pi_{eq})}{p_{eq} + \pi_{eq} + q_{eq}/2} = \frac{k_-}{1 + \frac{Ku_{eq}}{\left(1 + \frac{[T]}{K_1}\right)}} \tag{A-86}$$

Rearranging Eq. A-86 gives Equation A-87.

$$k_- = k_{off}\left\{1 + \frac{Ku_{eq}}{\left(1 + \frac{[T]}{K_1}\right)}\right\} \tag{A-87}$$

The only free parameter is $K_1$ for the probabilities and variables. To find the value of $K_1$, the probabilistic model is used to determine the value that provides the following ratio

$$\frac{(p_i + \pi_i + q_i^{+}/2 + q_i^{-}/2)_{i\to 1}}{p_{eq} + \pi_{eq} + q_{eq}/2} = 4.2 \qquad \text{(A-88)}$$

APPENDIX B
MATLAB CODES

## B.1 13-Protofilament Microtubule Model

This stochastic program simulates a 13-protofilament MT polymerizing against a motile surface with a constant load. The values of *f* and sigma can be varied to determine the resulting velocity of the microtubule and each of the protofilament end positions. The kinetic parameters were estimated or used from literature values.

```
%  This program simulates a 13-protofilament MT polymerizing against a motile surface with a
constant load.

clear all;
hold off;

Tc = 5.3;  % Tubulin critical concentration (free filament) (uM)
Tb = 15;    % Tubulin dimer concentration (uM)

d=8;                % Size of tubulin dimer (nm)
nf=13;              % Number of protofilaments
kT = 4.14;          % Thermal energy (pN-nm) - Howard J 2001
sigma=10;           % 5 (nm)
kappa=kT/(sigma^2); % (pN/nm)
f = 1000;           % Affinity modulation (Kd reduced by a factor of f)
v=167;              % velocity of MT end growth (nm/s)
Lhalf=700;          % half length of MT (nm)
koff=v/Lhalf;       % off rate of both EB1 arms coming off 2 adjacent T-GDP's (s^-1)
kD=0.5;             % Dissociation rate constant for both EB1 arms on taxol-stabilized MT
wal(uM)
L=10;               % (nm)
rho=1/(L^2);        % (nm^-2)
%conversion=1.66e6;  % conversion from uM to nm^3
%ksol=koff/(kD*f);
ksol=5e7;                                          % ksol: on-rate for both EB1 arms on MT in
solution (nm^3/s)
k1on=8.9/13;                                             % k1+:  kon for tubulin dimer on MT
(1/(uM-s))
k1off=44/13;                                             % k1-:  koff for tubulin dimer on MT
(1/s)
k3on=((rho*ksol)/((sigma)*(2*pi)^0.5));               % k3+:  kon for 1 EB1 arm on MT wall (1/s)
(1.6*10^3)
k3off=(1/2)*koff+(1/2)*((koff^2)+(4*k3on*koff))^0.5;  % k3-:  koff for 1 EB1 arm from MT wall
(1/s) (19.6)
k2on=k3on;                                            % k2+:  kon for 1 EB1 arm between T-GTP/T-
GDP (1/s) (1.6*10^3)
k2off=k3off/f;                                        % k2-:  koff for 1 EB1 arm between  T-
GTP/T-GDP(1/s) (0.02)

dt=4.8e-6;                % dt should be at least 0.1 x 1/fastest time constant (s)
tim=1;                    % initialize time
nt=round(tim/dt);         % Number of time steps
nshow0=1000;              % Initial value for dummy index used to minimize number of 'n'
and'z0's displayed
nshow=nshow0;             % Let nshow equal 100 for first iteration
nplot=round(nt/nshow0);   % Set number of time steps that will be stored
t=(1:nplot)*nshow0*dt;    % Calculate time from number of time steps taken (has 1000 elements)

F=0;                           % Constant force applied to surface (pN)
q=0;                           % Initial value for dummy variable used in "position" loop
z0=zeros(1,nf);                % Initial filament equilibrium position
z=(1/nf)*sum(z0)-F/(nf*kappa); % Initial position of motile surface
n=zeros(1,nf);                 % Initial number of tubulin dimers on protofilament
ps=ones(1,nf);                 % Initial state of each protofilament
position=zeros(1,nplot);       % Initial vector of z for each time step

% State 1: One EB1 arm bound between terminal T-GTP/T-GDP
% State 2: One EB1 arm bound between terminal 2 T-GDP's
% State 3: One EB1 arm bound between terminal 2 T-GDP's, One arm btwn terminal T-GTP/T-GDP
```

```
% State 4: One EB1 arm bound between terminal 2 T-GDP's, One arm btwn lagging 2 T-GDP's
% State 5: One EB1 arm bound between lagging 2 T-GDP's
% State 6: One EB1 arm bound between lagging 2 T-GDP's, One arm btwn terminal T-GTP/T-GDP

rn1=rand(nf,nshow0);  % Generate a (nf x nt) matrix of random numbers (from 0 to 1) for loop.
                      % Generating random numbers OUTSIDE of loop makes program faster to run
rn2=rand(nf,nshow0); rn3=rand(nf,nshow0); rn4=rand(nf,nshow0);
rn5=rand(nf,nshow0); rn6=rand(nf,nshow0);
rn7=rand(nf,nshow0); rn8=rand(nf,nshow0);
rn9=rand(nf,nshow0); rn10=rand(nf,nshow0);

jshow=1; jstore=1;       % Indices for storing, plotting data
beta=d^2/2/sigma^2;      % shortcut parameter in calculating fordependence.
np=round(nt/nshow0);     % number of plotted points
zp = zeros(1,np); t=zp;  % storage vectors for position plot

for j=1:nt                                                          % from 1 to 100,000

    itst = [rn1(:,jshow)'<k1on*Tb*dt.*(ps==1)                        % 1 to 2
        rn2(:,jshow)'<k3on*exp(-beta*((1-(n-z)).^2))*dt.*(ps==1)  % 1 to 3
        rn3(:,jshow)'<k1off*dt.*(ps==2)                           % 2 to 1
        rn4(:,jshow)'<k2on*exp(-beta*((1+(n-z)).^2))*dt.*(ps==2)  % 2 to 3
        rn5(:,jshow)'<k3on*exp(-beta*((1-(n-z)).^2))*dt.*(ps==2)  % 2 to 4
        rn6(:,jshow)'<k3off*dt.*(ps==3)                           % 3 to 1
        rn7(:,jshow)'<k2off*dt.*(ps==3)                           % 3 to 2
        rn8(:,jshow)'<k1on*Tb*dt.*(ps==3)                         % 3 to 4
        rn9(:,jshow)'<k3off*dt.*(ps==4)                           % 4 to 2
        rn10(:,jshow)'<k1off*dt.*(ps==4)];                        % 4 to 3
    % 10 x nf  matrix containing ones where transition occurs
    %  Note z is dimensionless, scaled by d

    n=n+itst(1,:)-itst(3,:)+itst(8,:)-itst(10,:);                          % update numbers

    tnum = itst.*(ones(nf,1)*[2 3 1 3 4 1 2 4 2 3])';                      % matrix for updating ps

    ps = ps.*(1-(max(tnum)>0)) + max(tnum).*(max(tnum)>0);                 % update ps based on
transitions (note if one filament makes two transitions in one step (shouldn't happen often) only
one leading to larger ps value is used.

    fz = (ps==1).*n+(ps==2).*(n-1)+(ps==3).*(n-1+n)+(ps==4).*(n-1+n-2);  % Dimenionless forces
(correct for multiple springs in states 3,4

    ns = sum((ps==1)+(ps==2)+(ps==3)*2+(ps==4)*2);
    z=sum(fz)/ns - F/d/ns/kappa;  % New Equlibrium position (dimensionless)


 jshow=jshow+1;   % update jshow --

 if j==nshow               % when j is a multiple of 100*time step
       j/nt                % display percent of the loop performed
       n;                  % display number of dimers added (vector)
       z0;                 % display equilibrium position for protofilament (vector)
       nshow=nshow+nshow0;  % new value for loop
       %bar(n);             % Bar plot of subfilament lengths
       %drawnow;

      rn1=rand(nf,nshow0);  % regenerate numbers for running loop to make program faster to run
      rn2=rand(nf,nshow0); rn3=rand(nf,nshow0); rn4=rand(nf,nshow0);
      rn5=rand(nf,nshow0); rn6=rand(nf,nshow0);
      rn7=rand(nf,nshow0); rn8=rand(nf,nshow0);
      rn9=rand(nf,nshow0); rn10=rand(nf,nshow0);

      jshow=1;          % reset jshow for new random numbers
      zp(jstore)=z;     % Position of motile surface at each 'jstore' time step
      t(jstore)=j*dt;   % store data for only those positions plotted
      jstore=jstore+1;  % update index for storing data
   end
end  % end "j" loop

position=z*d
ksol
sigma
L
dt
subplot(2,1,1)
plot(t,zp*d,'r')                    % Plot Surface Position (z) vs. Time (t)
xlabel('Time (sec)')                % Label x-axis
ylabel('Surface Position (nm)')     % Label y-axis
title('Surface Position vs Time')   % Label title of plot
axis([0 1 -2 300])
%axis([0 dt*nt min(zp)*d max(zp)*d])  % Set axis plotting range
```

```
zproto=n*d;
subplot(2,1,2)
bar(zproto,'b')
hold on
zi=[position,position,position,position,position,position,position,position,position,position,pos
ition,position,position];
plot(zi,'r')
xlabel('Protofilament')               % Label x-axis
ylabel('Filament End Position (nm)')    % Label y-axis
```

## B.2 Protofilament Growth Model with Monovalent EB1

### B.2.1 Occupational Probability of Monovalent EB1 on a Non-Tethered Protofilament

This probabilistic model simulates the free growth of a single protofilament in the presence of monovalent, EB1 end-tracking motors. The value of the affinity modulation factor can be varied to determine the resulting EB1 density along a protofilament. The kinetic parameters were estimated or used from literature values.

```
% Probabalistic model – free MT's
% Simulates free MT's in presence of EB1
% Monovlanet EB1
% Plots: Occupation Probability vs Subunit

clear all;
n=400;          % number of subunits to simulate
tspan=[0 1000];

j=1:n;
x0=zeros(n,1);

% Parameters

% Fixed parameters

Tb = 10;        % uM  tubulin dimer concentration
MT = 10;        % uM  microtubule concentration
V = 170;        % nm/s;  % elongation speed
d = 8;          % nm;  % subunit length
% kf = 0.68; % uM^-1s^-1   on-rate for tubulin
% kr = 3.38; % s^-2

kf = V/d/Tb;    % uM^-1s^-1   on-rate for tubulin -taken assuming irreversible
 % elongation at  observed elongation speed
Tc = 5;         % uM plus-end critical concentration
kr = kf*Tc;         % s^-1 off-rate, assuming Tc=kr/kf;

thalf=2.6;      % s
kobs=log(2)/thalf;  % s^-1  observed decay rate constant of EB1 from MT sides
EB1tot = 0.27;  % uM  Total EB1 concentration
K1 = .2;        % uM  Equilibrium dissocation constant of Tb for E in solution –
 % determined be value need for 4.2:1 tip-to-middle concentration
Kd = 0.5;       %uM  Equilibrium dissocation constant of E for MT sides
E = EB1tot/(1+Tb/K1+MT/Kd);     %uM  Equilibrium value of EB1 concentration
TE = Tb/K1*E;       %uM  Equilibrium value of EB1-Tb concentration

kplus_side=kobs/(E+Kd);     % uM^-1 s^-1   on-rate constant for EB1 to MT side --
kminus_side=kplus_side*Kd;  % s^-1 off-rate constant for EB1 from MT side

enh = kf/kplus_side   % End binding Rate enhancement factor

% Roughly estimated parameters
```

```
f =  1000;      % affinity modulation factor
sigma = 10 ;        % nm   stdev of EB1 position fluctuations
kplus=enh*kplus_side; % uM^-1 s^-1   on-rate constant for EB1 to terminal subunit –
 % assumed same as on side
kminus=enh*kminus_side/f;   % s^-1 off-rate constant for EB1 from MT tip
kfE = kf;           % binding of TE to end;

% Dimensionless parameters

a = kminus_side/(kf*Tb);
as = kminus/(kf*Tb);

g = kplus_side*E/(kf*Tb);
gs = kplus*E/(kf*Tb);

b=kfE*TE/kf/Tb;

% Fed parameters
kT=4.14;
sigEB1 = 10;        % nm  stdev of EB1 linkage position
amp=100;        % EB1 local concentration increase factor
delta=1;        % nm  characteristic interaction distance
%stiffEB1=kT/sigEB1^2;
% EB1 linkage stiffness

av = a*ones(n,1); av(1)=as;
gv = g*ones(n,1); gv(1)=gs;

% gv = gv.*amp.*exp(-(0:n-1).^2.*(d./sigEB1)^2)'.*exp((0:n-1)*d*delta/sigEB1^2)';
% av=av.*exp((0:n-1)*d*delta/sigEB1^2)';

Trinv0=Tc/[Tb];
Trinv1=Tc/[Tb]*Kd/K1/f*kfE/kf;

[tout, xout]=ode23s(@(t,x0) sfrate(t,x0,av,gv,b,Trinv0,Trinv1),tspan,x0);

nt=length(tout); nmid=round(nt/2);
pmid=xout(nmid,j);
pend=xout(nt,j);
fluor=pend;
fluorm=pmid;
plot(1:n,pmid,'k:',1:n,pend,'k');

xlabel('subunit')
ylabel('occupation probability')


function f=sfrate(t,x,av,gv,b,Trinv0,Trinv1)

n=length(x);
j=1:n;
p=x(j);
u=1-p;

f=zeros(n,1);

Trinv=Trinv0*u(1)+Trinv1*p(1);

f(1) = gv(1)*u(1)-av(1)*p(1)-p(1)+b*u(1)+Trinv0*u(1)*p(2)-Trinv1*p(1)*u(2);

i=2:n-1;

f(i)= gv(i).*u(i)-av(i).*p(i)+(1+b)*(p(i-1)-p(i))+Trinv*(p(i+1)-p(i));

%f(n)=0;
f(n)=f(n-1);
```

### B.2.2 Occupational Probability of Monovalent EB1 on a Tethered Protofilament

This probabilistic model simulates the growth of a surface-tethered protofilament in the presence of monovalent, EB1 end-tracking motors. The value of the affinity modulation factor can be varied to determine the resulting EB1 density along a protofilament. The kinetic parameters were estimated or used from literature values.

```
% “brunode.m”
% Probabalistic model – tethered MT's
% Simulates tethered MT's in presence of EB1
% Monovlanet EB1
% Plots: Occupation Probability vs Subunit

clear all;
n=200;  % number of subunits to simulate
tspan=[0 1000];

j=1:n;
x0=zeros(2*n+2,1);

% Parameters

% Fixed parameters
kT = 4.1; % pN-nm   thermal energy
T = 10; % uM  tubulin dimer concentration
MT = 10; % uM  microtubule concentration
V = 170; % nm/s;  % elongation speed
d = 8; % nm;  % subunit length

kf = V/d/T; % uM^-1s^-1   on-rate for tubulin -taken assuming irreversible elongation
at  observed elongation speed
Tc = 5; % uM plus-end critical concentration
kr = kf*Tc; % s^-1 off-rate, assuming Tc=kr/kf;

thalf=2.6; % s
kobs=log(2)/thalf; %  s^-1  observed decay rate constant of EB1 from MT sides
EB1tot = 0.27; %  uM  Total EB1 concentration
K1 = .16;  % uM  Equilibrium dissocation constant of T for E in solution -- determined
be value need for 4.2:1 tip-to-middle concentration
Kd = 0.5;  %uM  Equilibrium dissocation constant of E for MT sides
E = EB1tot/(1+T/K1+MT/Kd);  %uM  Equilibrium value of EB1 concentration
TE = T/K1*E;  %uM  Equilibrium value of EB1-Tb concentration

kplus_side=kobs/(E+Kd); % uM^-1 s^-1   on-rate constant for EB1 to MT side --
kminus_side=kplus_side*Kd; % s^-1 off-rate constant for EB1 from MT side


% Roughly estimated parameters
f =  1; % affinity modulation factor


TcE = Tc*Kd/K1/f;

sigma = 5 ; % nm   stdev of EB1 position fluctuations
Delta = 0; % bond distance
kplus=kplus_side;   % uM^-1 s^-1   on-rate constant for EB1 to terminal subunit --
assumed same as on side
kminus=kminus_side/f;  % % s^-1 off-rate constant for EB1 from MT tip
kfE = kf;  % binding of TE to end;

ceff0 = 2/(2*pi)^(3/2)/sigma^3;  % concentration in nm^-3 -- based on 3-D normal
distribution on half-sphere
```

```
Ceff0 = ceff0/(6.022e23)*1e27/1000*1e6;  % conc in uM: nm^-3 x (1 mol/ 6.022e23) x
(1e27 nm^3/m^3) x (1 m^3/1000 L) x (10^6 uM/M)

% Varied parameters

Kt = 5;  % uM
Force =1*kT*log(T/Tc)/d;  % load in pN   positive if compressive, negative if tensile

%% Dimensionless parameters
alpha=kplus_side/kf;  %
alpha_s =kplus/kf;  %
gamma = 1;  %kt/kf;
delta = 1; %kfE/kf
eta = 1; %k1/kf;
chi = Ceff0/T;
beta = Kt/T;
mu = Kd/T;
psi = Tc/T;
xi = K1/T;
epsilon=E/T;

deld = Delta/d;
kappa = kT/sigma^2; kappad= kappa*d^2/kT;
Fd = Force*d/kT;

pars = [alpha alpha_s gamma delta eta chi beta mu psi xi epsilon f kappad deld Fd];


alpha=pars(1)
alpha_s =pars(2)
gamma=pars(3)
delta=pars(4)
eta = pars(5)
chi = pars(6)
beta = pars(7)
mu = pars(8)
psi = pars(9)
xi = pars(10)
eps = pars (11)
f= pars(12)
kappad = pars(13)   % kappad = kappa*d^2/kT;
deld = pars(14)     % deld = Delta/d;
Fd = pars(15)      % Fd = F*d/kT   neg if under compression  Fnet*d/kT =
F*d/kT+kappa*i*d*(d/kT) = Fd +kappad*i

 [tout, xout]=ode23s(@(t,x0) bfrate(t,x0,pars),tspan,x0);

nt=length(tout); nmid=round(nt/2);
pmid=xout(nmid,2*j-1);
pend=xout(nt,2*j-1);
qmid= xout(nmid,2*j);
qend=xout(nt,2*j);
fluor=pend+qend;
fluorm=pmid+qmid;
plot(1:n,pmid,'k:',1:n,qmid,'b:',1:n,pend,'k',1:n,qend,'b',1:n,fluor,'g');

xlabel('subunit')
ylabel('occupation probability')

w = xout(nt,2*n+2);
v = xout(nt,2*n+1);

im = sum(qend.*(1:length(qend)))/sum(qend)
FT = (im-1)*kappad;
Fnetd = Fd+FT;

V1 = kf*T*(exp(-Fd)-Tc/T*(1-(qend(1)+pend(1))))
V2 = kfE*((TE+Ceff0*w)*exp(-Fd)-TcE*(qend(1)+pend(1)))

V=V1+V2
relV=V/(kf*T-kr)
```

```
Attachprob = 1-(1-sum(qend))^13

function ff=bfrate(t,x,pars)

n=(length(x)-2)/2;
j=1:n;
p=x(2*j-1);
q=x(2*j);
u=1-p-q;
v=x(2*n+1);
w=x(2*n+2);
y=1-v-w-sum(q);

fp=zeros(n,1);
fq=zeros(n,1);

ff=zeros(2*n+2,1);

alpha=pars(1) ;
alpha_s =pars(2);
gamma=pars(3);
delta=pars(4);
eta = pars(5) ;
chi = pars(6);
beta = pars(7);
mu = pars(8);
psi = pars(9);
xi = pars(10);
eps = pars (11);
f= pars(12);
kappad = pars(13);   % kappad = kappa*d^2/kT;
deld = pars(14);     % deld = Delta/d;
Fd = pars(15);       % Fd = F*d/kT   pos if under compression  Fnet*d/kT =
F*d/kT+kappa*(i-(im-1))*d^2/kT) = Fd +kappad*i

meani = 0;

if sum(q)>0
meani = sum(q.*j')/sum(q);
end

FT = (meani-1)*kappad;
Fnetd = Fd+FT;

%afac=exp(Fnetd);
%psi = psi*afac;
% alpha=alpha*exp(Fnetd); alpha_s=alpha_s*afac; gamma=gamma*afac; eta=eta*afac;

im =1;  %im = Fd/kappad+meani;  % mean subunit position for unstressed trackers

afac=exp(Fd);
psi = psi*afac;
alpha=alpha*afac; alpha_s=alpha_s*afac; gamma=gamma*afac; eta=eta*afac;

phi=exp(abs(j-im)*kappad*deld)';
theta=exp(-kappad/2*(j-im).^2)';
phi0 = exp(abs(im)*kappad*deld);
theta0 = exp(-kappad/2*(im).^2);

chiv=chi*theta(j).*phi(j);
chiv0 = chi*theta0*phi0;

line1 = alpha_s*(eps*u(1)-mu/f*p(1))-gamma*chiv(1)*y*p(1) - p(1)-delta*chiv0*w*p(1);
line2 = gamma*beta*phi(1)*q(1)+delta*eps/xi*(1-
p(1))+psi*(u(1)+delta*mu/f/xi*phi(1)*q(1))*p(2);
fp(1) = line1+line2-delta*psi*mu/xi/f*p(1)*(1-p(2));

line1 = (chiv(1)*(gamma*y*p(1)-alpha_s*v*u(1))+chiv0*phi0*w*(1-q(1)));
line2 = -(gamma*beta*phi(1)+alpha_s*mu/f*phi(1)+1+delta*eps/xi)*q(1);
line3 = psi*(u(1)+delta*mu/xi/f*p(1))*q(2)-delta*psi*mu/xi/f*phi(1)*q(1)*(1-q(1));
fq(1) =line1+line2+line3;
i=2:n-1;
```

```
line1 = alpha.*(eps*u(i)-mu*p(i))-gamma*chiv(i).*y.*p(i)+gamma*beta*phi(i).*q(i);
line2 = (1+delta*(eps/xi+chiv0*w))*(p(i-1)-p(i));
line3 = psi*(delta*mu/xi/f*(p(1)-theta(1)*q(1))+u(1))*(p(i+1)-p(i));
fp(i) = line1+line2+line3;

line1 = gamma*(chiv(i).*y.*p(i)-beta*phi(i).*q(i))+alpha*(chiv(i).*v.*u(i)-
mu*phi(i).*q(i));
line2 = (1+delta*eps/xi+delta*chiv0*w)*(q(i-1)-q(i));
line3 = psi*(delta*mu/xi/f*(p(1)-phi(1)*q(1))+u(1))*(q(i+1)-q(i));
fq(i)=line1+line2+line3;

ff(1)=fp(1);
ff(2)=fq(1);
ff(2*i-1)=fp(i);
ff(2*i) = fq(i);

line1 = gamma*(eps*y-beta*v)+eta*(xi*w-v)-alpha_s*(chiv(1)*v*u(1)-mu/f*phi(1)*q(1));
line2 = alpha*sum(mu*phi(2:n).*q(2:n)-v*chiv(2:n).*u(2:n));
ff(2*n+1) = line1+line2;

ff(2*n+2)= gamma*(eps/xi*y-beta*w)+eta*(v-xi*w)-delta*(chiv0*w-
psi*mu/xi/f*phi(1)*q(1));

V1 = (1+delta*eps/xi+delta*chiv0*w);
V2 = psi*(delta*mu/xi/f*(p(1)-phi(1)*q(1))+u(1));

line1 = alpha.*(eps*u(n)-mu*p(n))-gamma*chiv(n).*y.*p(n)+gamma*beta*phi(n).*q(n);
line2 = (1+delta*(eps/xi+chiv0*w))*(p(n-1)-p(n));
fp(n) = line1+line2;

line1 = gamma*(chiv(n).*y.*p(n)-beta*phi(n).*q(n))+alpha*(chiv(n).*v.*u(n)-
mu*phi(n).*q(n));
line2 = (1+delta*eps/xi+delta*chiv0*w)*(q(n-1)-q(n));
fq(n)=line1+line2;

ff(2*n-1)=fp(n);
ff(2*n)=fq(n);
```

## B.3 Protofilament Growth Model with Divalent EB1

### B.3.1 Occupational Probability of Divalent EB1 on a Non-Tethered Protofilament

This probabilistic model simulates the free growth of a single protofilament in the presence of divalent, EB1 end-tracking motors. The value of the affinity modulation factor can be varied to determine the resulting EB1 density along a protofilament. The kinetic parameters were estimated or used from literature values.

```
% Probabilistic model -- free-ended MT's
% Simulates free-ended MT's in presence of EB1
% Divalent EB1
% Inputs: kon
% Outputs: EB1 Tip: Side Binding Ratio
% Plots: Occupation Probability vs Subunit

n=400;                % number of subunits to simulate
tspan=[0 140];

j=1:n;
x0=zeros(3*n,1);

% Parameters
```

```
% Fixed parameters

Tb = 10;              % uM  tubulin dimer concentration
MT = 10;              % uM  microtubule concentration
V = 170;              % nm/s;  % elongation speed
d = 8;                % nm;  % subunit length
                      % kf = 0.68; % uM^-1s^-1   on-rate for tubulin
                      % kr = 3.38; % s^-2

kf = V/d/Tb;          % uM^-1s^-1   on-rate for tubulin -taken assuming irreversible
                        elongation at  observed elongation speed
Tc = 5;               % uM plus-end critical concentration
kr = kf*Tc;           % s^-1 off-rate, assuming Tc=kr/kf;

thalf=2.6;            % s
kobs=log(2)/thalf;    % s^-1  observed decay rate constant of EB1 from MT sides
EB1 = 0.27;           % uM  Total EB1 concentration

sigma = 10 ;          % nm   stdev of EB1 position fluctuations
ceff = 2*exp(-(8/10)^2/2)/(2*pi)^(3/2)/sigma^3;
                      % concentration in nm^-3 -- based on 3-D normal distribution on half-
                      sphere
Ceff = ceff/(6.022e23)*1e27/1000*1e6;
                      % nm-3 x (1 mol/ 6.022e23) x (1e27 nm^3/m^3) x (1 m^3/1000 L) x (10^6
                      uM/M)
K = 37; % equals kplus_side/kminus_side, valued required for Kdeff = 0.44

%%%% Guessed parameters

Kd1 = .65;      % Kd, Dissociation constant for EB1 subunit and Tb, Kd1=k1m/k1 (uM) - Value for
typical monovalent protein
%Kd1=Kd1vec(irun);
k1 = 10;    % On-rate for EB1 subunit and Tb (uM^-1*s^-1), Value for typical protein-protein
binding
k1m = k1*Kd1;  % Off-rate for EB1 subunit and Tb (s^-1)

%%%  Equlibria

E = EB1/((1+(Tb/Kd1))^2);  % [EB1], Concentration of EB1 dimer in sol'n
TE = 2*E*Tb/Kd1;           % [EB1-Tb], Concentration of EB1 dimer bound to 1 tubulin protomer
TTE = Tb*TE/(2*Kd1);       % [EB1-Tb^2], Concentration of EB1 dimer bound to 2 tubulin protomers

a=4*K^2*E/Ceff;
b=(1+Tb/Kd1)*2*K*E/Ceff+1;

u_eq = (-b+sqrt(b^2+4*a))/2/a
p_eq=2*K*E/Ceff*u_eq;
q_eq = 2*K*p_eq*u_eq;
pi_eq = Tb/Kd1*p_eq;

fl_eq=p_eq+pi_eq+q_eq/2   %%% Equilibrium flourescence conce
check = u_eq+p_eq+q_eq+pi_eq   %%% should equal one

%% Determine kminus_side, kplus_side, kon

kminus_side = kobs*(1+K*u_eq/(1+Tb/Kd1));  %% Based on FRAP half-life
kplus_side = K*kminus_side;  %% by definition
kon_side = kplus_side/Ceff;
f = 1000 ; % affinity modulation factor
%f=fvec(irun);

%% Mixed model -- chose kon, calculated koff from f
kon = 5; % uM-1s-1
fon =  kon/kon_side;  %%% accelerated on-rate at end
kplus = kon*Ceff;
foff = fon/f;
kminus=fon/f*kminus_side; %%% corresponding change off-rate at end

%%% Other parameters

kfE = kf % on-rate constant of TE and TTE to MT end  uM-1s-1;
krE = kfE*Tc/Kd1*kminus/kon  % off-rate constant of TE or TTE

%% Dimensionless parameters
pars =[kminus_side kminus kplus_side kplus kf kr krE kfE k1 k1m Tb E TE TTE Ceff];
x0(3*j-1)=p_eq;  %initial conditions
x0(3*j)=q_eq/2; x0(4)=0;
x0(3*j-2)=pi_eq;

[tout, xout]=ode23s(@(t,x0) dfrate(t,x0,pars),tspan,x0);
```

```
nt=length(tout); nmid=round(nt/2);
pimid=xout(nmid,3*j-2);
pmid=xout(nmid,3*j-1);
qpmid=xout(nmid,3*j);
piend=xout(nt,3*j-2);
pend=xout(nt,3*j-1);
qpend=xout(nt,3*j);
qmend=[0 qpend(1:n-1)];
qmmid=[0 qpmid(1:n-1)];
fluor=pend+.5*qpend+.5*qmend+piend;
fluorm=pmid+.5*qmmid+.5*qpmid+pimid;

pp=polyfit(20:150, log(fluor(20:150)-fl_eq),1);
fitf=exp(pp(2)+pp(1)*(1:n));
plot(1:n,fluor,'go',1:n,fitf+fl_eq);
xlabel('subunit')
ylabel('occupation probability')

tip_ratio=real(exp(pp(2))+fl_eq)/fl_eq
fl_eq

function f=dfrate(t,x,pars)

%pars = [kminus_side kminus kplus_side kplus kf kr krE kfE k1 k1m Tb E TE TTE Ceff];
kminus_side=pars(1);
kminus=pars(2);
kplus_side=pars(3);
kplus=pars(4);
kf=pars(5);
kr=pars(6);
krE=pars(7);
kfE=pars(8);
k1=pars(9);
k1m=pars(10);
Tb=pars(11);
E=pars(12);
TE=pars(13);
TTE=pars(14);
Ceff=pars(15);
kon_side=kplus_side/Ceff;
kon=kplus/Ceff;


n=length(x)/3;
j=1:n;
pid=x(3*j-2);
p=x(3*j-1);
qp=x(3*j);
qm=[0 qp(1:n-1)']';
u=1-p-qp-qm-pid;

konv = ones(n,1)*kon_side; konv(1)=kon;
kpv = konv*Ceff;
kmv=ones(n,1)*kminus_side; kmv(1)=kminus;


fp=zeros(n,1); fqp=fp; fqm=fp; fpi=fp; f=zeros(3*n,1);

Rp=kf*Tb+kfE*(TE+2*TTE)+kfE*Ceff*pid(1);
Rm=kr*u(1)+krE*(pid(1)+p(1)+qp(1));


i=2:n-1;

tmp1=2*konv(i)*E.*u(i)-kmv(i).*p(i)+k1m*pid(i)-k1*Tb*p(i)+kmv(i).*qp(i-1)-kpv(i+1).*p(i).*u(i+1);

tmp2=kmv(i+1).*qm(i+1)-kpv(i-1).*p(i).*u(i-1)+Rp*(p(i-1)-p(i))+Rm*(p(i+1)-p(i));

fp(i) = tmp1+tmp2;

fqp(i)=-kmv(i+1).*qm(i+1)-kmv(i).*qp(i)+kpv(i).*p(i+1).*u(i)+kpv(i+1).*p(i).*u(i+1)+Rp*(qp(i-1)-
qp(i))+Rm*(qp(i+1)-qp(i));

fpi(i)=konv(i)*TE.*u(i)-kmv(i).*pid(i)+k1*Tb*p(i)-k1m*pid(i)+Rp*(pid(i-1)-pid(i))+Rm*(pid(i+1)-
pid(i));

tmp1=2*kon*E*u(1)-kminus*p(1)+k1m*pid(1)-k1*Tb*p(1)+kminus_side*qm(2)-kplus_side*p(1)*u(2);

tmp2=kfE*TE*(1-p(1))-(kf*Tb+2*kfE*TTE)*p(1)+(kr*u(1)+krE*(pid(1)+qp(1)))*p(2)-krE*p(1)*(1-p(1));
```

```
fp(1)=tmp1+tmp2;

tmp1 = kon*TE*u(1)-kminus*pid(1)+k1*Tb*p(1)-k1m*pid(1);

tmp2 = 2*kfE*TTE*(1-pid(1))-(kf*Tb+kfE*TE)*pid(1)-
kfE*Ceff*pid(1)+krE*qp(1)+(kr*u(1)+krE*p(1))*pid(2)-krE*pid(1)*(1-pid(2));

fpi(1)=tmp1+tmp2;

tmp1= -kminus_side*qm(2)-kminus*qp(1)+kplus*p(2)*u(1)+kplus_side*p(1)*u(2);

tmp2= -(kf*Tb+kfE*TE+2*kfE*TTE)*qp(1)+kfE*Ceff*pid(1)-
krE*qp(1)+(kr*u(1)+krE*(pid(1)+p(1)))*qp(2);

fqp(1) =tmp1+tmp2;


fp(n)=0;
fqp(n)=0;
fpi(n)=0;


f(3*j-2)=fpi;
f(3*j-1)=fp;
f(3*j)=fqp;
```

### B.3.2 Average Fraction of divalent EB1-bound Protomers on Side of Protofilament

This stochastic model simulates the side-binding of divalent EB1 on a non-growing protofilament. The value of the affinity modulation factor can be varied to determine the time-averaged fluorescence of EB1 along the length of the protofilament and the state of the subunits in the protofilament. The kinetic parameters were estimated or used from literature values.

```
% Probabalistic model
% Simulates free-ended MT's in presence of EB1
% Divalent EB1
% Inputs: f, Kd1, kon
% Outputs: Time Avg Fluorescence
% Plots: Time Avg Fluorescence vs Subunit

clear all;
n=400;  % number of subunits to simulate - 400
tspan=[0 40]; - 40
j=1:n;
x0=zeros(3*n,1);


% Determine Parameters

% Fixed parameters

Tb = 10; % uM  tubulin dimer concentration
Tc = 5; % uM plus-end critical concentration
EB1 = 0.27; %  uM  EB1 concentration
d = 8; % nm;  % subunit length

V = 170; % nm/s;  % elongation speed
kf = V/d/Tb; % uM^-1s^-1   on-rate for tubulin -taken assuming irreversible elongation at
observed elongation speed
kr = kf*Tc; % s^-1 off-rate, assuming Tc=kr/kf;

thalf=2.6; % s
kobs=log(2)/thalf; %  s^-1  decay rate constant of EB1 from MT sides

sigma = 10 ; % nm   stdev of EB1 position fluctuations
ceff = 2*exp(-(8/10)^2/2)/(2*pi)^(3/2)/sigma^3;  % concentration in nm^-3 -- based on 3-D normal
distribution on half-sphere
```

```
Ceff = ceff/(6.022e23)*1e27/1000*1e6;  % nm-3 x (1 mol/ 6.022e23) x (1e27 nm^3/m^3) x (1 m^3/1000
L) x (10^6 uM/M)

K = 37; % equals kplus_side/kminus_side, valued required for Kdeff = 0.44


%%%% Guessed parameters

Kd1 = 0.65;      % Kd, Dissociation constant for EB1 subunit and Tb, Kd1=k1m/k1 (uM) - Value for
typical monovalent protein
%Kd1=Kd1vec(irun);
k1 = 10;    % On-rate for EB1 subunit and Tb (uM^-1*s^-1), Value for typical protein-protein
binding
k1m = k1*Kd1;  % Off-rate for EB1 subunit and Tb (s^-1)


%%%  Equlibria

E = EB1/((1+(Tb/Kd1))^2);  % [EB1], Concentration of EB1 dimer in sol'n
TE = 2*E*Tb/Kd1;           % [EB1-Tb], Concentration of EB1 dimer bound to 1 tubulin protomer
TTE = Tb*TE/(2*Kd1);       % [EB1-Tb^2], Concentration of EB1 dimer bound to 2 tubulin protomers

a=4*K^2*E/Ceff;
b=(1+Tb/Kd1)*2*K*E/Ceff+1;

u_eq = (-b+sqrt(b^2+4*a))/2/a
p_eq=2*K*E/Ceff*u_eq;
q_eq = 2*K*p_eq*u_eq;
pi_eq = Tb/Kd1*p_eq;

fl_eq=p_eq+pi_eq+q_eq/2   %%% Equilibrium flourescence conce
check = u_eq+p_eq+q_eq+pi_eq   %%% should equal one


%% Determine kminus_side, kplus_side, kon

kminus_side = kobs*(1+K*u_eq/(1+Tb/Kd1));  %% Based on FRAP half-life
kplus_side = K*kminus_side;  %% by definition
kon_side = kplus_side/Ceff;
f = 1000 ; % affinity modulation factor
%f=fvec(irun);


%% Mixed model -- chose kon, calculated koff from f
kon = 10; % uM-1s-1
fon =  kon/kon_side;  %%% accelerated on-rate at end
kplus = kon*Ceff;
foff = fon/f;
kminus=fon/f*kminus_side; %%% corresponding change off-rate at end


%%% Other parameters

kfE = 10 % on-rate constant of TE and TTE to MT end  uM-1s-1;
krE = kfE*Tc/Kd1*kminus/kon  % off-rate constant of TE or TTE


% Initial conditions

N=40;  % 50-number of subunits to simulate
S=ones(1,N);  %S = 1 if unocupplied; 2 if bound to E, 3 if bound to TEE, 4 if bound to +side of
doubly bound, 5 if bound to -side
tim=10; % 200-run time (s)
chartime=1/max([kfE*TTE kfE*TE kf*Tb kr krE kon*Tb k1*Tb k1 kplus kplus_side kminus
kminus_side]); %Characteristic time
dt = chartime/5;  %simulation time increment
nt=round(tim/dt);
rnside1=rand(nt,N);
radd = rand(nt,1);
previt=0; FLav=0*S;


for it=1:nt

   %% Side binding
   tst1=(S==1)& rnside1(it,:)<2*kon_side*E*dt;  % binds E
   tst2= (S==1)& rnside1(it,:)<(kon_side*TE*dt+2*kon_side*E*dt) &~tst1;  % or binds TE

   tst3=(S==2)& rnside1(it,:)<kminus_side*dt;  % dissociate E
   tst4=(((S==2)&[0 S(1:N-1)==1]) & rnside1(it,:)<(kplus_side*dt + kminus_side*dt)) &~tst3;  %
bind plus side
```

```
   tst5=(((S==2)&[S(2:N)==1 0]) & rnside1(it,:)<(kplus_side*dt + kplus_side*dt+kminus_side*dt))
&~(tst3|tst4); % bind minus side
   tst6=((S==2)& rnside1(it,:)<(k1*T*dt + 2*kplus_side*dt+kminus_side*dt)) &~(tst3|tst4|tst5); %
bind T

   tst7=(S==3)& rnside1(it,:)<k1m*dt; % dissociate T
   tst8=(S==4)& rnside1(it,:)<kminus_side*dt; % dissociate plus side
   tst9=(S==5)& rnside1(it,:)<kminus_side*dt; % dissociate minus side of bound E
   tst10=((S==3) & rnside1(it,:)<(kminus_side*dt+k1m*dt)) &~(tst7); %dissociate TE from side

   otst=(tst1+tst2+tst3+tst4+tst5+tst6+tst7+tst8+tst9+tst10);
   if sum(otst)>0

       ntav=it-previt;

       FL=(S==2)+(S==3)+.5*(S==5)+.5*(S==4);
       FLav=(previt*FLav+ntav*FL)/(ntav+previt);
       previt=it;
       ifnd1=find(tst1);
       S(ifnd1)=2;
       ifnd2=find(tst2);
       S(ifnd2)=3;
       ifnd3=find(tst3);
       S(ifnd3)=1;
       ifnd4=find(tst4);
       S(ifnd4)=5; S(ifnd4-1)=4;
       ifnd5=find(tst5);
       S(ifnd5)=4; S(ifnd5+1)=5;
       ifnd6=find(tst6);
       S(ifnd6)=3;
       ifnd7=find(tst7);
       S(ifnd7)=2;
       ifnd8=find(tst8);
       S(ifnd8)=1; S(ifnd8+1)=2;
       ifnd9=find(tst9);
       S(ifnd9)=1; S(ifnd9-1)=2;
       ifnd10=find(tst10);
       S(ifnd10)=1;

   it
   S;
   FLav
   plot(1:N,FLav,[1 N],[fl_eq fl_eq]); axis([0 N 0 1]); drawnow;
   end
 end
```

### B.3.3 Average Fraction of EB1-bound protomers during protofilament growth

This stochastic model simulates the time averaged fluorescence of EB1 along a non-tethered, single microtubule protofilament in the presence of divalent EB1 during protofilament growth. The value of the affinity modulation factor can be varied to determine its affect on the EB1 fluorescence. The state of the subunits in the protofilament can also be determined.

```
% Simulates free-ended MT's in presence of EB1
% Stochastic model
% Divalent EB1
% Inputs: f, Kd1, kon
% Outputs: Velocity, State of Subunits, Time Avg Fluorescence
% Plots: Time Avg Fluorescence vs Subunit

clear all;
tic;
N=200;  % number of subunits to simulate 200
tim=40; % run time (s)40
axmax=.2; % max y-axis.


% Determine Parameters

% Fixed parameters
```

```
T = 10; % uM  tubulin dimer concentration
V = 170; % nm/s;  % elongation speed
d = 8; % nm;  % subunit length

kf = V/d/T; % uM^-1s^-1   on-rate for tubulin -taken assuming irreversible elongation at
observed elongation speed
Tc = 5; % uM plus-end critical concentration
kr = kf*Tc; % s^-1 off-rate, assuming Tc=kr/kf;

thalf=2.6; % s
kobs=log(2)/thalf; %  s^-1  decay rate constant of EB1 from MT sides
EB1 = 0.27; %  uM  EB1 concentration

sigma = 10 ; % nm   stdev of EB1 position fluctuations
ceff = 2*exp(-(8/10)^2/2)/(2*pi)^(3/2)/sigma^3;  % concentration in nm^-3 -- based on 3-D normal
distribution on half-sphere
Ceff = ceff/(6.022e23)*1e27/1000*1e6;  % nm-3 x (1 mol/ 6.022e23) x (1e27 nm^3/m^3) x (1 m^3/1000
L) x (10^6 uM/M)
K = 37; % equals kplus_side/kminus_side, valued required for Kdeff = 0.44


%%%% Guessed parameters

Kd1 = .65;      % Kd, Dissociation constant for EB1 subunit and T, Kd1=k1m/k1 (uM) - Value for
typical monovalent protein
%Kd1=Kd1vec(irun);
k1 = 10;    % On-rate for EB1 subunit and T (uM^-1*s^-1), Value for typical protein-protein
binding
k1m = k1*Kd1;  % Off-rate for EB1 subunit and T (s^-1)

%%%  Equlibria

E = EB1/((1+(T/Kd1))^2);  % [EB1], Concentration of EB1 dimer in sol'n
TE = 2*E*T/Kd1;           % [EB1-T], Concentration of EB1 dimer bound to 1 tubulin protomer
TTE = T*TE/(2*Kd1);       % [EB1-T^2], Concentration of EB1 dimer bound to 2 tubulin protomers

a=4*K^2*E/Ceff;
b=(1+T/Kd1)*2*K*E/Ceff+1;

u_eq = (-b+sqrt(b^2+4*a))/2/a;
p_eq=2*K*E/Ceff*u_eq;
q_eq = 2*K*p_eq*u_eq;
pi_eq = T/Kd1*p_eq;

fl_eq=p_eq+pi_eq+q_eq/2;   %%% Equilibrium flourescence conce
check = u_eq+p_eq+q_eq+pi_eq;   %%% should equal one


%% Determine kminus_side, kplus_side, kon

kminus_side = kobs*(1+K*u_eq/(1+T/Kd1));  %% Based on FRAP half-life
kplus_side = K*kminus_side;  %% by definition
kon_side = kplus_side/Ceff;
f = 1 ; % affinity modulation factor
%f=fvec(irun);


%% Mixed model -- chose kon, calculated koff from f

kon = 5; % uM-1s-1
fon =  kon/kon_side;  %%% accelerated on-rate at end
kplus = kon*Ceff;
foff = fon/f;
kminus=fon/f*kminus_side; %%% corresponding change off-rate at end


%%% Other parameters

kfE = kf; % on-rate constant of TE and TTE to MT end  uM-1s-1;
%kfE = 1e-8;
krE = kfE*Tc/Kd1*kminus/kon;  % off-rate constant of TE or TTE


% Initial conditions

S=ones(1,N);  %S = 1 if unocupplied; 2 if bound to E, 3 if bound to TEE, 4 if bound to +side of
doubly bound, 5 if bound to -side
chartime=1/max([kfE*TTE kfE*TE kf*T kr krE kon*T k1*T k1 kplus kplus_side kminus kminus_side]);
%Characteristic time
dt = chartime/10;  %simulation time increment
```

```
nt=round(tim/dt);
rnside1=rand(nt,N);
radd = rand(nt,1);
roff=rand(nt,1);
previt=0; FLav=0*S;
nadd=1;

konv=[kon kon_side*ones(1,N-1)];
kminusv=[kminus kminus_side*ones(1,N-1)];
kplusv=[kplus kplus_side*ones(1,N-1)];
k1v=k1*ones(1,N);
k1mv=k1m*ones(1,N);

for it=1:nt

   %% Side binding

   tst1=(S==1)& rnside1(it,:)<2*konv*E*dt;  % binds E
   tst2= (S==1)& rnside1(it,:)<(konv*TE*dt+2*konv*E*dt) &~tst1;  % or binds TE

   tst3=(S==2)& rnside1(it,:)<kminusv*dt;  % dissociate E
   tst4=(((S==2)&[0 S(1:N-1)==1]) & rnside1(it,:)<(kplusv*dt + kminusv*dt)) &~tst3;  % bind plus
side
   tst5=(((S==2)&[S(2:N)==1 0]) & rnside1(it,:)<(kplusv*dt + kplusv*dt+kminusv*dt))
&~(tst3|tst4); % bind minus side
   tst6=((S==2)& rnside1(it,:)<(k1v*T*dt + 2*kplusv*dt+kminusv*dt)) &~(tst3|tst4|tst5); % bind T

   tst7=(S==3)& rnside1(it,:)<k1mv*dt; % dissociate T
   tst8=(S==4)& rnside1(it,:)<kminusv*dt; % dissociate plus side
   tst9=(S==5)& rnside1(it,:)<kminusv*dt; % dissociate minus side of bound E
   tst10=((S==3) & rnside1(it,:)<(kminusv*dt+k1mv*dt)) &~(tst7); %dissociate TE from side

       otst=(tst1+tst2+tst3+tst4+tst5+tst6+tst7+tst8+tst9+tst10);  % Anything happen?

   if sum(otst)>0

       Sold=S;  % Store old
       ntav=it-previt;  % number of additional steps in average

       FL=(S==2)+(S==3)+.5*(S==5)+.5*(S==4);  % EB1 fluorsescence
       FLav=(previt*FLav+ntav*FL)/(ntav+previt);  % Update time-averaged fluorescence
       previt=it;  % update

       ifnd1=find(tst1);
       S(ifnd1)=2;
       ifnd2=find(tst2);
       S(ifnd2)=3;
       ifnd3=find(tst3);
       S(ifnd3)=1;
       ifnd4=find(tst4);
       S(ifnd4)=5; S(ifnd4-1)=4;
       ifnd5=find(tst5);
       S(ifnd5)=4; S(ifnd5+1)=5;
       ifnd6=find(tst6);
       S(ifnd6)=3;
       ifnd7=find(tst7);
       S(ifnd7)=2;
       ifnd8=find(tst8);
       S(ifnd8)=1; S(ifnd8+1)=2;
       ifnd9=find(tst9);
       S(ifnd9)=1; S(ifnd9-1)=2;
       ifnd10=find(tst10);
       S(ifnd10)=1;

   S=S(1:N);
   FLav;
   plot(1:N,FLav,[1 N],[fl_eq fl_eq],'r'); axis([0 N 0 axmax]); drawnow;
        Veloc = nadd/it/dt*d;
   end

   % Tubulin addition

   ta1 = radd(it)<kf*T*dt;  % add T
   ta2 = radd(it)<(kfE*TE*dt+kf*T*dt) &~ ta1; % add TE
   ta3 = radd(it)<(2*kfE*TTE*dt+kfE*TE*dt+kf*T*dt) &~ (ta1|ta2); % add TTE
   ta4 = radd(it)<(kfE*Ceff*dt+kfE*2*TTE*dt+kfE*TE*dt+kf*T*dt)*(S(1)==3) &~(ta1|ta2|ta3);


   if ta1|ta2|ta3|ta4
       ntav=it-previt;
```

```
        FL=(S==2)+(S==3)+.5*(S==5)+.5*(S==4);
        FLav=(previt*FLav+ntav*FL)/(ntav+previt);
        previt=it;
        nadd=nadd+1;
        S(2:N)=S(1:N-1);
        if ta1
            S(1)=1;
        elseif ta2
           S(1)=2;
        elseif ta3;
           S(1)=3;
        elseif ta4
           S(1)=4; S(2)=5;
        end
    end

   % Tubulin removal

    ta5 = roff(it)<(S(1)==1)*kr*dt;
    ta6 = roff(it)<(S(1)==2)*krE*dt;
    ta7 = roff(it)<(S(1)==3)*krE*dt;
    ta8 = roff(it)<(S(1)==4)*krE*dt;
     if ta5|ta6|ta7|ta8
         Sold=S;
        ntav=it-previt;

        FL=(S==2)+(S==3)+.5*(S==5)+.5*(S==4);
        FLav=(previt*FLav+ntav*FL)/(ntav+previt);
        previt=it;
        nadd=nadd-1;
        S(1:N-1)=S(2:N);
        if S(N-1)==4
            S(N)=5;
        else
           S(N) = S(N-1);
        end
        if ta8
          S(1)=3;
        end
     end

     if S(1)==5
         [ta1 ta2 ta3 ta4 ta5 ta6 ta7 ta8];
         otst;
         pause
     end
     it/nt
end

% Velocity(irun)=Veloc;
```

### B.3.4 Tethered Protofilament Growth with Divalent EB1

This stochastic model simulates the growth of a single microtubule protofilament in the presence of divalent, EB1 end-tracking motors and an applied force. The value of the affinity modulation factor, applied force, and $K_T$ can be varied to determine the resulting velocity. This model also provides the state of the terminal subunit, position of the tracking unit, the time average fluorescence along the protofilament, and time spent in each pathway. The kinetic parameters were estimated or used from literature values.

```
% Stochastic model
% Simulates tethered MT's in presence of EB1
% Divalent EB1
% Inputs: f, Kd1, kon
```

```
% Outputs: Velocity, State of Subunit, Position of Track
% Plots: Time Avg Fluorescence vs Subunit

%clear all;
tic

rnside1=0;
radd = 0;
roff=0;
rndT=0;

tim=1; % run time (s)
axmax=1; % max y-axis.

% Determine Parameters

% Fixed parameters
T = 10  ; % uM  tubulin dimer concentration
V = 170; % nm/s;  % elongation speed
d = 8; % nm;  % subunit length

kf = V/d/T; % uM^-1s^-1   on-rate for tubulin -taken assuming irreversible elongation at
observed elongation speed
Tc = 5; % uM plus-end critical concentration
kr = kf*Tc; % s^-1 off-rate, assuming Tc=kr/kf;

thalf=2.6; % s
kobs=log(2)/thalf; %  s^-1  decay rate constant of EB1 from MT sides
EB1 = 0.27; %  uM  EB1 concentration

sigma = 10 ; % nm   stdev of EB1 position fluctuations
ceff = 2*exp(-(8/10)^2/2)/(2*pi)^(3/2)/sigma^3;  % concentration in nm^-3 -- based on 3-D normal
distribution on half-sphere
Ceff = ceff/(6.022e23)*1e27/1000*1e6;  % nm-3 x (1 mol/ 6.022e23) x (1e27 nm^3/m^3) x (1 m^3/1000
L) x (10^6 uM/M)

K = 37; % equals kplus_side/kminus_side, valued required for Kdeff = 0.44

Kd1 = .65;      % Kd, Dissociation constant for EB1 subunit and T, Kd1=k1m/k1 (uM) - Value for
typical monovalent protein
%Kd1=Kd1vec(irun);

k1 = 10;    % On-rate for EB1 subunit and T (uM^-1*s^-1), Value for typical protein-protein
binding
k1m = k1*Kd1;  % Off-rate for EB1 subunit and T (s^-1)


%%%  Equlibria

E = EB1/((1+(T/Kd1))^2);  % [EB1], Concentration of EB1 dimer in sol'n
TE = 2*E*T/Kd1;           % [EB1-T], Concentration of EB1 dimer bound to 1 tubulin protomer
TTE = T*TE/(2*Kd1);       % [EB1-T^2], Concentration of EB1 dimer bound to 2 tubulin protomers

a=4*K^2*E/Ceff;
b=(1+T/Kd1)*2*K*E/Ceff+1;

u_eq = (-b+sqrt(b^2+4*a))/2/a;
p_eq=2*K*E/Ceff*u_eq;
q_eq = 2*K*p_eq*u_eq;
pi_eq = T/Kd1*p_eq;

fl_eq=p_eq+pi_eq+q_eq/2;   %%% Equilibrium flourescence conc
check = u_eq+p_eq+q_eq+pi_eq;   %%% should equal one


%% Determine kminus_side, kplus_side, kon

kminus_side = kobs*(1+K*u_eq/(1+T/Kd1));  %% Based on FRAP half-life
kplus_side = K*kminus_side;  %% by definition
kon_side = kplus_side/Ceff;

%f = 1; % affinity modulation factor
f=fvec(irun);

%% Mixed model -- chose kon, calculated koff from f
kon = 5; % uM-1s-1
fon =  kon/kon_side;  %%% accelerated on-rate at end
kplus = kon*Ceff;
foff = fon/f;
kminus=fon/f*kminus_side; %%% corresponding change off-rate at end
```

```
%%% Other parameters

kfE = kf; % on-rate constant of TE and TTE to MT end  uM-1s-1;
krE = kfE*Tc/Kd1*kminus/kon;  % off-rate constant of TE or TTE


% Initial conditions

S=ones(1,N);  %S = 1 if unocupplied; 2 if bound to E, 3 if bound to TEE, 4 if bound to +side of
doubly bound, 5 if bound to -side
previt=0; FLav=0*S;
nadd=1;

konv=[kon kon_side*ones(1,N-1)];
kminusv=[kminus kminus_side*ones(1,N-1)];
kplusv=[kplus kplus_side*ones(1,N-1)];
k1v=k1*ones(1,N);
k1mv=k1m*ones(1,N);


%KT =10;% 5;  % eq. dissoc const. for tracker binding to EB1
KT=KTvec(irun);
kfT = 5; %
krT = KT*kfT;

%%%%% Tracking unit parameters
sigT = 10; % nm; tracking unit stdev
kT=4.1; %pN-nm
d=8; %nm - spacing
gamT = kT/sigT^2; % pN/nm  Tracking unit stiffness
CpT0 = 100; %% uM - effective concentration of Tracking unit end MT end
delta = 1; % nm -- transition state distance

%q=0;
q=qvec(irun);
Force = q*log(T/Tc)*kT/d;  %pN
Ffac = exp(-Force*d/kT);

konTv = konv.*CpT0.*exp(-gamT*((1:N)-1).^2*d^2/2/kT+gamT*((1:N)-1)*delta*d/kT);  % Effect of
stretching on Tracker-bound Eb1 binding
kfEp = kfE*CpT0;  % forward rate for transfer of tubulin from tracking unit (based on detailed
balance)
kfTv = kfT.*CpT0.*exp(-gamT*((1:N)-1).^2*d^2/2/kT+gamT*((1:N)-1)*delta*d/kT);  % Effect of
stretching on Tracker binding to MT-bound EB1

Track = 0;
Trackdist=0*(1:N);

chartime=1/max([kfEp sum(konTv) sum(kfTv) kfT*TTE kfT*TE kfT*E kfE*TTE kfE*TE kf*T kr krE kon*T
k1*T k1 kplus kplus_side kminus kminus_side]); %Characteristic time
dt = chartime/20;  %simulation time increment
nt=round(tim/dt);
rnside1=rand(nt,N);
radd = rand(nt,1);
roff=rand(nt,1);
rndT=rand(nt,1);


for it=1:nt;  %% Start time loop

   %% Side binding

   tst1=(S==1)& rnside1(it,:)<2*konv*E*dt;  % binds E
   tst2= (S==1)& rnside1(it,:)<(konv*TE*dt+2*konv*E*dt) &~tst1;  % or binds TE

   tst3=(S==2)& rnside1(it,:)<kminusv*dt;  % dissociate E
   tst4=(((S==2)&[0 S(1:N-1)==1]) & rnside1(it,:)<(kplusv*dt + kminusv*dt)) &~tst3;  % bind plus
side
   tst5=(((S==2)&[S(2:N)==1 0]) & rnside1(it,:)<(kplusv*dt + kplusv*dt+kminusv*dt))
&~(tst3|tst4); % bind minus side
   tst6=((S==2)& rnside1(it,:)<(k1v*T*dt + 2*kplusv*dt+kminusv*dt)) &~(tst3|tst4|tst5); % bind T
to E

   tst7=(S==3)& rnside1(it,:)<k1mv*dt; % dissociate T from E
   tst8=(S==4)& rnside1(it,:)<kminusv*dt; % dissociate plus side
   tst9=(S==5)& rnside1(it,:)<kminusv*dt; % dissociate minus side of bound E
   tst10=((S==3) & rnside1(it,:)<(kminusv*dt+k1mv*dt)) &~(tst7); %dissociate TE from side

       otst=(tst1+tst2+tst3+tst4+tst5+tst6+tst7+tst8+tst9+tst10);  % Anything happen?
```

```
    if sum(otst)>0

        Sold=S;  % Store old
        ntav=it-previt;  % number of additional steps in average

        FL=(abs(S)==2)+(abs(S)==3)+.5*(abs(S)==5)+.5*(abs(S)==4);  % EB1 fluorsescence
        FLav=(previt*FLav+ntav*FL)/(ntav+previt);  % Update time-averaged fluorescence
        previt=it;  % update

        ifnd1=find(tst1);
        S(ifnd1)=2;
        ifnd2=find(tst2);
        S(ifnd2)=3;
        ifnd3=find(tst3);
        S(ifnd3)=1;
        ifnd4=find(tst4);
        S(ifnd4)=5; S(ifnd4-1)=4;
        ifnd5=find(tst5);
        S(ifnd5)=4; S(ifnd5+1)=5;
        ifnd6=find(tst6);
        S(ifnd6)=3;
        ifnd7=find(tst7);
        S(ifnd7)=2;
        ifnd8=find(tst8);
        S(ifnd8)=1; S(ifnd8+1)=2; S=S(1:N);
        ifnd9=find(tst9);
        S(ifnd9)=1; S(ifnd9-1)=2;
        ifnd10=find(tst10);
        S(ifnd10)=1;

        if ifnd3>0 & ifnd3(1)==1 | ifnd8>0 & ifnd8(1)==1| ifnd10>0 & ifnd10(1)==1;
            S1(1,irun)=S1(1,irun)+1;
        elseif ifnd1>0 & ifnd1(1)==1| ifnd7>0 & ifnd7(1)==1| ifnd9>0 & ifnd9(1)==2;
            S1(2,irun)=S1(2,irun)+1;
        elseif ifnd2>0 & ifnd2(1)==1| ifnd6>0 & ifnd6(1)==1;
            S1(3,irun)=S1(3,irun)+1;
        elseif ifnd4>0 & ifnd4(1)==2| ifnd5>0 & ifnd5(1)==1;
            S1(4,irun)=S1(4,irun)+1;
        end
    end

    if Track<1    %%% start unbound tracker loop

     % Tubulin addition
     ta1 = radd(it)<kf*Ffac*T*dt;  % add T
     ta2 = radd(it)<(kfE*Ffac*TE*dt+kf*Ffac*T*dt) &~ ta1; % add TE
     ta3 = radd(it)<(2*kfE*Ffac*TTE*dt+kfE*Ffac*TE*dt+kf*Ffac*T*dt) &~ (ta1|ta2); % add TTE
     ta4 = radd(it)<(kfE*Ffac*Ceff*dt+kfE*Ffac*2*TTE*dt+kfE*Ffac*TE*dt+kf*Ffac*T*dt)*(S(1)==3)
&~(ta1|ta2|ta3);

     if ta1|ta2|ta3|ta4
         ntav=it-previt;

         FL=(abs(S)==2)+(abs(S)==3)+.5*(abs(S)==5)+.5*(abs(S)==4);
         FLav=(previt*FLav+ntav*FL)/(ntav+previt);
         previt=it;
         nadd=nadd+1;
         S(2:N)=S(1:N-1);
         if ta1
             S(1)=1;
             count(1,irun)=count(1,irun)+1;
             S1(1,irun)=S1(1,irun)+1;
         elseif ta2
            S(1)=2;
            count(2,irun)=count(2,irun)+1;
            S1(2,irun)=S1(2,irun)+1;
         elseif ta3;
            S(1)=3;
            count(3,irun)=count(3,irun)+1;
             S1(3,irun)=S1(3,irun)+1;
         elseif ta4
            S(1)=4; S(2)=5;
            count(4,irun)=count(4,irun)+1;
            S1(4,irun)=S1(4,irun)+1;
         end
     end

    % Tubulin removal
     ta5 = roff(it)<(S(1)==1)*kr*dt;
     ta6 = roff(it)<(S(1)==2)*krE*dt;
     ta7 = roff(it)<(S(1)==3)*krE*dt;
```

```
   ta8 = roff(it)<(S(1)==4)*krE*dt;

    if ta5|ta6|ta7|ta8
       Sold=S;
       ntav=it-previt;
       FL=(abs(S)==2)+(abs(S)==3)+.5*(abs(S)==5)+.5*(abs(S)==4);
       FLav=(previt*FLav+ntav*FL)/(ntav+previt);
       previt=it;
       nadd=nadd-1;
       S(1:N-1)=S(2:N);
       if S(N-1)==4
           S(N)=5;
       else
          S(N) = S(N-1);
       end

       if ta5
        count(5,irun)=count(5,irun)+1;
       elseif ta6
        count(6,irun)=count(6,irun)+1;
       elseif ta7
        count(7,irun)=count(7,irun)+1;
       elseif ta8
         S(1)=3;
         count(8,irun)=count(8,irun)+1;
       end

       if S(1)==1;
           S1(1,irun)=S1(1,irun)+1;
       elseif S(1)==2;
           S1(2,irun)=S1(2,irun)+1;
       elseif S(1)==3;
           S1(3,irun)=S1(3,irun)+1;
       elseif S(1)==4;
           S1(4,irun)=S1(4,irun)+1;
       end
     end

%%% Track =0  Tracking unit unbound

    tTa = (Track==0)& rndT(it)<kfT*E*dt;  % Bind E
    tTb = ((Track==0)& rndT(it)<(kfT*TE*dt+kfT*E*dt)) &~ tTa;  % Bind TE
    tTc = ((Track==0)& rndT(it)<(kfT*TTE*dt+kfT*TE*dt+kfT*E*dt)) &~ (tTa|tTb);  % Bind TTE
    totA = cumsum((S==2).*kfTv*dt);
    tTd = ((Track==0) & rndT(it) < (totA(N)+kfT*TTE*dt+kfT*TE*dt+kfT*E*dt)) &~ (tTa|tTb|tTc);  %
Binding tracking unit to EB1 on MT
    totA2 =  cumsum((S==3).*kfTv*dt);
    tTe = ((Track==0) & rndT(it) < (totA2(N)+totA(N)+kfT*TTE*dt+kfT*TE*dt+kfT*E*dt)) &~
(tTa|tTb|tTc|tTd);  % Binding tracking unit to TE on MT
    totA3 =  cumsum((S==5).*kfTv*dt);
    tTf = ((Track==0) & rndT(it) < (totA3(N)+totA2(N)+totA(N)+kfT*TTE*dt+kfT*TE*dt+kfT*E*dt)) &~
(tTa|tTb|tTc|tTd|tTe);  % Binding tracking unit to doubly bound TE on MT

%%% Track = -1  Tracking unit bound w/ E
    tT1 = (Track==-1)& rndT(it)<2*k1*T*dt;  % Binding tracking unit to 1st tubulin
    totB = cumsum((S==1).*2.*konTv*dt); %
    tT2 = ((Track==-1)& rndT(it)<(totB(N)+2*k1*T*dt)) &~ tT1; % Binds MT
    tT3 =  ((Track==-1) & rndT(it) < (krT*dt + totB(N)+2*k1*T*dt)) &~ (tT1|tT2);  % release EB1


%%% Track = -2  Tracking unit bound w/ TE
    tT4 = (Track==-2)& rndT(it)<k1*T*dt;     % Binding tracking unit to 2nd tubulin
    tT5 = (Track==-2)& rndT(it)<(k1m*dt+k1*T*dt) &~tT4;  % dissociate 1st tubulin
    totC = cumsum((S==1).*konTv*dt);
    tT6 = ((Track==-2)& rndT(it)<(totC(N)+k1m*dt+k1*T*dt)) &~ (tT4|tT5); % Binds free MT site
    tT7 = ((Track==-2) & rndT(it)<(krT*dt+totC(N)+k1m*dt+k1*T*dt))&~ (tT4|tT5|tT6); % release TE
    tT8 = ((Track==-2) & rndT(it)<(kfEp*Ffac*dt+krT*dt+totC(N)+k1m*dt+k1*T*dt))&~
(tT4|tT5|tT6|tT7);  % transfer T to end


%%% Track = -3  Tracking unit bound w/ TTE
   tT9 = (Track==-3)& rndT(it)<2*k1m*dt;  % release one tubulin
   tT10 = ((Track==-3)& rndT(it)<(krT*dt+2*k1m*dt)) &~ tT9;  % release TTE
   tT11 = ((Track==-3)& rndT(it)<(2*kfEp*Ffac*dt+krT*dt+2*k1m*dt)) &~ (tT9|tT10);  % transfer
tubulin to end

   if tTa
       Track=-1;
   elseif tTb
       Track =-2;
   elseif tTc
```

```
        Track = -3;
    elseif tTd
        %% find which subunit bound
        ifnd=find(rndT(it)<(totA+kfT*TTE*dt+kfT*TE*dt+kfT*E*dt));
        Track=min(ifnd);
        S(Track)=-2;
        if Track==1;
            S1(6,irun)=S1(6,irun)+1;
        end
    elseif tTe
         %% find which subunit bound
        ifnd=find(rndT(it)<(totA2+totA(N)+kfT*TTE*dt+kfT*TE*dt+kfT*E*dt));
        Track=min(ifnd);
         S(Track)=-3;
         if Track==1;
            S1(7,irun)=S1(7,irun)+1;
         end
    elseif tTf
       %% find which subunit bound
        ifnd=find(rndT(it)<(totA3+totA2(N)+totA(N)+kfT*TTE*dt+kfT*TE*dt+kfT*E*dt));
        Track=min(ifnd);
        if Track>1
        S(Track)=-5;
        S(Track-1) = -4;
        end
        if Track-1==1;
            S1(8,irun)=S1(8,irun)+1;
        end
    elseif tT1
        Track = -2;
    elseif tT2
        %% find which subunit bound
        ifnd=find(rndT(it)<(totB+2*k1*T*dt));
        Track=min(ifnd);
        S(Track) = -2;
        if Track==1;
            S1(6,irun)=S1(6,irun)+1;
        end
    elseif tT3
        Track = 0;
    elseif tT4
        Track = -3;
    elseif tT5
        Track = -1;
    elseif tT6
        % find which subunit bound
        ifnd=find(rndT(it)<(totC+k1m*dt+k1*T*dt));
        Track=min(ifnd);
        S(Track) = -3;
        if Track==1;
            S1(7,irun)=S1(7,irun)+1;
        end
    elseif tT7
        Track =0;
    elseif tT8
        Track =1;
        S(2:N)=S(1:N-1);
        S(1)=-2;
        nadd=nadd+1;
        count(9,irun)=count(9,irun)+1;
        S1(6,irun)=S1(6,irun)+1;
    elseif tT9
        Track = -2;
    elseif tT10
        Track = 0;
    elseif tT11
        Track =1;
        S(2:N)=S(1:N-1);
        S(1)=-3;
        nadd=nadd+1;
        count(10,irun)=count(10,irun)+1;
        S1(7,irun)=S1(7,irun)+1;
    end

if Track==-3;
    T1(1,irun)=T1(1,irun)+1;
elseif Track==-2;
    T1(2,irun)=T1(2,irun)+1;
elseif Track==-1;
    T1(3,irun)=T1(3,irun)+1;
elseif Track==0;
```

```
    T1(4,irun)=T1(4,irun)+1;
else
    T1(Track,irun)=T1(Track,irun)+1;
end

  elseif Track>0
      Trackdist(Track)=Trackdist(Track)+1;
     ffac = exp(-gamT*(Track-.5)*d^2/kT);  % rate factor due to stretching tracking unit upon
addition

    % Tubulin addition
   ta1 = radd(it)<ffac*kf*Ffac*T*dt;  % add T
   ta2 = radd(it)<(ffac*kfE*Ffac*TE*dt+ffac*kf*Ffac*T*dt) &~ ta1; % add TE
   ta3 = radd(it)<(ffac*2*kfE*Ffac*TTE*dt+ffac*kfE*Ffac*TE*dt+ffac*kf*Ffac*T*dt) &~ (ta1|ta2); %
add TTE
   ta4 =
radd(it)<(ffac*kfE*Ffac*Ceff*dt+ffac*kfE*Ffac*2*TTE*dt+ffac*kfE*Ffac*TE*dt+ffac*kf*Ffac*T*dt)*(ab
s(S(1))==3) &~(ta1|ta2|ta3);  % add from TE-bound MT

   if ta1|ta2|ta3|ta4
       ntav=it-previt;

       FL=(abs(S)==2)+(abs(S)==3)+.5*(abs(S)==5)+.5*(abs(S)==4);
       FLav=(previt*FLav+ntav*FL)/(ntav+previt);
       previt=it;
       nadd=nadd+1;
       Track=Track+1;
       S(2:N)=S(1:N-1);
       if ta1
           S(1)=1;
       count(11,irun)=count(11,irun)+1;
       S1(1,irun)=S1(1,irun)+1;
       elseif ta2
          S(1)=2;
       count(12,irun)=count(12,irun)+1;
       S1(2,irun)=S1(2,irun)+1;
       elseif ta3;
          S(1)=3;
       count(13,irun)=count(13,irun)+1;
       S1(3,irun)=S1(3,irun)+1;
       elseif ta4
          if Track ==2
             S(1) = -4; S(2)=-5;  % bound tracking unit
              S1(8,irun)=S1(8,irun)+1;
          else
             S(1)=4; S(2)=5;  % unbound tracking unit
             S1(4,irun)=S1(4,irun)+1;
          end
          count(14,irun)=count(14,irun)+1;
       end

    if Track==-2;
         T1(2,irun)=T1(2,irun)+1;
    elseif Track==-1;
         T1(3,irun)=T1(3,irun)+1;
    elseif Track==0;
          T1(4,irun)=T1(4,irun)+1;
    else
          T1(Track,irun)=T1(Track,irun)+1;
    end

   end

  % Tubulin removal

   ta5 = roff(it)<(S(1)==1)*kr*dt;
   ta6 = roff(it)<(abs(S(1))==2)*krE*dt;
   ta7 = roff(it)<(abs(S(1))==3)*krE*dt;
   ta8 = roff(it)<(abs(S(1))==4)*krE*dt;
    if ta5|ta6|ta7|ta8
        Sold=S;
       ntav=it-previt;

       FL=(abs(S)==2)+(abs(S)==3)+.5*(abs(S)==5)+.5*(abs(S)==4);
       FLav=(previt*FLav+ntav*FL)/(ntav+previt);
       previt=it;
       nadd=nadd-1;
       if Track ==1
          if ta6
              Track = -2;
          elseif ta7
```

```
            Track = -3;
        end
    else
        Track=Track-1;
    end

    S(1:N-1)=S(2:N);

    if S(N-1)==4
        S(N)=5;
    elseif S(N-1)==-4
        S(N)=-5;
    else
       S(N) = S(N-1);
    end

    if ta5
     count(15,irun)=count(15,irun)+1;
    elseif ta6
     count(16,irun)=count(16,irun)+1;
    elseif ta7
     count(17,irun)=count(17,irun)+1;
    elseif ta8
      if S(1)==-5;
         S(1)=-3;
      else
        S(1)=3;
      end
      count(18,irun)=count(18,irun)+1;
    end

    if S(1)==1;
        S1(1,irun)=S1(1,irun)+1;
    elseif S(1)==2;
        S1(2,irun)=S1(2,irun)+1;
    elseif S(1)==3;
        S1(3,irun)=S1(3,irun)+1;
    elseif S(1)==4;
        S1(4,irun)=S1(4,irun)+1;
    elseif S(1)==-1;
        S1(5,irun)=S1(5,irun)+1;
    elseif S(1)==-2;
        S1(6,irun)=S1(6,irun)+1;
    elseif S(1)==-3;
        S1(7,irun)=S1(7,irun)+1;
    elseif S(1)==-4;
        S1(8,irun)=S1(8,irun)+1;
    end

   if Track==-3;
        T1(1,irun)=T1(1,irun)+1;
   elseif Track==-2;
        T1(2,irun)=T1(2,irun)+1;
   elseif Track==-1;
       T1(3,irun)=T1(3,irun)+1;
   elseif Track==0;
        T1(4,irun)=T1(4,irun)+1;
   else
         T1(Track,irun)=T1(Track,irun)+1;
   end
  end

  if Track>0

  %%% Tracking unit-E detachment
  kminusv =[kminus kminus_side.*ones(1,N-1)];
  ffac2 = exp(gamT*(Track-1)*d*delta/kT);
  ffac3 = exp(-gamT*(Track-.5)*d^2/kT);


  %%% Doubly bound EB1
  tst1 = (S(Track) == -5)& rndT(it)<kminusv(Track)*ffac2*dt;  %  detachment of minus-side EB1
head (doubly bound)
  tst1a = ((S(Track) == -5)& rndT(it)<(krT*ffac2*dt+kminusv(Track)*ffac2*dt)) &~ tst1;  %
detachment of tracking from doubly bound EB1
  tst1b = ((S(Track) == -5) & rndT(it)< (kminusv(Track-
(Track>1))*dt+krT*ffac2*dt+kminusv(Track)*ffac2*dt)) &~ (tst1|tst1a); %  detachment of plus-side
EB1 head (doubly bound)

  %%% bound T-E
  tst2 = (S(Track) == -3)& rndT(it)<kminusv(Track)*ffac2*dt;  % detachment of Track-TE from MT
```

```
   tst2a = ((S(Track) == -3)& rndT(it)<(krT*ffac2*dt+kminusv(Track)*ffac2*dt)) &~ tst2; % detach
Track from TE
   tst2b =  ((S(Track) == -3)& rndT(it)<(k1m*dt+krT*ffac2*dt+kminusv(Track)*ffac2*dt)) &~
(tst2|tst2a); % dissociate T


   %%% bound E
   tst3 = (S(Track) == -2)& rndT(it)<kminusv(Track)*ffac2*dt;  % detachment of Track-E from MT
   tst3a = ((S(Track) == -2)& rndT(it)<(krT*ffac2*dt + kminusv(Track)*ffac2*dt)) &~ tst3;  %
detach Tracker
   tst3b = ((S(Track) == -2)& rndT(it)<(k1*TE*dt+krT*ffac2*dt+kminusv(Track)*ffac2*dt)) &~
(tst3|tst3a); % add T
   tst3c = ((S(Track) == -2)& S(Track+1)==1 &
rndT(it)<(kplus_side*ffac3*ffac2*dt+k1*TE*dt+krT*ffac2*dt+kminusv(Track)*ffac2*dt)) &~
(tst3|tst3a|tst3b); % bind second head in minus-direction

   if Track>1
     tst3d = ((S(Track-1)==1 & S(Track) == -2)& rndT(it)<(kplusv(Track-
1)*dt+kplus_side*ffac3*ffac2*dt+k1*TE*dt+krT*ffac2*dt+kminusv(Track)*ffac2*dt)) &~
(tst3|tst3a|tst3b|tst3c); % bind second head in plus-direction
   else
     tst3d=0;
   end

   if tst1
       Track=Track-1;
       S(Track) = -2;
       S(Track+1) = 1;
       if Track==1;
       S1(6,irun)=S1(6,irun)+1;
       end
   elseif tst1a
       Track_old=Track;
       S(Track) = 5;
       S(Track-1)=4;
       Track = 0;
       if Track_old-1==1;
       S1(4,irun)=S1(4,irun)+1;
       end
   elseif tst1b
       S(Track) = -2;
       S(Track-1) = 1;
       if Track-1==1;
       S1(1,irun)=S1(1,irun)+1;
       end
   elseif tst2
       Track_old=Track;
       S(Track) = 1;
       Track = -2;
       if Track_old==1;
           S1(1,irun)=S1(1,irun)+1;
       end
   elseif tst2a
       Track_old=Track;
       S(Track) = 3;
       Track = 0;
       if Track_old==1;
          S1(3,irun)=S1(3,irun)+1;
       end
   elseif tst2b
       S(Track) = -2;
       if Track==1;
           S1(6,irun)=S1(6,irun)+1;
       end
   elseif tst3
       Track_old=Track;
       S(Track) = 1;
       Track = -1;
       if Track_old==1;
           S1(1,irun)=S1(1,irun)+1;
       end
   elseif tst3a
       Track_old=Track;
       S(Track) = 2;
       Track = 0;
       if Track_old==1;
           S1(2,irun)=S1(2,irun)+1;
       end
   elseif tst3b
       S(Track) = -3;
       if Track==1;
```

```
            S1(7,irun)=S1(7,irun)+1;
        end
    elseif tst3c
        Track_old=Track;
        S(Track+1) = -5;
        S(Track) = -4;
        Track=Track+1;
        if Track_old==1;
            S1(8,irun)=S1(8,irun)+1;
        end
    elseif tst3d
        Track_old=Track;
        S(Track) = -5;
        S(Track-1) = -4;
        if Track_old-1==1;
            S1(8,irun)=S1(8,irun)+1;
        end
    end

if Track==-3;
    T1(1,irun)=T1(1,irun)+1;
elseif Track==-2;
    T1(2,irun)=T1(2,irun)+1;
elseif Track==-1;
    T1(3,irun)=T1(3,irun)+1;
elseif Track==0;
    T1(4,irun)=T1(4,irun)+1;
else
    T1(Track,irun)=T1(Track,irun)+1;
end
    end % Ends "if Track>0" Loop
  end %Ends "if Track<1, elseif Track>0 Loop"

  irun
  percent=(nt*(irun-1)+it)/(nt*nrun)
  Veloc = nadd/it/dt*d;

end % Ends "for it=1:nt" time loop

kon_vect=kon*vector;
Kd1v=Kd1*vector;
timv=tim*vector;
Nv=N*vector;
F = (qvec*log(T/Tc)*kT/d);
Velocity(irun)=Veloc;
matrix=[kon_vect',Kd1v',KTvec',fvec',qvec',F',Velocity',timv',Nv'];

xlswrite('sim_track_M.xls', matrix','matrix');  % Save position & time data in Excel
xlswrite('sim_track_M.xls', count,'count');  % Save position & time data in Excel
xlswrite('sim_track_M.xls', S1,'S');  % Save
```

The following is a macro that runs the stochastic model above at various values of $f$, $K_T$, and $q$.

```
% This macro runs track for multiple parameter sets
% Inputs: f, KT, q
% Outputs: Velocity, state of subunit, location of tracking unit

clear all;
tic;

fvec=[1000*ones(1,20)];  % f
qvec=[0,0.25,0.5,1,2,3,4,5,6,7,0,0.25,0.5,1,2,3,4,5,6,7];
KTvec=[0.1*ones(1,10),10*ones(1,10)];

N=40;  % number of subunits to simulate
Velocity=0*fvec;
nrun=length(fvec);
vector=ones(1,nrun);
count=zeros(18,nrun);
S1=zeros(8,nrun);
T1=zeros(N+4,nrun);

for irun=1:nrun;
   track
end

Velocity(irun)=Veloc;
kon_vect=kon*vector;
```

```
Kd1v=Kd1*vector;
timv=tim*vector;
Nv=N*vector;

F = (qvec*log(T/Tc)*kT/d);

matrix=[kon_vect',Kd1v',KTvec',fvec',qvec',F',Velocity',timv',Nv'];

xlswrite('sim_track_M.xls', matrix','matrix');  % Save position & time data in Excel
xlswrite('sim_track_M.xls', count,'count');  % Save position & time data in Excel
xlswrite('sim_track_M.xls', S1,'S');  % Save state of subunit data in Excel

S'
Track
Velocity
time=toc/3600
```

## B.4 Ciliary Plug Model

This model simulates a 13-protofilament MT polymerizing in a ciliary plug against a motile surface with a constant load. The value of the applied force and protofilament length can be varied to determine the trajectory of the ciliary plug (position versus time) and the resulting velocity. The kinetic parameters were estimated or used from literature values.

```
%  Simulates MT-based motility in ciliary plugs based on the LLF model
%  Trajectory between steps not simulated (fast version)

clear all;
hold off;

% Filament Parameters
kT=4.14; % Thermal energy (pN-nm)
nf = 13;  % No. filaments
kappa = 0.15;  % Filament compression stiffness (pN/nm)
Df = 4e6;  %  Filament diffusivity (nm^2/s)
deltaf = kT/Df;   % Filament Drag (pN-s/nm)
v=167;  % Expected velocity (nm/s)
d = 8 ; % Subunit length (nm)
Tmin = d/v;% Mean time to load (s)
Kappa2 = 60; % filament stretch stiffness (pN/nm)
pn=1. ; % Positioning error (nm)

%% Simulation setup
z0f=rand(1,nf)*100; % random initial distributin of filament lengths
z0f(1)=-kappa/kappa2*sum(z0f(2:nf)); % Set filament 1 position to balance forces
dt=.005*Tmin;  % Simulation time increment
nt = 2^18;  % total time steps
zp = 0*(1:nt); t=0; z=0;  % Initialize t=time; z= position of motile surface
nplot = 2^4; dnplot=nplot;  % Time steps between plotting
ih=1; nh=nt/nplot; zh=zeros(1,nh); th=zh;  zhn=zh; %  Plotting storage vectors/variables
nbp=10*round(Tmin/(dnplot*dt))   % Sets plotting range based on number of expecte steps
runb=rand(dnplot,nf);  % Random numbers for first set (between plotting)
diffs=randn(1,dnplot)*sqrt(2*Df/nf*dt); % dW for first set
jsim=1;   % iteration index within set
zeq=0; kf=zeros(1,nf);

for i=1:nt
  unbind=(runb(jsim,:)<(kf*dt));   % Identify those that unbind
  if sum(unbind>=1) | i==1
      z0f=z0f+unbind*d;  % Shift those that rebind  Equilibrium position
      sF=1;
      kappai=kappa*((zeq)<=z0f)+kappa2*((zeq)>z0f);  % Vector of filament stiffness
      while sF^2>1e-10;
         zeq = kappai*z0f'/sum(kappai);
         kappai=kappa*((zeq)<=z0f)+kappa2*((zeq)>z0f);  % Vector of filament stiffnesses
        F=-kappai.*(zeq-z0f);   % Vector of forces
        sF=sum(F);
```

```
      end
        stiffness=sum(kappa*((zeq)<=z0f)+kappa2*((zeq)>z0f)); % total stiffness
        fvar=kT/stiffness;   %  Position variance
      Pr = d*F/kT;   % Dimensionless force
        tau = (exp(Pr)-1-Pr)./Pr.^2;  % Dimensionless Mean Time to Shift
        T = tau*d^2/Df;  % Mean Time to Shift (s)
      kf =1./(Tmin+T) ;  % Shift probability per unit time (s-1)
  end
  z=zeq+diffs(1,jsim)*sqrt(fvar);   % Noisy position
  zp(i) = z;         % Store position


  jsim=jsim+1;
  if i==nplot
      tp=(1:i)*dt;  th(ih)=t; % Store Time
      zh(ih)=zp(i);           % Store position
      zhn(ih)=zp(i)+pn*randn(1,1); % Noisy position
      tplot=th(max(ih-nbp,1):ih);
      zplot=zh(max(ih-nbp,1):ih);
      znplot=zhn(max(ih-nbp,1):ih);
      SUBPLOT(2,1,1), plot(tplot,znplot,'r',tplot,zplot,'b');  % Plot recent trajectory
      tmin=th(max(ih-nbp,1)); tmax = max([th .1]);
      zmin=zh(max(ih-nbp,1))-3; zmax = max(zh)+5;
      axis([tmin tmax zmin zmax]);  % Axes
      zrng=(zmin:5.4:zmax);
      nlin=length(zrng);
      tlin=[ones(nlin,1)*tmin ones(nlin,1)*tmax];
      zlin=[zrng' zrng'];
      line(tlin', zlin');

      SUBPLOT(2,1,2),  hist(z0f-zeq,-5:10:max(z0f-zeq)+5);  % Histogram of filament lengths
      drawnow;
      nplot=nplot+dnplot;   % Update next iteration to plot
       ih=ih+1;  % Update plot index
      runb=rand(dnplot,nf);  % Generate random numbers for next set
      diffs=randn(1,dnplot); % "
      jsim=1;   % Reset set index
   end
   t=t+dt;   % Update time
end
```

LIST OF REFERENCES

Abrieu, A., J. A. Kahana, K. W. Wood and D. W. Cleveland. 2000. CENP-E as an essential component of the mitotic checkpoint in vitro. *Cell*. 6:817-26.

Allen, C. and G. G. Borisy. 1974. Structural polarity and directional growth of microtubules of Chlamydomonas flagella. *J Mol Biol*. 2:381-402.

Askham, J. M., P. Moncur, A. F. Markham and E. E. Morrison. 2000. Regulation and function of the interaction between the APC tumour suppressor protein and EB1. *Oncogene*. 15:1950-8.

Bell, G. I. 1978. Models for the specific adhesion of cells to cells. *Science*. 4342:618-27.

Boal, D. H. 2002. Mechanics of the Cell. Cambridge University Press, Cambridge, U.K.

Bu, W. and L. K. Su. 2003. Characterization of functional domains of human EB1 family proteins. *J Biol Chem*. 50:49721-31.

Carlier, M. F., D. Didry, R. Melki, M. Chabre and D. Pantaloni. 1988. Stabilization of microtubules by inorganic phosphate and its structural analogues, the fluoride complexes of aluminum and beryllium. *Biochemistry*. 10:3555-9.

Chretien, D. and S. D. Fuller. 2000. Microtubules switch occasionally into unfavorable configurations during elongation. *J Mol Biol*. 4:663-76.

Chretien, D., S. D. Fuller and E. Karsenti. 1995. Structure of growing microtubule ends: two-dimensional sheets close into tubes at variable rates. *J Cell Biol*. 5:1311-28.

Coue, M., V. A. Lombillo and J. R. McIntosh. 1991. Microtubule depolymerization promotes particle and chromosome movement in vitro. *J Cell Biol*. 6:1165-75.

Dembo, M. 1994. Some Mathematical Problems in Biology: Lectures on Mathematics in the Life Sciences. American Mathematical Society, Providence, RI.

Dembo, M., D. C. Torney, K. Saxman and D. Hammer. 1988. The reaction-limited kinetics of membrane-to-surface adhesion and detachment. *Proc R Soc Lond B Biol Sci*. 1274:55-83.

Dentler, W. L. 1981. Microtubule-membrane interactions in cilia and flagella. *Int Rev Cytol*. 1-47.

Dentler, W. L. and J. L. Rosenbaum. 1977. Flagellar elongation and shortening in Chlamydomonas. III. structures attached to the tips of flagellar microtubules and their relationship to the directionality of flagellar microtubule assembly. *J Cell Biol*. 3:747-59.

Desai, A. and T. J. Mitchison. 1997. Microtubule polymerization dynamics. *Annu Rev Cell Dev Biol*. 83-117.

Dickinson, R. B., L. Caro and D. L. Purich. 2004. Force generation by cytoskeletal filament end-tracking proteins. *Biophys J*. 4:2838-54.

Dickinson, R. B. and D. L. Purich. 2002. Clamped-filament elongation model for actin-based motors. *Biophys J*. 2:605-17.

Dogterom, M. and B. Yurke. 1997. Measurement of the force-velocity relation for growing microtubules. *Science*. 5339:856-60.

Eigen, M. and G. G. Hammes. 1963. Elementary steps in enzyme reactions (as studied by relaxation spectrometry). *Adv Enzymol Relat Areas Mol Biol*. 1-38.

Farr, G. W., M. B. Yaffe and H. Sternlicht. 1990. Alpha-tubulin influences nucleotide binding to beta-tubulin: an assay using picomoles of unpurified protein. *Proc Natl Acad Sci U S A*. 13:5041-5.

Fodde, R., J. Kuipers, C. Rosenberg, R. Smits, M. Kielman, C. Gaspar, J. H. van Es, C. Breukel, J. Wiegant, R. H. Giles and H. Clevers. 2001a. Mutations in the APC tumour suppressor gene cause chromosomal instability. *Nature Cell BIology*. 9.

Fodde, R., J. Kuipers, C. Rosenberg, R. Smits, M. Kielman, C. Gaspar, J. H. van Es, C. Breukel, J. Wiegant, R. H. Giles and H. Clevers. 2001b. Mutations in the APC tumour suppressor gene cause chromosomal instability. *Nat Cell Biol*. 4:433-8.

Folker, E. S., B. M. Baker and H. V. Goodson. 2005. Interactions between CLIP-170, Tubulin, and Microtubules: Implications for the Mechanism of CLIP-170 Plus-End Tracking Behavior. *Mol Biol Cell*. 11:5373-84.

Gache, V., M. Louwagie, J. Garin, N. Caudron, L. Lafanechere and O. Valiron. 2005. Identification of proteins binding the native tubulin dimer. *Biochem Biophys Res Commun*. 1:35-42.

Gardiner, C. W. 1986. Handbook of Stochastic Methods: for Physics, Chemistry and the Natural Sciences. Springer Series in Synergetics,

Gittes, F., B. Mickey, J. Nettleton and J. Howard. 1993. Flexural rigidity of microtubules and actin filaments measured from thermal fluctuations in shape. *J Cell Biol*. 4:923-34.

Green, R. A. and K. B. Kaplan. 2003. Chromosome instability in colorectal tumor cells is associated with defects in microtubule plus-end attachments caused by a dominant mutation in APC. *J Cell Biol*. 5:949-61.

Hayashi, I., A. Wilde, T. K. Mal and M. Ikura. 2005. Structural basis for the activation of microtubule assembly by the EB1 and p150Glued complex. *Mol Cell*. 4:449-60.

Hill, T. L. 1985. Theoretical problems related to the attachment of microtubules to kinetochores. *Proc Natl Acad Sci U S A*. 13:4404-8.

Honnappa, S., C. M. John, D. Kostrewa, F. K. Winkler and M. O. Steinmetz. 2005. Structural insights into the EB1-APC interaction. *Embo J*. 2:261-9.

Howard, J. 2001. Mechanics of Motor Proteins and the Cytoskeleton. Sinauer, Sunderland, MA.

Inoue, S. 1981. Cell division and the mitotic spindle. *J Cell Biol*. 3 Pt 2:131s-147s.

Inoue, S. 1982. Developmental Order: its Origin and Regulation. Alan R. Liss, New York.

Inoue, S. and E. D. Salmon. 1995. Force generation by microtubule assembly/disassembly in mitosis and related movements. *Mol Biol Cell*. 12:1619-40.

Juwana, J. P., P. Henderikx, A. Mischo, A. Wadle, N. Fadle, K. Gerlach, J. W. Arends, H. Hoogenboom, M. Pfreundschuh and C. Renner. 1999. EB/RP gene family encodes tubulin binding proteins. *Int J Cancer*. 2:275-84.

Kaplan, K. B., A. A. Burds, J. R. Swedlow, S. S. Bekir, P. K. Sorger and I. S. Nathke. 2001. A role for the Adenomatous Polyposis Coli protein in chromosome segregation. *Nat Cell Biol*. 4:429-32.

Ligon, L. A., S. S. Shelly, M. Tokito and E. L. Holzbaur. 2003. The microtubule plus-end proteins EB1 and dynactin have differential effects on microtubule polymerization. *Mol Biol Cell*. 4:1405-17.

Ligon, L. A., S. S. Shelly, M. K. Tokito and E. L. Holzbaur. 2006. Microtubule binding proteins CLIP-170, EB1, and p150Glued form distinct plus-end complexes. *FEBS Lett*. 5:1327-32.

Lodish, H., A. Berk, L. S. Zipursky, P. Matsudaira, D. Baltimore and J. Darnell. 1995. Molecular Cell Biology. W.H. Freeman and Company, New York.

Maddox, P., A. Straight, P. Coughlin, T. J. Mitchison and E. D. Salmon. 2003. Direct observation of microtubule dynamics at kinetochores in Xenopus extract spindles: implications for spindle mechanics. *J Cell Biol*. 3:377-82.

Maiato, H., J. DeLuca, E. D. Salmon and W. C. Earnshaw. 2004. The dynamic kinetochore-microtuuble interface. *J Cell Sci*. 23:5461-5477.

Matthies, H. J., R. J. Baskin and R. S. Hawley. 2001. Orphan kinesin NOD lacks motile properties but does possess a microtubule-stimulated ATPase activity. *Mol Biol Cell*. 12:4000-12.

McEwen, B. F., G. K. Chan, B. Zubrowski, M. S. Savoian, M. T. Sauer and T. J. Yen. 2001. CENP-E is essential for reliable bioriented spindle attachment, but chromosome alignment can be achieved via redundant mechanisms in mammalian cells. *Mol Biol Cell*. 9:2776-89.

Mickey, B. and J. Howard. 1995. Rigidity of microtubules is increased by stabilizing agents. *J Cell Biol*. 4:909-17.

Miller, J. M., W. Wang, R. Balczon and W. L. Dentler. 1990. Ciliary microtubule capping structures contain a mammalian kinetochore antigen. *J Cell Biol*. 3:703-14.

Mimori-Kiyosue, Y., I. Grigoriev, G. Lansbergen, H. Sasaki, C. Matsui, F. Severin, N. Galjart, F. Grosveld, I. Vorobjev, S. Tsukita and A. Akhmanova. 2005. CLASP1 and CLASP2 bind to EB1 and regulate microtubule plus-end dynamics at the cell cortex. *J Cell Biol*. 1:141-53.

Mimori-Kiyosue, Y., N. Shiina and S. Tsukita. 2000. The dynamic behavior of the APC-binding protein EB1 on the distal ends of microtubules. *Curr Biol*. 14:865-8.

Mimori-Kiyosue, Y. and S. Tsukita. 2003. "Search-and-capture" of microtubules through plus-end-binding proteins (+TIPs). *J Biochem (Tokyo)*. 3:321-6.

Mitchison, T. J. and M. W. Kirschner. 1987. Some thoughts on the partitioning of tubulin between monomer and polymer under conditions of dynamic instability. *Cell Biophys*. 35-55.

Mitchison, T. J. and E. D. Salmon. 2001. Mitosis: a history of division. *Nat Cell Biol*. 1:E17-21.

Mogilner, A. and G. Oster. 1996. Cell motility driven by actin polymerization. *Biophys J*. 6:3030-45.

Nakamura, M., X. Z. Zhou and K. P. Lu. 2001. Critical role for the EB1 and APC interaction in the regulation of microtubule polymerization. *Curr Biol*. 13:1062-7.

O'Brien, E. T., W. A. Voter and H. P. Erickson. 1987. GTP hydrolysis during microtubule assembly. *Biochemistry*. 13:4148-56.

Olmsted, J. B. and G. G. Borisy. 1973. Microtubules. *Annu Rev Biochem*. 507-40.

Pedersen, L. B., S. Geimer, R. D. Sloboda and J. L. Rosenbaum. 2003. The Microtubule plus end-tracking protein EB1 is localized to the flagellar tip and basal bodies in *Chlamydomonas reinhardtii*. *Curr Biol*. 22:1969-74.

Peskin, C. S., G. M. Odell and G. F. Oster. 1993. Cellular motions and thermal fluctuations: the Brownian ratchet. *Biophys J*. 1:316-24.

Piehl, M. and L. Cassimeris. 2003. Organization and dynamics of growing microtubule plus ends during early mitosis. *Mol Biol Cell*. 3:916-25.

Rieder, C. L. and S. P. Alexander. 1990. Kinetochores are transported poleward along a single astral microtubule during chromosome attachment to the spindle in newt lung cells. *J Cell Biol*. 1:81-95.

Rieder, C. L., R. W. Cole, A. Khodjakov and G. Sluder. 1995. The checkpoint delaying anaphase in response to chromosome monoorientation is mediated by an inhibitory signal produced by unattached kinetochores. *J Cell Biol*. 4:941-8.

Rieder, C. L. and E. D. Salmon. 1998. Motile kinetochores and polar ejection forces dictate chromosome position on the vertebate mitotic spindle. *Trends in Cell Biology*. 310-318.

Rieder, C. L., A. Schultz, R. Cole and G. Sluder. 1994. Anaphase onset in vertebrate somatic cells is controlled by a checkpoint that monitors sister kinetochore attachment to the spindle. *J Cell Biol*. 5:1301-10.

Rogers, S. L., G. C. Rogers, D. J. Sharp and R. D. Vale. 2002. Drosophila EB1 is important for proper assembly, dynamics, and positioning of the mitotic spindle. *J Cell Biol*. 5:873-84.

Salmon, E. D. 1989. Microtubule dynamics and chromosome movement. In: Mitosis: Molecules and Mechanisms, ed. Academic Press Limited, New York.

Schilstra, M. J., S. R. Martin and P. M. Bayley. 1987. On the relationship between nucleotide hydrolysis and microtubule assembly: studies with a GTP-regenerating system. *Biochem Biophys Res Commun*. 2:588-95.

Schroder, J. M., L. Schneider, S. T. Christensen and L. B. Pedersen. 2007. EB1 Is Required for Primary Cilia Assembly in Fibroblasts. *Curr Biol*. 13:1134-9.

Schuyler, S. C. and D. Pellman. 2001. Microtubule "plus-end-tracking proteins": The end is just the beginning. *Cell*. 4:421-4.

Severin, F. F., P. K. Sorger and A. A. Hyman. 1997. Kinetochores distinguish GTP from GDP forms of the microtubule lattice. *Nature*. 6645:888-91.

Skibbens, R. V., V. P. Skeen and E. D. Salmon. 1993. Directional instability of kinetochore motility during chromosome congression and segregation in mitotic newt lung cells: a push-pull mechanism. *J Cell Biol*. 4:859-75.

Sloboda, R. D. and L. Howard. 2007. Localization of EB1, IFT polypeptides, and kinesin-2 in Chlamydomonas flagellar axonemes via immunogold scanning electron microscopy. *Cell Motil Cytoskeleton*.

Stewart, R. J., K. W. Farrell and L. Wilson. 1990. Role of GTP hydrolysis in microtubule polymerization: evidence for a coupled hydrolysis mechanism. *Biochemistry*. 27:6489-98.

Suprenant, K. A. and W. L. Dentler. 1988. Release of intact microtubule-capping structures from Tetrahymena cilia. *J Cell Biol*. 6 Pt 1:2259-69.

Tirnauer, J. S., J. C. Canman, E. D. Salmon and T. J. Mitchison. 2002a. EB1 targets to kinetochores with attached, polymerizing microtubules. *Mol Biol Cell*. 12:4308-16.

Tirnauer, J. S., S. Grego, E. D. Salmon and T. J. Mitchison. 2002b. EB1-microtubule interactions in Xenopus egg extracts: role of EB1 in microtubule stabilization and mechanisms of targeting to microtubules. *Mol Biol Cell*. 10:3614-26.

Walker, R. A., E. T. O'Brien, N. K. Pryer, M. F. Soboeiro, W. A. Voter, H. P. Erickson and E. D. Salmon. 1988. Dynamic instability of individual microtubules analyzed by video light microscopy: rate constants and transition frequencies. *J Cell Biol*. 4:1437-48.

Yahara, I. and G. M. Edelman. 1975. Modulation of lymphocyte receptor mobility by locally bound concanavalin A. *Proc Natl Acad Sci U S A*. 4:1579-83.

Zeeberg, B. and M. Caplow. 1979. Determination of free and bound microtubular protein and guanine nucleotide under equilibrium conditions. *Biochemistry*. 18:3880-6.

# BIOGRAPHICAL SKETCH

Luz Elena Caro was born and raised in Delaware, and graduated from Middletown High School in Middletown, DE. She attended the University of Delaware and obtained her B.ChE. in Chemical Engineering. During her time at the university, Luz Elena completed two summer internships at Merck & Co., Inc. After graduation, she interned at General Mills for a summer before joining the chemical engineering department at the University of Florida for her graduate degree. Upn receiving her doctoral degree, Luz Elena will join the drug metabolism department at Merck & Co., Inc. in West Point, PA as a senior research pharmacokineticist.